Temporary modification strategies of Vibration Dampers for Offshore Wind Turbines

J.C.W. Daamen

December 19, 2017

TU Delft Delft University of Technology

SIEMENS Gamesa RENEWABLE ENERGY

Temporary modification strategies of Vibration Dampers for Offshore Wind Turbines

Master of Science Thesis

For the degree of Master of Science in Mechanical Engineering at Delft University of Technology

Author: J.C.W. Daamen

Committee:

Prof.dr. A. Metrikine	TU Delft - Chairman
Dr.ir. A. Jarquin Laguna	TU Delft
Dr.ir. K.N. van Dalen	TU Delft
Dr.ir. S.N. Voormeeren	Siemens Gamesa Renewable Energy
Ir. F. Wenneker	Siemens Gamesa Renewable Energy

Bottom Founded Offshore Structures, Arctic & Wind - Offshore and Dredging Engineering
Faculty of Mechanical, Maritime and Materials Engineering (3mE) - Delft University of Technology

December 19, 2017

TU Delft Delft University of Technology

- CONFIDENTIAL -

SIEMENS Gamesa RENEWABLE ENERGY

Summary

Trends towards higher capacity offshore wind turbines (OWTs) and deeper offshore wind farm sites, make wave-induced vibrations more dominant in its structural design. In order to design economically feasible monopile-type support structures for these next generation OWTs, additional damping is required during idling phases. A specific damper, the Tuned Liquid Column Damper (TLCD), can potentially be very effective in achieving this without requiring many components in its design.

Besides the structural design, installation is a significant cost-driver for offshore wind energy. For next-generation OWTs, increased wave-induced vibrations may result in installation workability reductions as high as 50%. Dampers that are designed for the operational life of an OWT will not improve installation workability sufficiently because they are not effective at off-tuned natural frequencies of partially installed OWTs. The application of TLCDs to OWTs imposes new constraints on the damper's design. As a result, existing methods for increasing effectiveness at off-tuned frequencies are not applicable.

The main objective of this thesis is, therefore, the reduction of wave-induced vibrations during OWT installation by non-invasive modification strategies of off-tuned TLCDs.

To this end, a novel period adjustment strategy was investigated: the Airflow Obstructed Tuned Liquid Column Damper (AO-TLCD). Identical to the intensively researched Tuned Liquid Column Gas Damper (TLCGD), the vertical compartments are enclosed from the environment, resulting in an additional gas-spring. The proposed modification utilises controllable valves in the gas system to regulate the pressures inside the gas compartments. The vast amount of research performed on the passive and active TLCGD make the AO-TLCD a promising option. Moreover, modifications are made away from the regular geometrical design. As a consequence, the operational effectiveness of the TLCD can be maintained.

The first part of this research fulfils the first objective: the development and validation of the AO-TLCD model. A closed-form differential equation was formulated for the polytropic pressure difference in the compartments, assuming quasi-steady and quasi-1D gas flow. For the operational conditions of the AO-TLCD, simplified forms of the massflow and pressure equations have differences smaller than 10% compared to their fully non-linear and incompressible counterparts. Using small-scale experimental data, the model was validated to accurately predict the steady-state response of the passive AO-TLCD.

For the passive AO-TLCD, adjustment to off-tuned frequencies introduces large amounts of viscous dissipation into the system, effectively reducing the restoring force with respect to the host structure. As a result, period adjustment using passive airflow obstruction (AO) is not possible while maintaining significant effectiveness of the TLCD. For low obstruction, a large influence of the AO on the internal damping of the TLCD was observed without affecting other properties of the system. Hence, passive AO can be used as an alternative design parameter for the internal damping of a TLCD.

The second part of this research fulfils the main objective: the development of an effective TLCD modification for OWT installation. Semi-active control of the valves was used to minimize the dissipation that renders the passive AO-TLCD ineffective. Contrary to active control, semi-active control cannot add mechanical energy through its actuator. This results in relatively low requirements for additional components and yields an inherently stable system, making it more suitable for offshore applications.

To reduce the complexity of the device further, the valve was controlled in a bi-state discrete manner

(bang-bang control). In other words, the actuator can only be switched between its open and closed state. Based on literature on semi-active dampers, two control laws were defined: a simple hybrid control law that switches between continuous systems through discrete control actions and a clipped Linear Quadratic Regulator, i.e. a semi-active variant of optimal full-state feedback control.

The behaviour of the semi-active AO-TLCD was solely tested for an OWT installation case study because the narrow-banded and strongly non-linear response of the semi-active AO-TLCD results in an excitation dependent performance. Environmental loads were limited to regular sea states with high occurrence. As a result, the first mode of the support structure is dominant. Modal reduction was performed on the stand-alone support structure including the non-participating TLCD weight. The semi-active AO-TLCD was coupled through the first mode shape of the OWT.

The semi-active control laws behaved as designed. The internal parameters of the TLCD were improved and energy was effectively absorbed from the host. Across all load cases, wave-induced tower top displacements were reduced up to 60% even though relatively small liquid strokes were observed. A sensitivity study found that the effectiveness of the semi-active AO-TLCD was independent of the operational TLCD's design frequency. At optimally tuned conditions, the semi-active AO-TLCD outperformed its passive counterpart by more than 10%. Inclusion of actuator dynamics was not detrimental to the performance.

The developed modification strategy was further investigated through a more general framework of periodic linear time-variant systems. The inherent stability of the damper was demonstrated further. Moreover, it was shown that the two proposed control laws have relatively optimal performance.

The design of the proposed modification is of low complexity compared to existing TLCDs capable of period adjustment. Depending on the design of the AO-TLCD, the airflow obstruction can be implemented as a temporary modification or its effects on the operational TLCD can be minimised. Most importantly, the damper effectively reduces wave-induced vibrations independent of the passive TLCD design. Consequently, the semi-active AO-TLCD will be sufficiently effective in improving workability for the whole OWT installation range. Therefore, it can be concluded that the main objective of this thesis is fulfilled.

Further development of the semi-active AO-TLCD is required. The semi-active AO-TLCD should be validated experimentally; namely, unmodelled dynamics that are potentially introduced through semi-active control of the valves should be investigated. Additionally, the effects of sensor noise on the performance of the controller should be investigated.

Acknowledgements

Exactly one year ago I was in a completely different environment; exploring the rural part of Vietnam on a motorbike. I must admit this feels like ages ago. Though, my time here at Siemens hasnt been tedious at all.

I would like to thank Sven and Frits for their insights during our various meetings. I appreciate the way you helped me shape my research and bring it to a higher level. But mostly, I would like to thank you for your patience in trying to understand the more than frequent chaotic presentations of my progress. I would also like to thank Antonio for his refreshing views and for helping me keep the overall picture. Besides my daily supervisors, I would like to thank Marc, the knowledge you provided on the topic during my research has been really valuable. Even more, I appreciate how you involved me in numerous meetings and discussions.

What I enjoyed most about this research was the freedom it provided to combine different fields of study into a single topic. Even though, at multiple instants over the past year I was wondering where I had gotten myself into. With this in mind, I would like to thank the people from the TU who helped me regardless of not being involved in my research. Dr. Ferdinand Schrijer and Dr. Rene Pecnik; without your help I wouldn't have been able to proceed my work with such confidence. Moreover, I would like to thank Professor Jan-Willem van Wingerden for our intriguing discussions.

Last but not least, I would like to thank my parents for their relentless support over the past 25 years. Without you, I literally couldn't have done it.

The Hague, Decemeber 2017

Joris Daamen

Contents

Summary i

Acknowledgements iii

List of Figures vii

List of Tables ix

Nomenclature x

1 Introduction 1
- 1.1 Motivation . . . 1
- 1.2 Research context . . . 1
- 1.3 Problem statement . . . 2
- 1.4 Research objective and scope . . . 2
- 1.5 Thesis outline . . . 3

I Passive TLCD modification 5

2 Dynamic Vibration Absorbers 6
- 2.1 Structural control . . . 6
- 2.2 Tuned Mass Dampers . . . 7
- 2.3 Tuned Liquid Column Dampers . . . 9
- 2.4 Period adjustment strategies . . . 12

3 Modelling of Airflow Obstructed TLCDs 17
- 3.1 Working principle and assumptions AO-TLCD . . . 17
- 3.2 Brief review of gas dynamics . . . 18
- 3.3 Compression . . . 21
- 3.4 Massflow . . . 22
- 3.5 Modelling simplifications airflow obstruction . . . 24
- 3.6 Stand-alone model AO-TLCD . . . 26

4 Validation and dynamic behaviour passive AO-TLCD model 29
- 4.1 Experimental set-up . . . 29
- 4.2 Verification and validation of the AO-TLCD model . . . 31
- 4.3 Additional analysis . . . 34
- 4.4 Modification valves . . . 35
- 4.5 Discussion . . . 35

II Semi-Active TLCD modification for OWT installation **37**

5 Semi-active control **38**
5.1 Semi-active structural control devices . . . 38
5.2 Modelling and control components . . . 42
5.3 Control laws . . . 45

6 Modelling of OWT installation with semi-active AO-TLCDs **53**
6.1 Installation case study . . . 53
6.2 Modelling of offshore wind turbines . . . 55
6.3 Coupled model of OWT and AO-TLCD . . . 56
6.4 Verification and benchmark coupled model . . . 57

7 Results Case Study **61**
7.1 General statistical results . . . 61
7.2 Additional observations . . . 63
7.3 Sensitivity to frequency variations . . . 65
7.4 Sensitivity to actuator dynamics . . . 66
7.5 Discussion . . . 68

8 Periodically time-variant systems framework **71**
8.1 Linear time varying systems . . . 71
8.2 Stability of LTV systems . . . 72
8.3 Modulation of Single DoF systems . . . 75
8.4 Semi-active AO-TLCD . . . 77
8.5 Discussion . . . 81

9 Conclusions and Recommendations **83**
9.1 Conclusions . . . 83
9.2 Recommendations . . . 85

Appendices **88**

A Methods **88**
A.1 Energy considerations extended . . . 88
A.2 Derivation spring-element concept . . . 91
A.3 Extended review of gas dynamics . . . 92
A.4 Massflow . . . 94
A.5 Experimental calibration . . . 97
A.6 Fundamental matrix of Meissner's equation . . . 99
A.7 Performance evaluation using the growth matrix . . . 100

B Figures and tables **101**
B.1 In-depth analysis LQR strategy . . . 101
B.2 Results periodic LTV framework . . . 102

Bibliography **107**

Definitions **111**

List of Figures

2.1 Classification structural control strategies. . . . 7
2.2 Single DoF host structure with a passive TMD. . . . 7
2.3 Dynamic amplification host structure with optimally tuned TMD as a function of damping. 8
2.4 Regular sealable TLCD. . . . 9
2.5 Effectiveness TLCD attached to a white noise excited host structure, for variable damping and tuning, including operational regions OWT. . . . 11
2.6 Effectiveness optimally damped TLCGD attached to a white noise excited host structure, including operational regions OWT. . . . 12
2.7 Concept for Period-Adjustment Liquid Column Damper. . . . 13
2.8 Additional gas volume requirement for period adjustment TLCD. . . . 14
2.9 Additional spring-element concept for period adjustment TLCD. . . . 14

3.1 Overview of AO-TLCD with control valves. . . . 17
3.2 Comparison linear pressure and equivalent linear pressure with non-linear form for a two-sided sealed TLCD. . . . 24
3.3 Comparison massflow equations for very low obstruction. . . . 25
3.4 Comparison massflow equations for pressure release from previously 1-sided compressed compartment. . . . 26

4.1 Diagram experimental set-up. . . . 30
4.2 Actual experimental set-up. . . . 30
4.3 Numerical steady state response comparison of the liquid displacements for open/sealed TLCD and very low-/high obstructed AO-TLCD. . . . 31
4.4 Numerical and experimental steady state response of the liquid displacements for variable number of open valves. . . . 32
4.5 Numerical and experimental steady state response of the pressure difference for variable number of open valves. . . . 33
4.6 Numerical results for equivalent parameters of the AO-TLCD with variable number of open valves. . . . 34
4.7 Comparison energy dissipation TLCD and gas-system for a variable number of open valves. 35

5.1 MR-fluid damper device 39
5.2 MR-fluid damper attached to a multi-story structure. . . . 39
5.3 Variable orifice damper. . . . 40
5.4 Variable stiffness semi-active TMD. . . . 40
5.5 Variable orifice TLCD. . . . 41
5.6 MR-TLCD. . . . 41
5.7 Variable column TLCD. . . . 41
5.8 Tuned liquid column gas damper 41
5.9 Force-displacement/velocity diagrams: Clipping of AO-TLCD input for a followed reference stiffness. . . . 46

5.10 Force-displacement/velocity diagram of pressure-force on liquid: minimal clipping of AO-TLCD input. . . . 46
5.11 Schematic overview of effect of pressures on host and liquid. . . . 47
5.12 Schematic overview simple hybrid system. . . . 47
5.13 Simplified schematic of non-optimal hybrid control scheme. . . . 48
5.14 Simplified schematic of improved and final hybrid control scheme. . . . 48
5.15 Frequency response of active LQR controlled AO-TLCD and passive TLCDs for the host and liquid displacements. . . . 50
5.16 Comparison control inputs active and semi-active LQR schemes resulting from a stochastic load case. . . . 51

6.1 Installation workability graph for case study site for wind-speeds $v < 16m/s$. . . . 54
6.2 Effectiveness optimally damped TLCGD attached to a white noise excited host structure, including hub-installation frequency. . . . 55
6.3 Diagram OWT-coupled SA AO-TLCD. . . . 58
6.4 Displacements benchmark solutions for critical loadcase III seed 1. . . . 58
6.5 Comparison between working points of benchmark solutions with linear TLCD effectiveness for a white noise excited host structure. . . . 59

7.1 Average standard deviation TT displacements semi-active across seeds. . . . 61
7.2 Convergence mean tower-top displacement standard deviations. . . . 62
7.3 Dynamic amplification host for all set-ups. . . . 63
7.4 Force-displacement/velocity diagrams for hybrid control strategy. . . . 64
7.5 Sensitivity of semi-active control strategies to adjusted 'open' TLCD stiffness. . . . 65
7.6 Equivalent internal properties TLCD for semi-active control strategies with variable 'open' TLCD stiffness. . . . 65
7.7 Step response of a 'slow' and 'fast' actuator to control input. . . . 66
7.8 Sensitivity of semi-active control strategies to actuator rise time. . . . 67
7.9 Force-displacement/velocity trajectory comparison hybrid control strategy with and without actuator dynamics. . . . 67

8.1 Discretised system matrix over a single period. . . . 74
8.2 Shape of modulation signal $p(t)$ of Meissner's equation. . . . 76
8.3 Stability chart for Meissner's equation with variable damping. . . . 77
8.4 Diagram of the periodically varying LTV semi-active AO-TLCD. . . . 78
8.5 Square modulation signal over two modulation periods. . . . 78
8.6 Computational procedure stability and performance of the homogeneous LTV SA AO-TLCD. 80
8.7 Stability and performance of the periodical LTV system. . . . 80

A.1 Comparison massflow equations for very low obstruction. . . . 96
A.2 Dynamic amplification liquid. Comparison calibrated model with open experimental set-up. 97
A.3 Loss factor approximation for all experiments . . . 98
A.4 Sensor noise and distortion experimental data. . . . 98

B.1 Force-displacement/velocity trajectories for clipped-LQR strategy. . . . 101
B.2 Damping modulation of a second order differential equation for δ=0.25. . . . 102
B.3 Comparison of the responses between the LTV and the NL TD model. . . . 103
B.4 Comparison mechanical energy results of the growth- and the transition matrix. . . . 103
B.5 Cross section of the performance figure at $D = 1$ corresponding to the passive TLCD. . . . 104
B.6 Cross section of the performance figure with variable duty cycle. . . . 104
B.7 Boxplot of 'duty cycles' observed in the non-linear TD simulations of the case study 105

List of Tables

2.1 Morphological overview of existing and new TLCD modification. 15

4.1 Air-system set-ups used for verification. 29
4.2 Calibrated parameters for numerical model obtained with experimental data. 30

5.1 Overview of control laws used in case study. 52

6.1 Overview normalized properties of support structure during installation steps. 53
6.2 Hydrodynamic load cases and stand-alone tower response including total weight TLCD. . . 56

7.1 Performance passive and semi-active strategies. 62

8.1 Variables and constants used in the stability and performance analysis of the LTV SA AO-TLCD. 79
8.2 Effectiveness of the LTV system at specific points corresponding to passive AO-TLCD settings. 81

Nomenclature

Latin symbols

$\mathbf{A}$	System matrix state space	
$\mathbf{A}_k$	Discrete constant system matrix	
$\mathbf{B}$	Input vector state space	
A_B	Area horizontal pipe TLCD	m^2
A_H	Area liquid column TLCD	m^2
B	Width TLCD	m
$\mathbf{C},\ c$	Damping matrix/constant	Ns/m
c	Speed of sound	m/s
D	Duty cycle	$-$
$\bar{f}$	Velocity independent moody friction factor	$-$
F	Force	N
f	Mass normalized force	N/kg
g	Gravitational constant	m/s^2
H	Height liquid column TLCD	m
h	Enthalpy	J
h_{eff}	Effective height gas compartment	m
J	Cost function LQR	
$\mathbf{K_g}$	State feedback gain LQR	
$\mathbf{K},\ k$	Stiffness matrix/constant	N/m
K	Flow loss factor	$-$
Δk	Discrete time interval $t_k - t_{k-1}$	s
K_o	Air-obstruction parameter	
K_{oi}	Inverse obstruction parameter	
L_{eff}	Effective length TLCD	m
L_{em}	Mass length TLCD	m
$m,\ m_{act}$	Damper mass / active fluid mass	kg
M	Mach number	$-$
M	Mass host	kg
m_0	Initial mass gas compartment	$-$
m_f	Fluid mass	kg
m_{pas}	Passive fluid mass	kg
Δm	Displaced gas mass	kg
$\mathbf{M}$	Mass matrix	N/m
n	Polytropic constant	$-$

N_c	Number of sealed compartments	$-$
n_v	Number of parallel valves	$-$
p	Pressure	Pa
$\mathbf{Q}$	State weighing matrix LQR	
q	Generalized (modal) coordinate	m
$\mathbf{R}$	Input weighing matrix LQR	
R	Specific gas constant for dry air	$Jkg^{-1}K^{-1}$
$r_{1,2}$	Set of roots/eigenvalues of second order differential equation	
$\mathbf{s}$	Position vector TLCD	
s	Number of full cycles	
t_r	Rise time step response	s
T	Temperature	K
T	Modulation period	s
u	Input	
u_f	Liquid displacement	m
V	Volume	m^3
v	Gas flow speed	m/s
V_0	Initial gas compartment volume	m^3
w	Host horizontal displacement	m
$\mathbf{x}$	State vector	

Greek symbols

α	Area ratio TLCD A_H/A_B	$-$
β^2	Area ratio valve/liquid column	$-$
δ	Tuning factor ω_A/ω_s	$-$
δ_L	Headloss coefficient	m^{-1}
δ	Modulation frequency ratio	$-$
ϵ	Inverse air-spring stiffness	Pa/m
ϵ	Modulation depth	$-$
ζ_A	Linearized damping TLCD	$crit$
ζ_S	Structural damping Host	$crit$
γ	Isentropic constant	$-$
γ	Normalized excitation frequency	$-$
γ	Normalized damping	$-$
$\bar{\kappa}$	Geometrical parameter 2 TLCD	$-$
κ	Geometrical parameter 1 TLCD	$-$
Λ	Characteristic multipliers	
λ	Characteristic exponents	
μ	Modal mass ratio TLCD/Host	$-$
$\phi_{i,j}$	Phase angle between i and j	deg
$\boldsymbol{\phi}_j$	Mode vector j	$-$
$\phi_{j,i}$	Mode vector j at location i	$-$
$\boldsymbol{\phi}(t)$	Fundamental matrix	
$\boldsymbol{\Phi}(t, t_0)$	Transition matrix between time t_0 and time t	

$\mathbf{\Phi}_0(t)$	Transition matrix between time $t_0 = 0$ and time t	
ρ	Density	kg/m^3
τ	Normalized time	s
ω	Excitation frequency	rad/s
ω_A	Natural frequency TLCD	rad/s
ω_S	Natural frequency Host	rad/s
χ	Normalized liquid displacements	$-$

Subscripts

a	Absorber/damper
eq	Equivalent (energy) linearised property
f	Fluid/liquid
g	Gas
opt	Optimal TLCD property
0	Initial property when related to gas system
0	Amplitude when referred to TLCD responses
p	Properties used for the spring-element concept
s	System/host
v	Actuator

Superscripts

$*$	Modal property, periodic varying property

Abbreviations

AO	Airflow Obstruction
AO-TLCD	Airflow Obstructed Tuned Liquid Column Damper
CFD	Computational Fluid Dynamics
DoF	Degree of Freedom
SDoF/MDoF	Single/Multiple Degree of Freedom
ER-fluid	Electro Rheological fluid
(G)AS	(Global) Asymptotic Stability
LQR	Linear Quadratic Regulator
C-LQR	Clipped Linear Quadratic Regulator
LTI	Linear time-invariant (system)
LTV	Linear time-variant (system)
MR-fluid	Magneto Rheological fluid
MMS	Method of Multiple Scales
OWT	Offshore Wind Turbine
SA	Semi-active
STMD	Semi-Active Tuned Mass Damper
TLCD	Tuned Liquid Column Damper
TLCGD	Tuned Liquid Column Gas Damper
TMD	Tuned Mass Damper
TT	Tower top
VA	(Dynamic) Vibration Absorber

Chapter 1

Introduction

1.1 Motivation

In order to make offshore wind energy a viable option in the long term, further costs reductions are required. One of the key factors in achieving cost-competitiveness is the introduction of higher capacity turbines (up-scaling) [1].

As these trends continue, the natural frequency of the Offshore Wind Turbine (OWT) will decrease further into the wave-spectrum. In combination with the low inherent structural damping, wave-induced fatigue may play an even larger role in the structure's design and lifetime assessment.

Besides the structural design, installation is a significant cost driver for offshore wind energy. The wave-induced vibrations will also pose problems for installation workability. In other words: the probability that installation can be performed is affected negatively by these trends.

In order to design an economically feasible monopile-type support structure for the next generation OWTs, damping needs to be increased during idling phases. This can be achieved through structural control with vibration absorber (VA) devices. A specific device, the Tuned Liquid Column Damper (TLCD), can potentially be very effective while not requiring many components in its design. Hence, the use of TLCDs in offshore applications can be very promising.

The application of TLCDs in OWTs introduces new problems, especially for the purpose of improving installation workability. VAs can be very sensitive to their tuning to specific frequencies. A damper designed for the operational life (fatigue lifetime) is not effective at frequencies typical during installation steps. Existing methods for period adjustment of TLCDs are not sufficient because they do not comply with additional constraints imposed by OWTs. Therefore, this research focusses on new period adjustment strategies of TLCDs designed for OWTs.

1.2 Research context

In this section, additional context is provided regarding OWTs and structural control, including a brief overview of relevant literature.

Installation of OWTs

The installation phase plays an important role in the levelised cost of energy of an offshore wind farm [2]. Installation vessels are only able to operate in mild environmental conditions. Traditionally these conditions do not have a high probability to correlate with large structural vibrations of the partially installed OWT.

Reduction of the OWT's natural frequency, increases the wave-induced response for highly probable sea states. As a result, wave-induced vibrations may dominate the installation process. In order

to continue the trends towards higher capacity turbines and deeper waters, while using monopile foundations, these vibrations have to be reduced.

During installation the structure has a larger natural frequency, as not the whole top mass has been installed. A VA designed for the operational natural frequency, will not be effective.

Structural Control

Structural control through VAs has been intensively researched and applied to onshore civil structures. For the TLCD alone, multiple modifications and geometrical variations have been investigated [3][4]. The most intensively researched and applied period adjustment strategy for a TLCD was first introduced by Hochrainer in the form of additional gas springs: the tuned liquid column gas damper (TLCGD) [5]. Some (semi)-active devices were also proposed including an active variation of the TLCGD [6]. Most recently, a novel method for semi-active period adjustment was proposed, using variable vertical column geometry [7]. These existing methods are not capable of non-complex and broad-range period adjustment for low-frequency TLCDs.

Structural Control for OWTs

The use of structural control in OWTs is in a more exploratory phase than their onshore application [8]. The potential benefits of Tuned Mass Dampers (TMDs) and TLCDs [9] for OWTs have been investigated using both high-fidelity wind- and soil models [10][11][12]. Generally, results show a potential reduction of OWT vibrations for both wind/wave- and seismic excitation [9]. The largest improvements have been obtained for wind/wave misalignment and low/high wind speeds [11] (low aerodynamic damping). Though, large uncertainties in the soil model can render passive control ineffective [12]. Most recently, the use of a semi-active TMD for monopile OWTs has been studied [13]. Unlike the passive system, it was able to cope with foundation damage and soil uncertainty. Furthermore, the semi-active system was shown to out-perform its passive counterpart while having a smaller stroke.

1.3 Problem statement

As explained in the previous paragraphs, vibration reduction during OWT installation plays an important role in ensuring economic feasibility of monopile-type support structures for next-generation OWTs. The use of TLCDs for this reduction gives rise to the following problems:

- TLCDs designed for the operational OWT are not effective[1] around natural frequencies typical during installation steps.
- Permanent modifications of the passive damper properties are undesired due to reduced effectiveness during the operational life of the OWT. Temporary modifications of the passive damper properties, besides additional gas-springs, are prevented by geometrical constraints.
- Current control strategies capable of increased effectiveness at largely off-tuned frequencies are limited to active control; requiring large amounts of energy supply and components.

1.4 Research objective and scope

Main objective

Reduction of wave-induced vibrations during OWT installation by a novel non-invasive[2] strategy for period adjustment of off-tuned TLCDs: passive/semi-active[3] airflow obstruction.

[1] Effectiveness is the ability of the damper to reduce dynamic vibrations of the host system.
[2] Non-invasive modifications are defined to have a negligible effect on the operational damper's design and effectiveness.
[3] Semi-active devices have means of control but cannot add mechanical energy into the system through its actuators.

Scope

In order to evaluate the main objective, numerical time-domain simulations are performed on the OWT support structure including the modified TLCD. For this, first a numerical model describing the dynamical behaviour of the Airflow Obstructed Tuned Liquid Column Damper (AO-TLCD) is required. For efficient analysis, this model requires sufficient simplicity.

Therefore, the first part of this research focusses on the passive stand-alone TLCD. For this, two sub-objectives can be identified: '*development and validation of a simple*[4] *numerical model*' and '*investigation of the dynamical behaviour of the passive AO-TLCD*'. The modification mainly involves gas dynamics; potentially requiring complex and computationally expensive models. Several assumptions, like quasi-steady gas-flow and polytropic compression, are made. Thereafter, these assumptions are justified through validation of the passive AO-TLCD model using small-scale experimental data.

The second part of this research aims to fulfil the main objective of this research. Again, two sub-objectives can be identified: '*robust period adjustment of the AO-TLCD*' and '*evaluation of the effect of the AO-TLCD on installation workability*'. To ensure robust performance, semi-active control of the airflow obstruction is investigated. The main focus is on actuator implementation and general feasibility. Advanced control theory is outside the scope of this research. Therefore, control is limited to two sub-optimal state-feedback strategies with on/off actuators. For the evaluation of the installation workability, the same level of detail is assumed for the OWT. A modal reduced form of a support structure model is used. Of which, soil-structure interaction is approximated through p-y curves. Due to the inherent non-linear nature of the semi-active modification, the effects are investigated for a single case study and a limited set of environmental conditions.

To further ensure robustness and general applicability of the AO-TLCD strategy. Its performance and stability is analysed through a more general framework of periodic time varying systems.

1.5 Thesis outline

As mentioned in the previous section, this thesis has been split up in two parts based on the structural control strategy. Part I is limited to the modelling and the behaviour of a stand-alone passive AO-TLCD. Part II introduces semi-active control of the AO-TLCD and evaluates its performance for OWT installation.

The first part starts in Chapter 2 with an introduction to structural control in general. Furthermore, current and proposed methods for period adjustment of a TLCD are discussed. In Chapter 3 the proposed modification is investigated in greater depth. The model of a stand-alone passive AO-TLCD is derived. A brief review of gas dynamics modelling is also given. To finalize part I, the AO-TLCD model is validated in Chapter 4 using data from small-scale experiments.

The second part starts in Chapter 5, with a review of semi-active structural control and control theory. Afterwards, in Chapter 6, additional information is given on OWT installation and modelling of OWTs during this phase. Moreover, the semi-active AO-TLCD is coupled to the OWT model. Part II is concluded in Chapter 7 with results from an installation phase case study including the fully coupled AO-TLCD model.

In order to obtain a broader analysis of the performance and stability of the semi-active AO-TLCD, the damper is analysed through a more general framework of periodic time variant systems in Chapter 8.

In Chapter 9, the main conclusions of this research are listed and recommendations for future work are given.

[4] A simple numerical model is assumed to be limited to a set of algebraic- and ordinary differential equations with a limited amount of degrees of freedom.

Part I

Passive TLCD modification

Chapter 2

Dynamic Vibration Absorbers

Dynamic vibration absorbers and their dynamic interaction with structures lie at the basis of this thesis work. Consequently, this first chapter focusses on understanding the behaviour of such devices. For this, a portion of the chapter is devoted to Tuned Mass Dampers (TMDs), as their working principle largely dictates the workings of Tuned Liquid Column Dampers (TLCDs). In essence, the TLCD can be considered as a specific class of TMDs.

First, the classification of vibration absorbers is defined. Afterwards, Section 2.2 explains the working principle and dynamical behaviour of TMDs. In Section 2.3, the Equations of Motion of TLCDs are given. Additionally, a comparison with regular TMDs is made. Afterwards, in Section 2.4 a review is given on existing and new modifications for period adjustment of TLCDs. In this review, (semi)-active methods are included briefly for completeness.

2.1 Structural control

Structural control of civil structures is a rich field of research. Numerous classes of strategies and devices have been proposed, tested and applied in structures like high-rise buildings and bridges. This research focusses on a single class of structural control devices: dynamic vibration absorbers (VAs), since these are applicable in offshore wind turbines (OWTs).

Application of VAs in OWTs is in a more exploratory phase. The main difference with onshore applications is that they should be designed to mitigate wave-induced vibrations instead of more broad band wind and seismic vibrations. Furthermore, targeted frequencies are generally lower and spatial restrictions are larger.

Classification structural control

Structural control through VAs can be classified in terms of type of control [4], as is seen in Figure 2.1. The main focus of this research is on passive and semi-active devices.

- Passive devices are most simplistic but require careful tuning. The dynamic properties of a passive device are determined by its geometrical design. In this research, damper modifications are considered passive when they occur on much larger time scales than the natural period of the device.
- Active devices require additional components like sensors, computers and (force)-actuators. This enables the device to deal with off-tuning and vastly out-perform passive devices. Drawbacks are that they require many components and large amounts of energy. Moreover, they can potentially to destabilize the host structure.

- Semi-active devices cannot add mechanical energy into the system through its actuator. Instead passive device parameters, like damping, can be controlled and changed in real-time. As a consequence, energy requirements are minimal and destabilization of the host is impossible. Semi-active devices generally out-perform their passive counterparts and can deal with off-tuning. In case of a failure in the control components, a passive system remains.

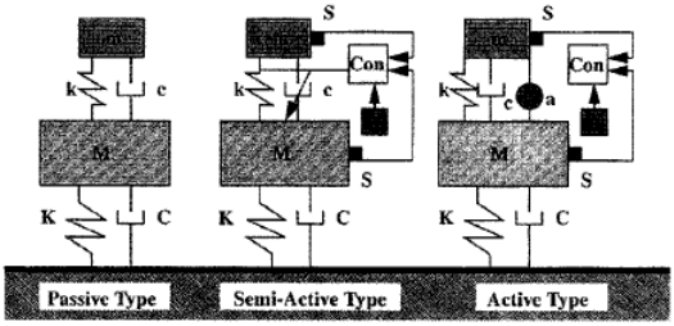

Figure 2.1: Classification structural control strategies (s = sensor, a = actuator, con = controller) [14].

2.2 Tuned Mass Dampers

The working principle of a passive TMD can be best explained through a linear 2DoF system as depicted in Figure 2.2. Here the host system and the absorber are denoted by subscripts S and A respectively. The equations of motion are given by Equation 2.1. Here, $u = w - x$ is the relative displacement of the damper and $\mu = m/M$ indicates the TMD mass ratio. As a result, the natural frequency of the host and the absorber can be expressed as $\omega_S^2 = k_S/M$ and $\omega_A^2 = k_A/m$, respectively. The damping ratio ζ is obtained in the same fashion.

The idea behind a TMD, or VAs in general, is that the damper is excited by the host structure, in effect absorbing part of its energy. Subsequently, this energy is dissipated by additional mechanisms introduced by the damper. The behaviour of the 2DoF system largely depend on the damper parameters. For a properly designed damper, the dynamic characteristics of the host system can be improved significantly.

$$\begin{bmatrix} 1+\mu & \mu \\ 1 & 1 \end{bmatrix} \begin{bmatrix} \ddot{w} \\ \ddot{u} \end{bmatrix} + \begin{bmatrix} 2\zeta_S\omega_S & 0 \\ 0 & 2\zeta_A\omega_A \end{bmatrix} \begin{bmatrix} \dot{w} \\ \dot{u} \end{bmatrix} + \begin{bmatrix} \omega_S^2 & 0 \\ 0 & \omega_A^2 \end{bmatrix} \begin{bmatrix} w \\ u \end{bmatrix} = \begin{bmatrix} F(t)/M \\ 0 \end{bmatrix} \tag{2.1}$$

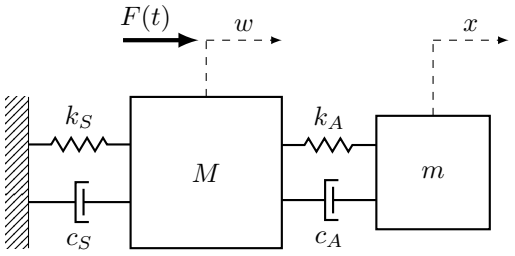

Figure 2.2: Single DoF host structure with a passive TMD.

A good understanding of the effect of the TMD can be obtained by through the energy balance of the host system. For the steady-state response of a stationary stochastic excited system, the expectation

$E[.]$ of kinetic and potential energy must go to zero, resulting in Equation 2.2. For the damper energy flow, an equivalent additional linear damping can be defined by matching the energies with such a fictive damping (Equation 2.3). The full derivation can be found in Appendix A.1.

$$2\zeta_s\omega_s E\left[\dot{w}\dot{w}\right] + \mu E\left[\ddot{u}\dot{w}\right] = \frac{1}{M} E\left[F(t)\dot{w}\right] \tag{2.2}$$

$$\Delta\zeta_s = \frac{\mu \cdot E\left[\ddot{u}\dot{w}\right]}{2\omega_s \cdot E\left[\dot{w}^2\right]} \tag{2.3}$$

Equation 2.3 shows how the additional dissipation is influenced by the damper parameters. For optimal performance, the phase difference between $\dot{w}$ and $\ddot{u}$ must be kept at a minimum while the magnitude of the forcing term should be as high as possible. This requires a natural frequency close to that of the host and low TMD damping. Though, for low internal damping, the effect of the damper may be too narrow banded. Therefore, an optimal damping value exists, depending on the type of excitation.

An approach for finding these optimal parameters was first introduced by Den Hartog [15] and later expanded for additional types of excitations by Constantinou [16]. Both methods assume an undamped host structure and optimal performance over the whole frequency band. Therefore, it may not be applicable for narrow-banded excitation. Such excitations require either numerical optimization or optimal parameter definitions using higher order filters [17]. Moreover, constraints may require reduction of the TMD response through increased damping.

In Figure 2.3 the dynamic amplification of a lightly damped host structure, including an optimally tuned TMD, is given as a function of the excitation ratio γ for different damping values[1]. The optimal tuning ratio δ and damping ζ_A were computed for a statistically random excitation and are listed in Equation 2.4. Infinite internal damping, $\zeta_A = \infty$, represents the stand-alone host system including damper mass.

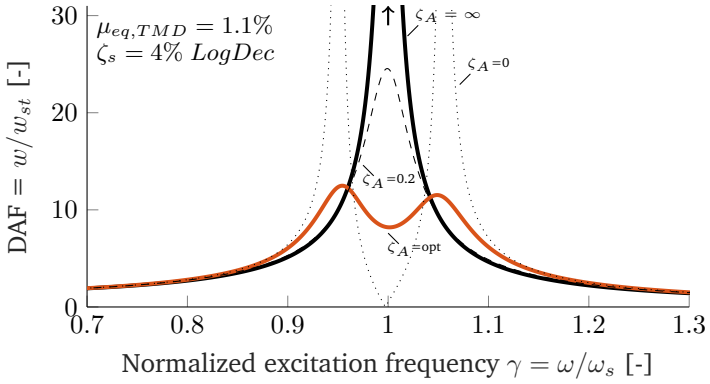

Figure 2.3: Dynamic amplification host structure with optimally tuned TMD as a function of ζ_A.

$$\begin{aligned} \delta_{opt} &= \sqrt{\frac{1+0.5\mu}{(1+\mu)^2}} \\ \zeta_{A,opt} &= \sqrt{\frac{\mu(1+0.75\mu)}{4(1+\mu)(1+0.5\mu)}} \end{aligned} \tag{2.4}$$

[1] In this research, the use of 'damping' without any further clarification always refers to the TLCD. Alternatively 'internal damping' may be used. For inherent structural damping, always some reference to the host or structure is given. Damping added by the TLCD to the host, equivalent structural damping, will be referred to as 'effectiveness'.

2.3 Tuned Liquid Column Dampers

With the working principle for a linear TMD defined, we can start looking at the similarities and differences of a TLCD.

2.3.1 General description

A tuned liquid column damper, generally is a U-shaped container containing a Newtonian liquid, as can be seen in Figure 2.4. Unlike a TMD, it does not require additional components to represent a full mass-dashpot-spring system. Stiffness results from the restoring weight of the liquid and damping is a result of viscous and turbulent pressure losses along the streamline. Additional stiffness and damping can be obtained through sealing of the gas compartments and the use of orifices in the liquid, respectively. The TLCD can be closed from the environment to prevent corrosion, as long as the interconnecting pipe conveys free gas flow.

The simplicity of the TLCD can be an advantage, especially in offshore applications where high reliability is of importance. A disadvantage, for the application in OWTs, is the required volume to obtain the desired mass ratio, due to the relatively low density of the liquid compared to TMD masses comprised of steel or concrete.

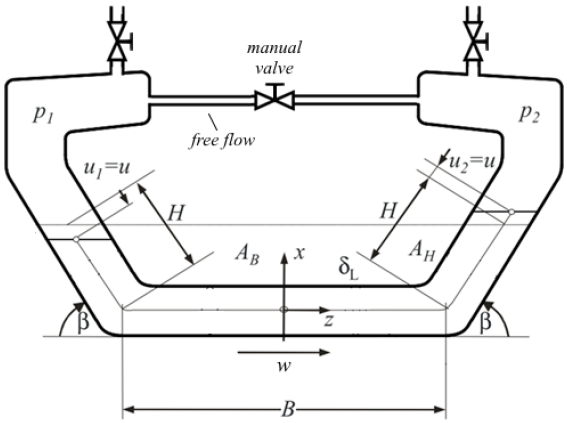

Figure 2.4: Regular sealable TLCD attached to host with accelerations $\ddot{w}$ [5].

2.3.2 Equation of motion

Assumptions have to be made in order to derive the equations of motion of the TLCD. Most importantly, we assume that the liquid is incompressible and moves uniformly across a streamline. The viscous and turbulent losses are combined into a single headloss parameter δ_L dependent on the TLCD configuration. For a TLCD without orifice, the turbulent losses caused by liquid moving between horizontal and inclined/vertical sections are most dominant [18].

Using Lagrange one can derive the equation of motion for a TLCD illustrated in Figure 2.4, including the possibility of sealed gas compartments. Fluid properties and displacements are generally denoted by subscript f. An U-shaped container with $\beta = 90°$ is assumed, which simplifies the equations for the reaction forces and parameters.

$$\ddot{u}_f + \delta_L |\dot{u}_f| \dot{u}_f + \frac{\Delta p}{\rho_f L_{eff}} + \omega_A^2 u_f = -\kappa \ddot{w} \tag{2.5}$$

Reaction forces The conservation of momentum is used to derive the reaction forces [5] listed in Equation 2.6 to Equation 2.7. Here, m_f denotes the fluid mass. The vertical force in Equation 2.7 excludes gravitational forces.

$$f_x = -m_f \left(\ddot{w} + \bar{\kappa}\ddot{u}\right) \tag{2.6}$$

$$f_z = 0 \tag{2.7}$$

Parameters The main parameters of the TLCD are listed in Equation 2.8 - 2.12. The effective length, L_{eff}, can be viewed as the equivalent energy length of the fluid. The equivalent mass length, L_{em}, is related to the fluid mass m_f through the vertical TLCD area A_H. Both lengths, are influenced by the area ratio $\alpha = A_H/A_B$. The headloss coefficient δ_L is obtained experimentally. Though, Equation 2.11 provides insight in the geometric scaling of the headloss for constant fluid resistance λ. Finally, geometric factors influencing the reaction forces are listed in Equation 2.12.

$$L_{eff} = 2H + \alpha B \tag{2.8}$$

$$L_{em} = 2H + \alpha^{-1} B \tag{2.9}$$

$$\omega_A = \sqrt{\frac{2g}{L_{eff}}} \tag{2.10}$$

$$\delta_L = \frac{\lambda}{2L_{eff}} \tag{2.11}$$

$$\kappa = \frac{B}{L_{eff}} \ , \ \bar{\kappa} = \frac{B}{L_{em}} \tag{2.12}$$

Gas pressure The pressure difference for a sealed TLCD, or Tuned Liquid Column Gas Damper (TLCGD), can be approximated by Equation 2.13. Where, ϵ is the inverse linear gas-spring stiffness. The gas compartments are studied in more detail in Section 3.3.

$$\Delta p = p_2 - p_1 = \epsilon^{-1} u_f \tag{2.13}$$

2.3.3 Comparison with the linear TMD

The main differences between the TLCD and the TMD described in Section 2.2 are: its non-linear damping and the introduction of geometry factors in the coupling forces. First, the efficiencies of both dampers are compared based on the geometry factors. Afterwards, the non-linear damping characteristics are analysed further.

Geometry

An analogy between a linearised TLCD and a TMD can be made that shows the influence of the geometric parameters listed in Equation 2.12. The most important result of this transformation is the introduction of the active mass m_{act} and the passive mass m_{pas} [5] (not to be confused with the classification in Section 2.1). For a larger value of $\kappa\bar{\kappa}$, the equivalent TMD mass ratio of the TLCD decreases, reducing its effectiveness directly [19]. The active mass can be maximized by increasing the horizontal mass of the TLCD through the width B and the ratio α. For OWT applications this can be relatively difficult compared to onshore civil structures, as the low natural frequency and space restrictions require a high value of α. For the remainder of this research whenever the mass ratio is quantified it is expressed as in Equation 2.16. Though in most equations, the normal modal mass ratio μ is used.

$$m_{act} = \kappa\bar{\kappa}m_f \tag{2.14}$$

$$m_{pas} = m_f - m_{act} \tag{2.15}$$

$$\mu_{Eq,TMD} = \frac{\kappa\bar{\kappa}\mu}{1+\mu(1-\kappa\bar{\kappa})} \tag{2.16}$$

Damping

In reality the TLCD damping is not linear as was assumed in the previous paragraph. Though, its non-linearity can be linearised with reasonable accuracy for a stationary excitation. The derivation of Equation 2.17 can be found in Appendix A.1. In Equation 2.17, U_{f0} expresses the observed or expected liquid displacement amplitude of the non-linear TLCD response. In Equation 2.18, $\sigma_{\dot{u}_f}$ is the liquid velocity standard deviation of the non-linear TLCD response.

1. Using harmonic linearisation (e.g. equivalent dissipated energy in one cycle or harmonic balancing) [5] [18]:

$$\zeta_A = \frac{4}{3\pi}\frac{\omega}{\omega_A}U_{f0}\delta_L \text{ with } U_{f0} = max(u_f) \text{ for irregular excitation} \tag{2.17}$$

2. Using statistical linearisation (assuming Gaussian random white-noise excitation) [17] :

$$\zeta_A = \frac{\delta_L}{\omega_A}\sqrt{\frac{2}{\pi}}\sigma_{\dot{u}_f} \tag{2.18}$$

The design of an optimal TLCD is a cumbersome process due to its non-linear damping, as the optimal headloss coefficient is inversely proportional to the excitation intensity [18]. This results in sub-optimal performance of the damper at excitations deviating from its 'design' excitation.

To illustrate this, approximate effectiveness graphs can be very useful. Moreover, these graphs provide insight in the effect of internal TLCD properties on the host in general. In Figure 2.5, such a graph is given. Here, the structural damping of the host is 4% LogDec and the equivalent mass ratio is 1.1%, corresponding to one of the case-studies defined later in this research.

Assuming white noise excitation of the host, a frequency domain approximation can be computed for the effectiveness of the TLCD using Equation 2.3. The effectiveness depends on the internal linear damping indicated on the x-axis and the tuning ratio of the TLCD, indicated by different lines.

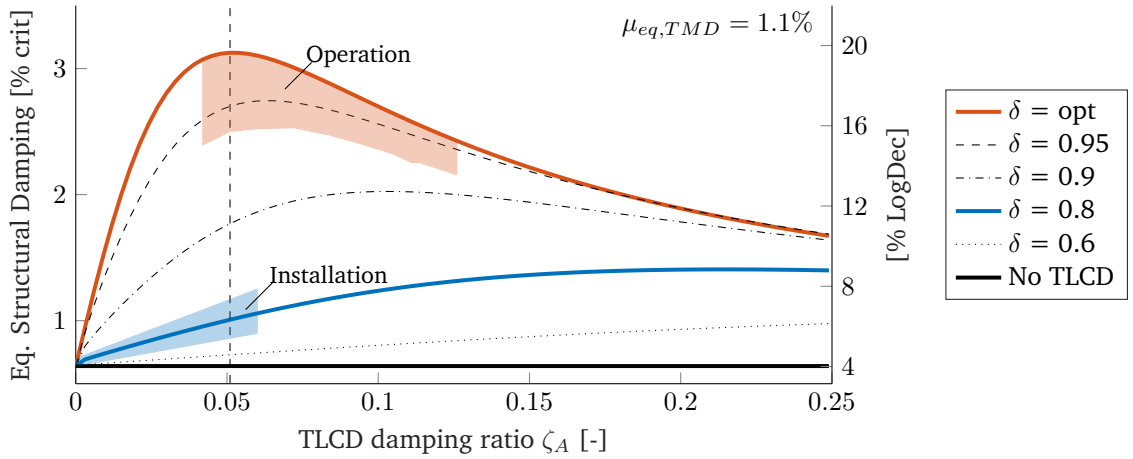

Figure 2.5: Effectiveness TLCD attached to a white noise excited host structure, for variable damping and tuning, including typical operational regions of the OWT.

A typical region of an operational TLCD has been indicated by the orange area. Tuning may vary across OWTs in a single offshore wind farm due to uncertainties and variations of the host natural frequency across the farm. The linearised damping, for a single OWT varies depending on the excitation intensity. A properly designed TLCD, is generally over-damped [2] and have near optimal tuning.

A possible region for a TLCD during installation is indicated by the blue area. The TLCD is off-tuned due to an increase of the structure's natural frequency. The TLCD is under-damped because critical load cases during installation are milder compared to dominant fatigue load cases. Consequently, resulting in a lower linearised damping.

The effect of different OWT phases on the internal properties of the TLCD is discussed and demonstrated further in Chapter 6.

2.4 Period adjustment strategies

To illustrate the narrow-banded effect of the damper further, the effectiveness of an optimally damped TLCD is plotted in Figure 2.6 against the normalized host frequency. Three different passive settings can be obtained for a single TLCD design through sealing of the gas compartments containing air at atmospheric conditions:

- Open TLCD: Both gas compartments of the TLCD are fully open or connected by an interconnecting pipe conveying free flow.
- 1-sided sealed TLCD: A single gas compartment is fully closed while the other compartment is fully open to the surroundings.
- 2-sided sealed TLCD: Both gas compartments are fully closed.

Again, typical operational and installation frequencies have been indicated with orange and blue areas respectively. The host frequency has been normalized by the 'regular' open TLCD.

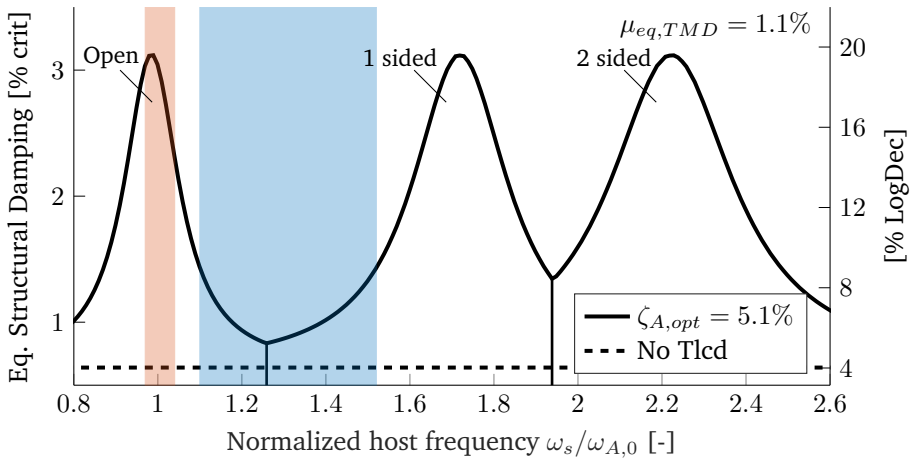

Figure 2.6: Effectiveness optimally damped TLCGD attached to a white noise excited host structure, including operational regions OWT.

Natural frequencies of multiple installation steps lie in the region indicated by blue. In some cases, such low damper effectiveness could be detrimental for the installation workability. For the case study presented at the end of this thesis, a workability decrease up to 50% is observed for the worst-case scenario. Therefore, additional methods are required to adjust the natural period of the damper.

[2] With respect to the TLCD, 'over-damped' refers to damping values larger than optimal. 'Under-damped' conditions refer to damping values smaller than optimal. In this definition, optimal damping is based on the optimally tuned TLCD.

2.4.1 Current methods

Existing and proposed period-adjustment strategies are divided up into three classes based on the location where it is applied. An overview of these methods and their constraints is given in Table 2.1.

Additional devices

The first class of modifications was proposed by Teramura [20] and can be found in Figure 2.7. Additional mechanisms are introduced to control the gas-spring stiffness: the secondary TLCD and the valve/pendulum stiffness. This method is assumed to be too exotic for an offshore application due to the relatively high number of components.

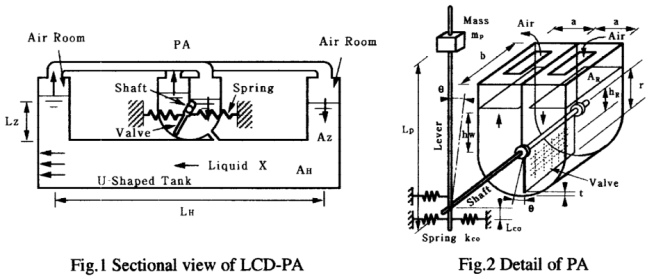

Figure 2.7: Concept for Period-Adjustment Liquid Column Damper (LCD-PA) [20].

Gas compartments

The second class of methods found in literature, is based on further modification of the gas-springs. Two ways to to achieve this are: modification of the compartment's volume and pressurization.

An increase of the gas compartment's volume, effectively decreases the gas-spring stiffness. This has also been shown to work with consecutive gas volumes that can be switched to tune to a multitude of frequencies [21]. The downside is the requirement for a potentially large additional gas volume. The normalized additional gas volume V_{add} required for the design in this research, can be seen in Figure 2.8.

Pre-pressurization of the gas compartments has also been shown to be an effective way to change the gas-spring stiffness [5]. When the sealed frequency needs to be reduced, this requires lower than atmospheric pressures, potentially resulting in large hoop stresses and buckling [22].

An active counterpart of the TLCGD has also been investigated and can be effective for period adjustment [6].

Liquid compartments

Semi-active strategies that utilize control of the fluid's viscosity, through magneto rheological (MR) fluids [23], are considered too expensive and invasive for the operational TLCD.

Various research has been performed on using semi-active control of a variable orifice [17][24]. Since this method only provides limited control over the viscous damping forces in the TLCD, its application for period adjustment is limited.

Most recently a novel semi-active strategy has been proposed to obtain control over the natural frequency and damping of a TLCD [7]. Movable panels were installed in the vertical columns resulting in a variable effective length of the TLCD. The strategy is deemed un-practical due to the potentially complex geometry of a TLCD fitted in an OWT. Moreover, immersed moving components are considered too unreliable for offshore applications.

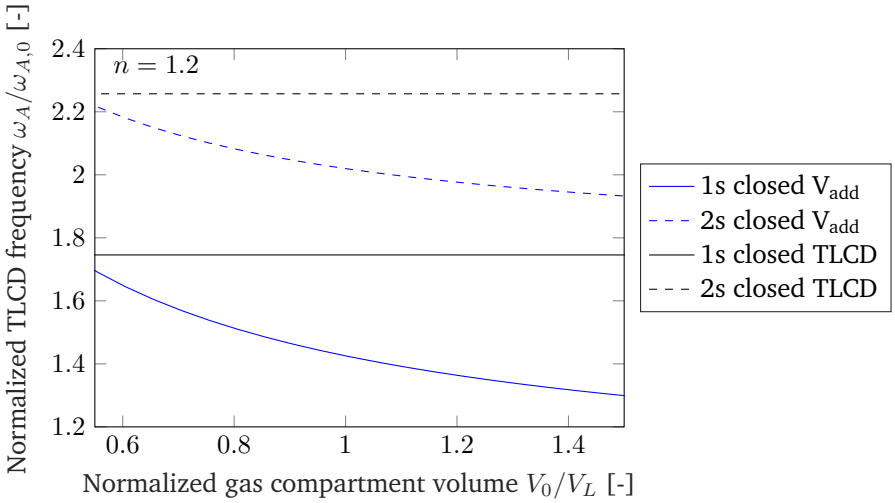

Figure 2.8: Additional gas volume requirement for period adjustment TLCD.

2.4.2 Additional methods

All of the above methods violate at least one of the following restrictions formulated in the problem statement:

- Operational effectiveness TLCD affected
- Geometrical constraint
- Large number of (unreliable) additional components
- High energy requirements

Two additional methods are discussed, both based more or less on existing methods. These variations alleviate one or more of the constraints listed above.

Additional spring-element

A passive method based on a simplification of the LCD-PA proposed by Teramura, would be to use a spring in series with the gas-spring. This could be achieved through some kind of piston or a impermeable flexible membrane in the gas compartments. In this manner, the large number of components of the LCD-PA concept is reduced. A schematic overview is given in Figure 2.9.

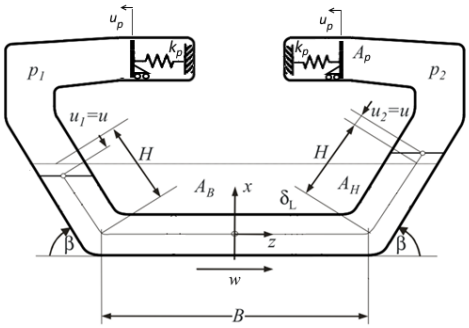

Figure 2.9: Additional spring-element concept for period adjustment TLCD.

Neglecting mass/damping of the piston and assuming a linear spring, Equation 2.19 is obtained for the natural frequency of the TLCD. The factor f_p introduces additional control over the natural frequency compared to a regular sealed TLCD. Here, k_p is the piston spring stiffness, ϵ is the original inverse gas-spring stiffness and β_p^2 is the area ratio between the piston A_P and the vertical compartment A_H. The piston displacement u_p can be found according to Equation 2.20. Note that reduction of the gas spring stiffness requires large values for f_p which may result in large piston displacements. The complete derivation can be found in Appendix A.2.

$$\omega_A^2 = \frac{2g}{L_{eff}} + \frac{1 - f_p}{\epsilon \rho_f L_{eff}} \tag{2.19}$$

$$u_p = f_p \frac{1}{\beta_p^2} u_f \tag{2.20}$$

$$f_p = \frac{1}{1 + \frac{V_0 k_p}{n p_0 A_p^2}} \tag{2.21}$$

For the target TLCD response, large piston deflections/volumes may occur in case of period adjustment to low frequencies. For extreme TLCD responses, expected piston deflections may be even larger, or the spring should contain hardening characteristics. It is deemed un-practical to implement an adjustable spring in the gas compartments including these requirements.

Air-obstruction

Passive or semi-active variations on the active TLCGD may also be able to achieve effectiveness at intermediate frequencies. These variations, that can be achieved through controllable valves in the gas system, do not violate the energy requirement constraint. Furthermore, additional components are kept relatively low and all modifications can be made away from the regular TLCD, in the gas system. Lastly, the vast amount of research performed on TLCGDs including experimental validation make it an attractive option. In the next chapter, and the remainder of this research, this Airflow Obstructed Tuned Liquid Column Damper (AO-TLCD) is studied in greater depth.

Overview

An overview of the strategies mentioned in this section is given in Table 2.1. Here, a minus indicates violation of one of the constraints mentioned in Chapter 1.

Table 2.1: Morphological overview of existing and new TLCD modifications (+ : good , 0 = neutral , - = violation constraint, none = N/A).

Modifications	Effectiveness PA	Op. effectiveness	Geometrical	Components	Energy
LCD-PA	0	0	+	-	
Passive TLCGD	+	+	-	0	
Active TLCGD	+	+	0	-	-
Vertical compartments	-	+	+	-	0
Semi-active damping	-	+	+	0	0
Spring series	+	+	-	+	
AO-TLCD	+	+	+	0	0

Chapter 3

Modelling of Airflow Obstructed TLCDs

In the previous chapter a new TLCD period adjustment strategy was introduced. This chapter elaborates further on this airflow obstruction (AO) strategy, including the derivation of a numerical model and the physics behind it.

Firstly, a more detailed overview of the strategy and its underlying modelling assumptions are given. In Section 3.2 some fundamentals on gas dynamics and compressible flow are briefly discussed. Section 3.3 - 3.5 apply and simplify these fundamental concepts into the pressure and massflow equations. Afterwards, in Section 3.6 these 'ingredients' are used for the derivation of the AO-TLCD model. Additionally, further analyses are performed to increase the understanding of the behaviour of the airflow system.

3.1 Working principle and assumptions AO-TLCD

Compared to the sealed TLCD, gas pressures are released partially through massflow. As a result, the restoring force on the liquid can be influenced and reduced, resulting in modified behaviour and properties of the TLCD. A representation can be found in Figure 3.1. For now, the AO-TLCD is still assumed to be passive. In other words, the properties of the control valve can only be changed on time scales far greater than the damper its natural period.

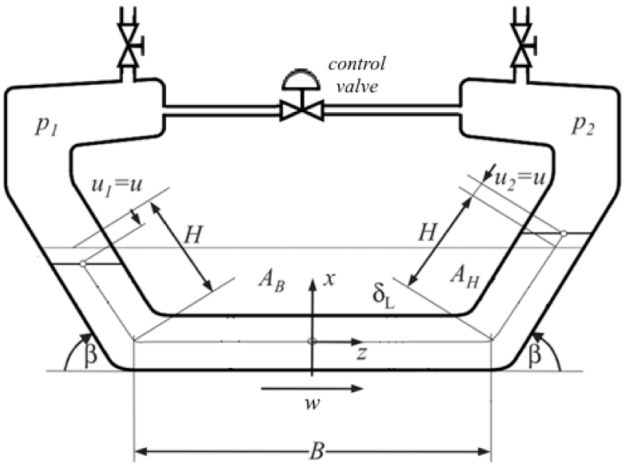

Figure 3.1: Overview of AO-TLCD with control valves.

3.1.1 Assumptions

For a numerical model to be derived, assumptions have to be made regarding the behaviour of the gas. These are the following:

Quasi-steady

Temporal variations in the flow are much smaller than spatial variations, and can be neglected. The flow in-between the two reservoirs 'responds' instantaneous to reservoir conditions. This assumption is explained in greater depth in Section 3.2.2.

Compression

Uniform reservoir conditions are assumed. Furthermore, the compression follows polytropic relations. A more thorough review is given in Section 3.3.

Massflow

For the massflow we assume:

- Subsonic: The flow does not become supersonic. No discontinuities exist in the pressures across the total gas volume.
- Adiabatic flow: There is no net heat exchange; even though heat is generated through viscous losses.
- (In)-compressibility: The flow's properties may change as a function of the flow speed.
- Quasi-1D: The flow can be analysed along one-dimensional streamlines.
- Viscid: Losses occur in the system. Turbulent losses can be approximated through empirical relations.

Some of the flow equations derived in Section 3.4 may also assume isentropic conditions, meaning that the flow is reversible and adiabatic (not viscid). This holds as long as the bulk of the flow is not affected by irreversible effects. In other words: as long as the boundary layer is small.

Other assumptions

The additional volume of the gas system is neglected.

3.2 Brief review of gas dynamics

Since the application of this thesis is outside the field of gas dynamics, a brief review on its relevant fundamentals is given. This review encompasses terminology required to formulate the model of the AO-TLCD. Moreover, it includes the laws of conservation, thermodynamics and the concept of compressible flow. The latter is mainly used as a basis to formulate the compressible massflow equations in Section 3.4. In the end, these compressible forms are only used for the justification of the simplified forms in Section 3.5.

Terminology

For gas properties like pressures, temperatures and densities different reference definitions exist. The difference between these definitions is important for the upcoming sections. Below an example is given for the pressure p at location i.

- p_i Static: These refer to the properties which are 'felt' for a reference frame moving along the gas at local velocity. If a property is referred to without further specification it can be interpreted to be static. These properties are often also referred to as local properties.
- p_{0i} Stagnation: These refer to the properties if the flow would be brought to a rest isentropically. The difference between the static and the stagnation pressure is the dynamic pressure.
- p_{ti} Total: The total properties are generally the same as the stagnation properties. The exception is the total pressure, which also includes the gravitational pressure. For gasses the gravitational forces can be neglected, so the terms total and stagnation can be interchanged.
- p_i^* Sonic: The static properties at sonic speed.

Additionally the terms are illustrated in Equation 3.1 using the Bernoulli equation, which is a derivation of the energy equation. Here, H represents the total head of the system.

$$\underbrace{p_t}_{\text{total}} = H\rho g = \overbrace{\underbrace{p_i}_{\text{static}} + \underbrace{0.5\rho \mathrm{v}^2}_{\text{dynamic}}}^{\text{stagnation}} + z\rho g \tag{3.1}$$

3.2.1 Fundamental equations

Below the conservation laws and the state relation for a caloric perfect gas are given. The conservation laws are given in a steady one-dimensional form. Depending on the equation, additional assumptions are included. An extended review of the fundamental equations, including the general derivative form of the conservation laws, can be found in Appendix A.3. For a thorough review of the conservation laws and thermodynamics the interested reader is referred to Chapter 2 and Chapter 7 of Anderson, respectively [25].

Laws of conservation

A steady 1D integral form of the conservation of mass, i.e. the continuity equation, is given in Equation 3.2. Here, ρ is the static density, v is the velocity and C is a constant.

$$\rho A \mathrm{v} = C \tag{3.2}$$

A steady 1D derivative form of the conservation of momentum is given in Equation 3.3 Here, f_x can be a combination of forces acting in the x-direction (e.g. wall friction).

$$\rho \mathrm{v} \frac{\partial \mathrm{v}}{\partial x} = -\frac{\partial p}{\partial x} + \rho f_x \tag{3.3}$$

An isentropic steady 1D integral form of the conservation of energy is given in Equation 3.4. Here h denotes the enthalpy.

$$h + 0.5\mathrm{v}^2 = C \tag{3.4}$$

Thermodynamics

The equation of state for a perfect gas, or the 'ideal gas law', is given by Equation 3.5 . Here, R is the specific gas constant.

$$p = \rho R T \tag{3.5}$$

3.2.2 Compressible flow

Depending on the dimensions and design of the airflow system, the gas flow may become compressible. A flow is said to be compressible when "changes in fluid momentum cause important variations in the fluid pressure and density" [26]. For low-speed flow of a gas "the actual magnitude of the pressure changes throughout the flow field is small compared with the pressure itself" [25].

Incompressible flow obeys purely mechanical laws and does not require thermodynamic considerations, while compressible flow is dependent on thermodynamics. The relation for incompressibility can be derived from the continuity equation in its steady derivative form and is given by Equation 3.6.

$$\bigtriangledown (\rho \mathbf{v}) = 0 \rightarrow \mathrm{v}\frac{\partial \rho}{\partial x} \ll \rho \frac{\partial \mathrm{v}}{\partial x} \tag{3.6}$$

Classification compressible flow regimes

Below the classification of compressible flow regimes is listed. Here, M is the Mach number. Depending on the design, the AO-TLCD is either in the incompressible or in the sub-sonic region.

- Incompressible flow (M<0.3): Property variations due to momentum can be neglected.
- Subsonic flow (0.3<M<1): The flow must be assumed compressible.
- Transonic flow (0.8<M<1.2): Shock waves may appear and lead to rapid increase of losses. This type of flow can be hard to analyse.
- Supersonic flow (1<M<3): Shock waves are generally present.

Speed of sound

The speed of sound c, or wave speed, can be derived by analysing the flow properties across a pressure wave. By combining the continuity equation (neglecting higher order terms) with the momentum equation (neglecting viscous stresses and assuming steady flow) and using isentropic relations, Equation 3.7 is obtained. Here, γ is the isentropic constant which is equal to 1.4 for air around atmospheric conditions.

$$c = \sqrt{\gamma R T} \tag{3.7}$$

For a caloric perfect gas, the local speed of sound only depends on the local temperature.

$$c = c_0 \left(\frac{T}{T_0}\right)^{0.5} \tag{3.8}$$

The local Mach number is defined as:

$$M = \frac{\mathrm{v}}{c} \tag{3.9}$$

Quasi-steady

In essence, quasi-steady means that the time is 'frozen' at every instant and the problem is solved as if it were steady. In reality compression and flow does not occur instantaneous.

Instead, a pressure wave is formed that moves across the gas at the local wave speed. Therefore, two separate locations in a gas can only 'communicate' with each other with the speed of sound. For our application, the time for a pressure wave to move in-between the two gas compartments is far smaller than the natural period of the TLCD ($L_{duct} \cdot c^{-1} << 0.01 T_n$). Therefore, quasi-steady conditions can be assumed.

Isentropic compressible flow

As described at the start of this chapter, gas properties may vary due to a change in the fluid's momentum. Compared to their stagnation properties, local properties decrease as a function of the Mach number. Assuming isentropic conditions these relations can be derived. They can be found in Appendix A.3.

3.3 Compression

Compression of the gas is also assumed to occur quasi-steady (e.g. the compartments have uniform properties). During compression, temperature changes as a result of the work performed on the gas. The amount of heat exchange with the environment, as a result of the temperature changes, influences the actual pressures. For an ideal gas compression can be described by the polytropic process, which assumes heat exchange to be proportional to the compressive work. Therefore, it lies in-between isentropic compression (very fast and thus no heat exchange) and isothermal compression (very slow and thus maximum heat exchange).

Polytropic index

The polytropic assumption for passive TLCGDs, has been validated experimentally. In small-scale experiments a polytropic index of 1.2 was obtained [22]. Though, the polytropic index is influenced by frequency (compressive speed), TLCD geometry (scaling laws), TLCD material and other properties. As mentioned by Hochrainer: "it depends on each TLCGD design, the polytropic index $1 \leq$ n ≤ 1.4 is determined experimentally in practical applications" [6]

Polytropic relations

The polytropic relation along a streamline is given by Equation 3.10. In Equation 3.11 the integral form of this relation is given. Here, $h_{eff} = V_0/A_H$ is the effective height of the gas compartment depending on the initial volume V_0. The total mass that has been displaced is indicated by Δm. In general the reservoir conditions in both compartments are fully determined with only two known variables (e.g.: p_{01}, u_f).

$$\text{General form: } \frac{p}{\rho^n} = C \tag{3.10}$$

$$\text{Integral form: } p_{0i} = p_0 \left(\frac{(1 - \Delta m/m_0)}{(1 - u_f/h_{eff})} \right)^n \tag{3.11}$$

The differential form, given by Equation 3.12, is found by combining the time derivative of the massflow and the density. Here, $V = V_0 - A_h u_f$ is the instantaneous volume of the gas compartment. Similarly, m and h are the instantaneous mass and height.

$$\dot{m} = \frac{d(\rho V)}{dt} = V\dot{\rho} + \rho\dot{V} = m\left(\frac{\dot{u}_f}{h} + \frac{\dot{\rho}}{\rho}\right)$$

$$\dot{\rho} = \frac{d\rho}{dt} = \frac{d}{dt}\left(\rho_0 \left(\frac{p}{p_0}\right)^{n^{-1}}\right) = \frac{\rho\dot{p}}{np}$$

$$\dot{p_i} = np_i\left(\frac{\dot{u}_f}{h_i} - \frac{\dot{m}}{m_i}\right) \tag{3.12}$$

3.4 Massflow

This section focusses on massflow in-between two gas reservoirs with differing reservoir conditions. First, the working principle behind the massflow is explained. Afterwards, derivations of incompressible and compressible flow equations are presented. Inviscid flow, i.e. reversible flow, is not covered in this research, as it does not represent realistic massflow. Especially not in case when controllable valves are used.

3.4.1 Working principle

Massflow occurs when upstream reservoir pressures differ from downstream conditions by Δp. For the momentum to be at balance, the static exit pressure p_e must equal the downstream reservoir pressure p_{02}. In other words, Δp can be balanced by two mechanisms: by viscid losses across the flow or by an increase in dynamic pressure.

Equation 3.13 shows the effect of these two mechanisms. Here, Δp describes the pressure difference between the two gas reservoirs with index 1 and 2. The pressure losses p_{loss} occur due to flow between upstream reservoir 1 and exit e. The increase of dynamic pressure influences the ratio between the local and the stagnation pressures at the exit e.

$$\Delta p = p_{01} - (p_{01} - p_{loss}) \left(\frac{p_e}{p_{0e}} \right) \tag{3.13}$$

3.4.2 Incompressible flow

So-called 'local losses' are often the most dominant dissipative mechanism in an incompressible flow. These losses result from complex flow patterns due to geometry changes (e.g. sudden exits/entrances, bends and valves). For some flow elements, these losses can be approximated through empirical correlations (instead of CFD simulations). Average design values for these loss factors can be found in numerous engineering handbooks. More specific values can be found in manufacturers brochures. In this research the loss factor definition K is used together with average design values [27]. This results in Equation 3.14. Manufacturers often use factors K_v or C_v. The relation between these definitions and the values used for K, can be found in Appendix A.4.1.

$$p_{loss} = 0.5 \sum K \rho_1 \mathrm{v}_1^2 \tag{3.14}$$

Additionally, friction occurs across the walls. Wall shear stresses are assumed to be correlated by the Darcy friction factor f, which is found in the Moody chart [28]. For the fully turbulent regime this simplifies into a velocity independent loss factor. Here, L and D denote the length and diameter of the duct, respectively.

$$K_{friction} = \frac{\bar{f} L}{D} \tag{3.15}$$

In Equation 3.16, Equation 3.14 is written in terms of massflow. Here $n_{v,j}\beta_j^2$ is the area ratio between the nominal flow area at location j and the reservoir area. Dynamic outlet losses need to be taken into account by either an additional factor K equal to 1 or by an empirical correlation for losses due to a sudden exit (often close to 1).

$$\dot{m} = A_H n_{v,j} \beta_j^2 sgn(\Delta p) \sqrt{\frac{2\rho_1 |\Delta p|}{\sum K_j}} \tag{3.16}$$

3.4.3 Compressible flow

Depending on the flow, effects due to compressibility may not be negligible. Compressible flow equations can result in completely different conditions. Therefore, it is important to define these equations and to compare their results with the incompressible flow equations.

Similar to incompressible flow we can derive analytical expressions for the massflow when assuming a Moody-type pipe friction problem. Specifically one with "large changes in kinetic energy and enthalpy" [27]. Due to compressibility and viscid losses, both the gas' local and stagnation density drop across the flow. As a result, downstream flow velocities increase. Inclusion of these effects in the steady momentum equation yields the Fanno flow equations. Below a brief summary of the results is given. For a more thorough review, the reader is referred to Chapter 9 of White [27].

$$\left(\frac{\bar{f}L}{D}\right)_{i,ref} = \frac{1-M_i^2}{\gamma M_i^2} + \frac{\gamma+1}{2\gamma} ln\left(\frac{(\gamma+1)\,M_i^2}{2+(\gamma-1)\,M_i^2}\right) \tag{3.17}$$

$$\frac{p_i}{p^*} = \frac{1}{M_i}\sqrt{\frac{\gamma+1}{2+(\gamma-1)\,M_i^2}}\,, \qquad \frac{p_2}{p_1} = \frac{p_2}{p^*}\frac{p^*}{p_1} \tag{3.18}$$

$$\left(\frac{\bar{f}L}{D}\right)_{2,ref} = \left(\frac{\bar{f}L}{D}\right)_{1,ref} - \frac{\bar{f}L}{D} \tag{3.19}$$

If the length of the duct is larger than the so-called critical length L^*, exit flow velocities approach sonic conditions. Contrary to nozzles, the flow cannot become supersonic. Further losses require an increase in entropy, which is at its maximum at the sonic point. Consequently, the massflow will start to choke. Further decrease of the back-pressure does not change the massflow. Oblique shock-waves may occur at the exit.

$$if\ L > L^*\ \rightarrow \left(\frac{\bar{f}L}{D}\right)_{1,ref} = \left(\frac{\bar{f}L^*}{D}\right) \tag{3.20}$$

Alternatively, the equations can be rewritten into terms of initial and final properties. In combination with the isentropic compressible flow Equations A.35 - A.37, these can be used for more direct computation of the pressure drop. However, a closed form for the massflow for a given pressure drop does not exist. Hence, interpolation or iteration is required.

$$\frac{p_{02}}{p_{01}} = \frac{M_1}{M_2}\left(\frac{T_2}{T_1}\right)^{\frac{\gamma+1}{2(1-\gamma)}} \tag{3.21}$$

$$\frac{T_2}{T_1} = \frac{1+0.5\,(\gamma-1)\,M_1^2}{1+0.5\,(\gamma-1)\,M_2^2} \tag{3.22}$$

To include local losses, the friction losses in Equation 3.19 can be replaced by the total loss factor K. Although, the range of Mach numbers where this formulation is valid depends on the range for which the empirical factor K has been derived for.

3.5 Modelling simplifications airflow obstruction

In order to enhance computational speed and to analyse the behaviour of the AO-TLCD more thoroughly, further simplifications of the numerical model are required. In this section, the pressure and massflow equations are simplified. Moreover, the range for which these expressions are accurate is investigated.

Pressures

Linear expressions for the pressures can be obtained through the time derivative of the Taylor series expansion of Equation 3.11 or by assuming constant reservoir conditions for Equation 3.12. As liquid displacement and massflow are opposite for both compartments, the pressure difference can be expressed according to Equation 3.23. Here, ϵ is the inverse air spring stiffness given by Equation 3.24. Here, N_c indicates the number of closed compartments.

$$\Delta\dot{p} \approx np_0N_c\left(\frac{\dot{u}}{h_{eff}} - \frac{\dot{m}}{m_0}\right) = \epsilon^{-1}\left(\dot{u} - \frac{\dot{m}}{\rho_0 A_H}\right) \tag{3.23}$$

$$\epsilon = \frac{h_{eff}}{np_0N_c} \tag{3.24}$$

The linear expression for the pressure difference is accurate for a large range of inputs, as is shown in Figure 3.2. Pressure differences are given for constant mass and constant reservoir volume on the left and on the right, respectively. For a 2-sided sealed TLCD, errors due to volume changes are dominant and smaller than 10% for normalized displacements χ smaller than 0.3. For $\chi > 0.3$, the linear expression may still be accurate in case the displaced mass is also large (resulting in low pressures).

In some cases the potential energy of the gas springs may be more important than the magnitude of the pressures. Using the equivalent linearisation method given in Appendix A.1, one can derive a linear pressure relation with the same potential energy as its non-linear counterpart. For χ = 0.3, this equivalent stiffness shows an even better agreement with Equation 3.23.

For a 1-sided sealed TLCD, errors in the pressure magnitude are larger. While, the error in equivalent energy flow over a whole cycle is the same as for 2-sided sealed TLCDs. Therefore, above assumptions may not hold in case a TLCD is intermittently closed 1-sided in an a-symmetric manner during a single cycle.

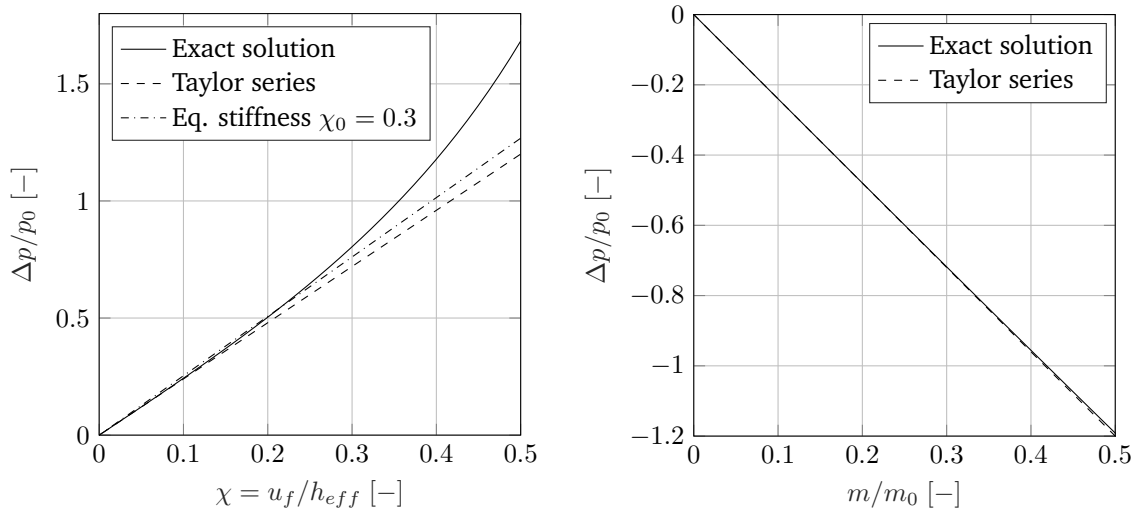

(a) For constant mass

(b) For constant volume

Figure 3.2: Comparison linear pressure and equivalent linear pressure with non-linear form for a two-sided sealed TLCD with n=1.2.

Massflow

The incompressible massflow Equation 3.16 can be simplified further when the reservoir pressures are computed with the linear polytropic relation. Additionally, changes in the upstream density can be neglected, result in Equation 3.25. A flow obstruction parameter K_O is introduced to address multiple flow elements with different nominal diameters. The full derivation can be found in Appendix A.4.3.

$$\dot{m} = \frac{A_H \rho_0}{K_O} sgn(\Delta p) |\Delta p|^{0.5} \tag{3.25}$$

$$K_O = \sqrt{\sum_j \left(\frac{K_j}{n_{v,j}^2 \beta_j^4} \right) \frac{\rho_0}{2}} \tag{3.26}$$

In Figure 3.3, Equation 3.25 is compared with the incompressible and compressible massflow equations derived in Section 3.4. The massflow is given for pressure differences across the two reservoirs. Moreover, the corresponding normalized liquid displacements required for such compression, are indicated. For this, the non-linear polytropic relation was used with zero massflow. As a result the relation between χ and Δp in Figure 3.3b corresponds to Figure 3.2a. Hence, it illustrates the massflow rate from a previously sealed reservoir at the moment of instantaneous opening of the valve.

Errors for the simplified massflow equation can get up to 15% for $\chi < 0.3$, especially for 1-sided under-pressures. Though, the conditions in Figure 3.3 are extremely rare and temporary. These conditions can only occur for strong TLCD responses in combination with very sudden changes in the valve opening. Moreover, for such a release, pressures will decrease quickly to acceptable values (with respect to the error margin).

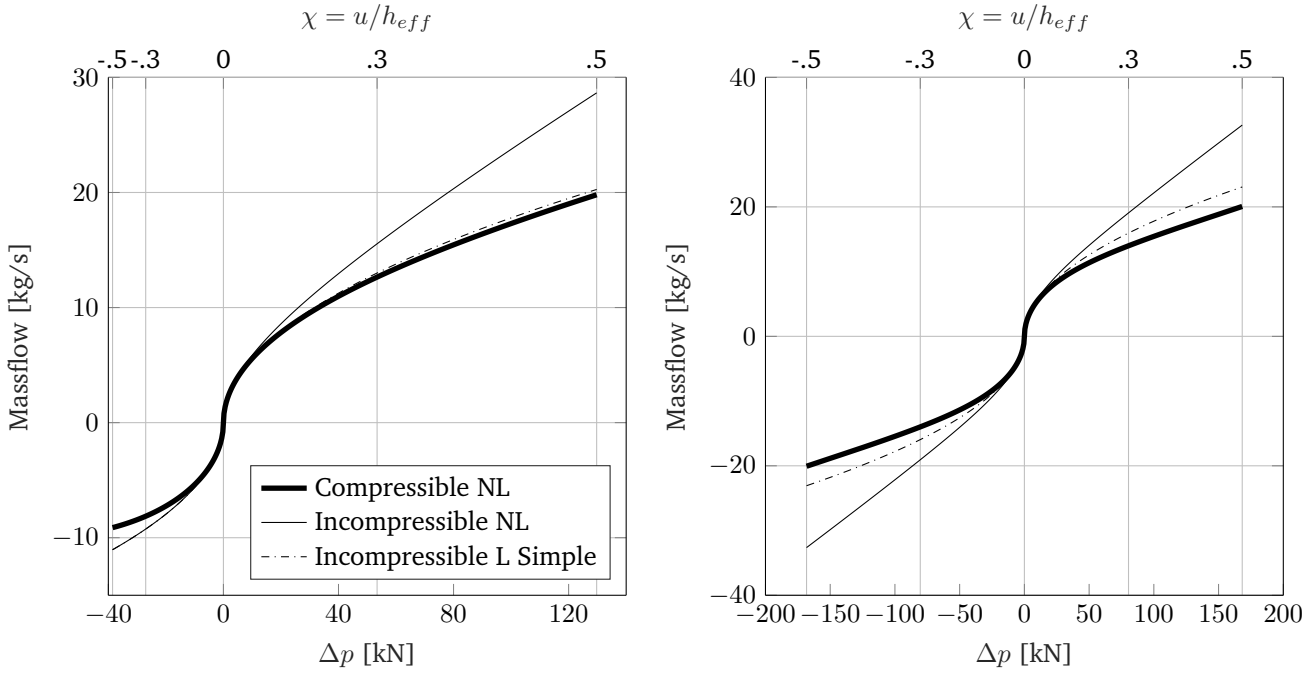

(a) 1-sided sealed

(b) 2-sided sealed

Figure 3.3: Comparison massflow equations for very low obstruction with n=1.2.

Massflow release

To illustrate this, such a release is shown in Figure 3.4. Here the pressure release can be found for a 1-sided sealed TLCD, compressed up to $\Delta p = -27kPa$ ($\chi \approx -0.3$). On the left, valves open instantaneously. On the right, valve dynamics are included using a critically damped second order low-pass filter with a normalized rise time of 8.7% of the TLCD natural period (time to open/close for 95%). The 'non-linear' massflow equations were used in combination with non-linear pressure differential Equation 3.12. While the simplified massflow equation was combined with the linear differential form. As a consequence, both the error in massflow and the error due to decompression are tested.

As expected, errors are negligible due to an improvement of the regime during the release. Additionally, the agreement between the different formulations is improved further due to inclusion of actuator dynamics. During intermediate opening of the valve, obstruction is larger. Pressure differences across the valve can be maintained using lower flow speeds. Therefore, the flow is less compressible, effectively improving the regime illustrated in Figure 3.3

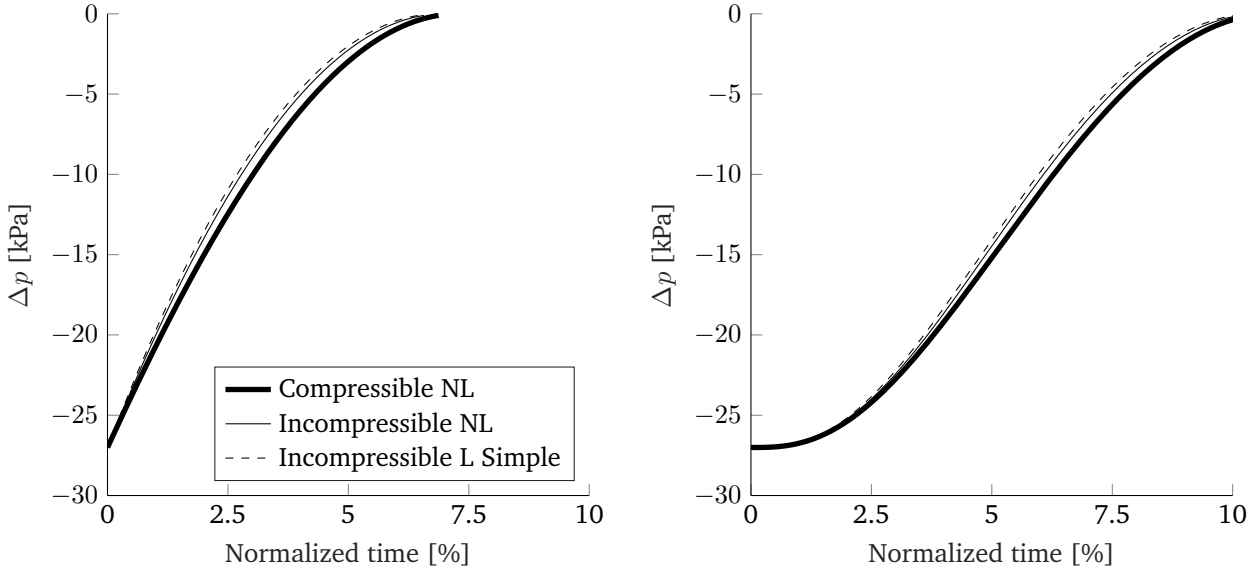

(a) With instantaneous valve

(b) With valve dynamics included

Figure 3.4: Comparison massflow equations for pressure release from previously 1-sided compressed compartment with n=1.2.

3.6 Stand-alone model AO-TLCD

Using the simplified expressions for pressure and massflow as described in Equation 3.23 and Equation 3.25 we arrive at the equations of motion.

$$\ddot{u}_f + \delta_L |\dot{u}_f| \dot{u}_f + \frac{\Delta p}{\rho_w L_{eff}} + \omega_A^2 u_f = -\kappa \ddot{w} \tag{3.27}$$

$$\Delta \dot{p} + \frac{1}{\epsilon} \frac{\dot{m}}{A_H \rho_0} = \frac{1}{\epsilon} \dot{u}_f \tag{3.28}$$

$$\dot{m} = f(\Delta p) = \frac{A_H \rho_0}{K_O} sgn(\Delta p) |\Delta p|^{0.5} \tag{3.29}$$

Equation 3.27 - 3.29 can be rewritten into their first-order differential form. Here the state $\mathbf{x}$ is given by Equation 3.30.

$$\mathbf{x} = \begin{bmatrix} u_f & \Delta p & \dot{u} \end{bmatrix}^T \tag{3.30}$$

$$\dot{\mathbf{x}} = - \begin{bmatrix} 0 & 0 & -1 \\ 0 & 0 & -\frac{1}{\epsilon} \\ \omega_A^2 & \frac{1}{\rho_w L_{eff}} & \delta_L |x_3| \end{bmatrix} \mathbf{x} + \begin{bmatrix} 0 \\ 0 \\ \kappa \ddot{w} \end{bmatrix} + \begin{bmatrix} 0 \\ -f\left(\Delta p\right) \\ 0 \end{bmatrix} \tag{3.31}$$

Low obstruction

In line with one of the constraints, the operational effectiveness of the TLCD must remain unaffected by the proposed modification. Moreover, we must find a way to size the air system accordingly. For this, the effect of the fully open airflow system on the TLCD can be approximated.

For these conditions we assume the pressure difference across the reservoirs to be negligible. As a consequence, we may assume the gas flows freely and in phase with the liquid velocities. Contradictory, it is still assumed losses occur due to this flow. Since they are in phase with liquid velocities, these losses result in additional internal damping of the TLCD. This effect has also been observed by Hochrainer in experiments with fully open TLCGDs [6].

Assuming a linear response, we can derive Equation 3.32 for the additional headloss $\Delta\delta_L$ introduced by the airflow system. The full derivation can be found in Appendix A.1.3.

$$\Delta\delta_L = \frac{K_O^2}{\rho_W L_{eff}} \tag{3.32}$$

Linear pressure drop valves

In case the pressure drop over the valves is assumed linear with respect to massflow, differential Equation 3.28 can be solved to gain more insight in the effect and dependencies of the air system. In the frequency domain, the linear form of Equation 3.29 results in the complex amplitude of the pressures. Relations for additional damping and stiffness can be obtained and the air-system DoF can be eliminated.

The results show that for passive (linear) airflow obstruction the additional damping and stiffness are related [29][30]. As a consequence, they cannot be modified independently without violating constraints.

These valves exist in the forms of permeable membranes (commercially available carpets) and honeycomb filters.

Chapter 4

Validation and dynamic behaviour passive AO-TLCD model

The purpose of this chapter is two fold: validation of the proposed AO-TLCD model and analysis of the passive airflow obstructed behaviour. These two purposes are closely related because the validation requires interpretation of the AO-TLCD's behaviour.

Validation is performed using small-scale experimental data. First, this experimental set-up and its limitations are discussed in Section 4.1. Afterwards, results are given and analysed. Section 4.2 treats the validation of the numerical model. Section 4.3 shows a more in-depth analysis of the AO-TLCD's behaviour. At the end of this chapter, in Section 4.5, the results for part I of this research are summarized and discussed. Furthermore, some additional observations and recommendations are made, including the reason for part II of this research: semi-active damper modifications.

4.1 Experimental set-up

The main goal of experimental validation is to check assumptions regarding the massflow and its effects on the gas pressures. The validation regarding compression is of less importance, as polytropic compression of TLCGDs has already been validated in experimental studies [22]. Assumptions regarding compressible flow could not be checked with the experimental data because flow-speeds were low due to its small-scale set-up.

4.1.1 Set-up

The small-scale set-up can be found in Figure 4.1 and 4.2. A sine-sweep was performed on multiple air-system set-ups, which can be found in Table 4.1. The steady-state response of the damper was obtained using ultrasonic displacement sensors and pressure sensors. Liquid displacements were measured on both sides.

Table 4.1: Air-system set-ups used for verification.

#	Set-up	nClose	Obstruction	Comment
1	Open	0	No	Only numerical
2	1sided-closed	1	∞	Only numerical
3	2 valves	1	Medium	
4	4 valves	1	Low	
5	6 valves	1	Low	
6	Interconnecting pipe	2	Very low	Used for calibration

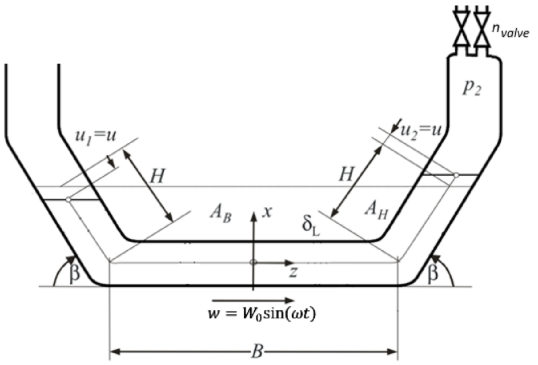

Figure 4.1: Diagram experimental set-up.

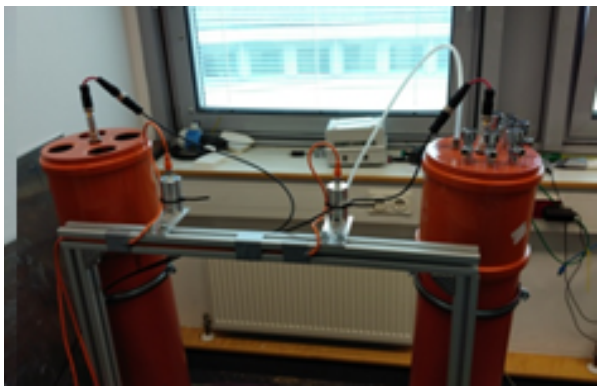

Figure 4.2: Actual experimental set-up.

4.1.2 Calibration numerical model

Some damper and flow parameters require calibration to ensure good comparison between the numerical model with the experimental data. This mainly includes geometric factors, the headloss and the valve loss factors. It was found that the losses introduced by the interconnecting pipe of set-up number 6 were significant. As a result, the headloss coefficient could not be calibrated. Instead it was assumed to be 0.5, which is a conservative estimation based on theoretical loss factors [27]. An overview of the calibration is given in Table 4.2. More detailed information can be found in Appendix A.5.

Table 4.2: Calibrated parameters for numerical model obtained with experimental data.

Parameter	Value	Unit	Deterimined from	Comment
κ	0.46	$[-]$	High frequency response	
K_{valve}	7	$[-]$	max(Δp), max($\dot{u}_f$)	
δ_L	0.5	$[m^{-1}]$	Loss factors [27]	Rough estimation

4.1.3 Limitations experimental data

The major limitation of the available experimental data is disturbance of the ultrasonic liquid displacement sensors. In general ultrasonic measurements of the liquid displacements were not smooth as can be seen in Figure A.4. This was mainly observed at high frequencies due to increased sloshing and liquid velocities.

Visual observations verified a non-smooth liquid surface. Splashing liquid droplets are most likely the main cause of these disturbances. Measurement of the distance to these droplets causes an overestimation of the liquid displacement by the ultrasonic sensors. Furthermore, this may have affected the shape of the measured signal, resulting in potential phase-shifts. Both may have had an effect on the calibration of the parameters and the comparison of the steady-state response.

4.2 Verification and validation of the AO-TLCD model

In this section the implementation of the AO-TLCD model and its accuracy is verified and validated.

4.2.1 Comparison frequency- and time domain

First, the implementation is checked using the numerical model alone. The steady-state results of the non-linear model can be compared to the (iterative) frequency domain solution. Furthermore, the natural frequencies of the TLCD can be checked.

In Figure 4.3 the steady-state response of the liquid is displayed for the 'open' and '1-sided closed' set-up. Furthermore, the airflow system was included for negligible obstruction and for very large obstruction. Both the dynamic amplification and phase lag relate the liquid displacement to the shaker table displacements.

From these results it can be concluded that the model has been implemented correctly because the same steady-state response is observed for the linear and non-linear solution. Furthermore, the very low and very high obstructed AO-TLCD approximately corresponds to the "open" and "1-sided closed" set-up respectively.

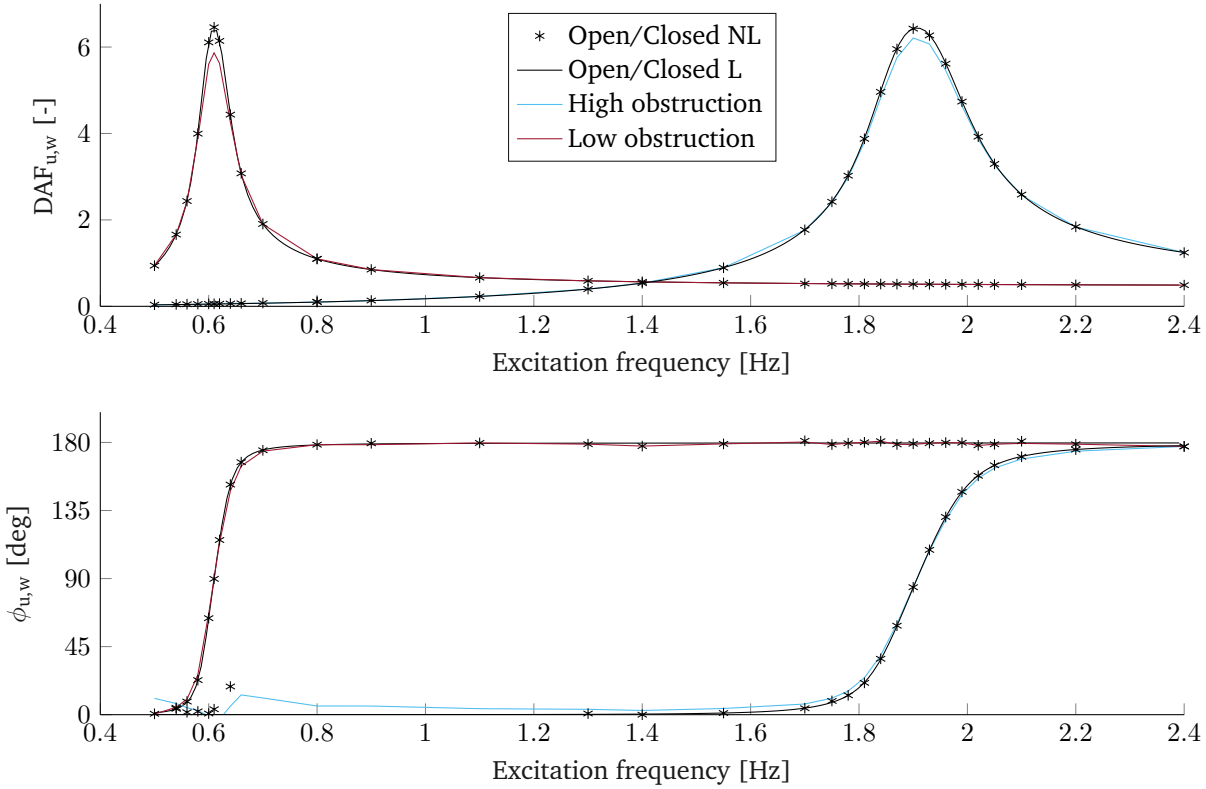

Figure 4.3: Numerical steady state response comparison of the liquid displacements for open/sealed TLCD and very low-/high obstructed AO-TLCD.

4.2.2 Steady-state response liquid

The airflow obstruction still requires validation. Errors in the AO modelling and coupling can potentially have a large influence on the liquid response. Hence, the steady-state response of the liquid is compared first in Figure 4.4 for the cases found in Table 4.1. Numerical results were obtained using the simplified AO-TLCD equations with the parameters listed in Section 4.1.2. Experimental results are indicated by dashed lines.

Both qualitatively as quantitatively, a good agreement is found for the dynamic amplification of the liquid displacements. These specific set-ups predominantly introduce additional damping in the TLCD. For the '2 valves' set-up some resonance occurs at high frequencies. The steady-state response was observed to be very sensitive to changing obstruction parameters. Therefore, errors in the calibration and in the measurements may cause deviations.

For a 2 DoF system, we expect a phase-lag transition between 0 and 180 degrees around the natural frequency. High internal damping results in smoother transitions. The experimental results deviate somewhat from this expectation. A phase-shift is observed at the natural frequency. As this phase-shift increases for higher frequencies, it is concluded that it is a result of distorted liquid displacement sensors mentioned in Section 4.1.2.

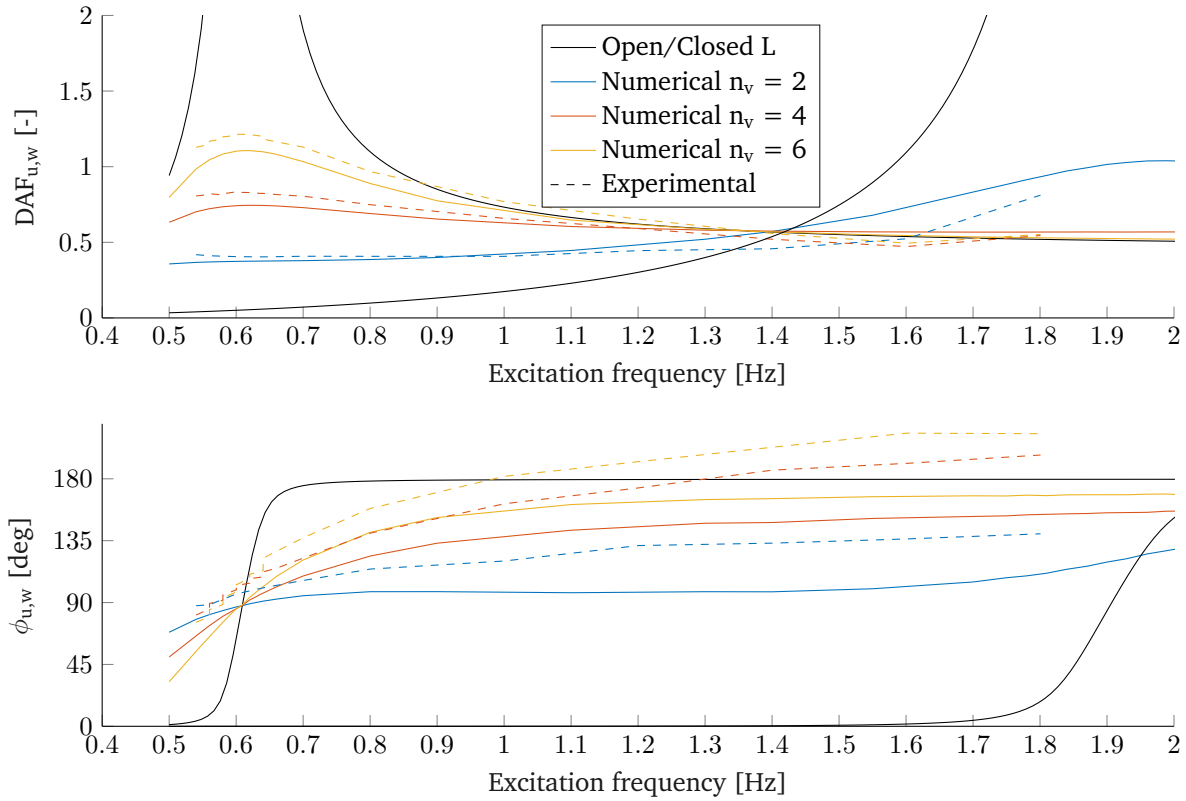

Figure 4.4: Numerical and experimental steady state response of the liquid displacements for variable number of open valves.

4.2.3 Steady-state response pressures

For additional validation, the steady-state response of the pressures is compared. Moreover, it is used to explain the physical behaviour behind the observed damped response in Figure 4.4.

In Figure 4.5 the peak pressures and phase-lag between the pressures and liquid displacements are shown. The phase-shift described in the previous section would distort the phase-lag between the pressures and the liquid. Therefore, the experimental pressure's phase is compared to the numerical liquid displacement phase instead.

Qualitatively and somewhat quantitatively, the same behaviour is observed. The sensitivity to AO parameters is also true for the pressures. For example, a lower headloss coefficient and a slightly larger obstruction parameter increases the pressures while maintaining a similar liquid response. The quantitative difference of the phase-lag remains mostly unexplained.

Figure 4.5 gives better insight in the behaviour of the passive AO-TLCD. At low-obstruction and/or low compressive velocities, almost all mass flows through the valves. Pressure magnitudes are small and out-of-phase with the liquid displacements. Effectively, adding (non-linear) damping to the TLCD. For high obstruction and/or high compressive velocities, mass hardly flows through the valves. Pressure magnitudes are larger and move in-phase with the liquid displacements. Effectively adding stiffness to the TLCD.

One can conclude that the airflow system has strong dependencies on the obstruction parameter, the excitation intensity and the excitation frequency. Furthermore, control over the stiffness/damping ratio is most likely very limited, since a phase-lag close to zero can't be obtained without near closed pressure magnitudes.

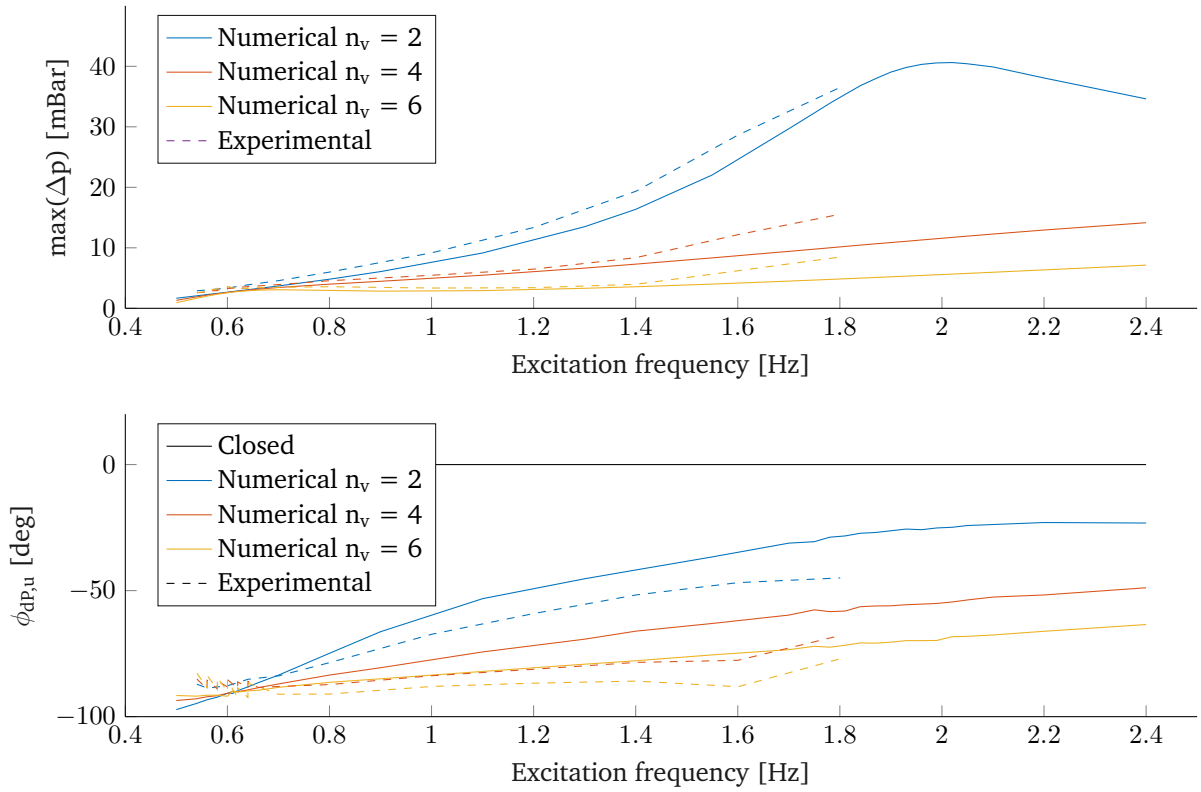

Figure 4.5: Numerical and experimental steady state response of the pressure difference for variable number of open valves.

4.3 Additional analysis

In this section some additional analyses are given to provide more insight in the behaviour of the passive AO-TLCD. For this, only numerical results are used.

4.3.1 Equivalent parameters AO-TLCD

To quantify the effect of the air-system, the equivalent parameters are shown in Figure 4.6. In order to show a more favourable configuration in terms of period adjustment, additionally a set-up with $n_{valve} = 0.5$ is shown. Obviously, half a valve is not realistic. However, an equivalent K_O can be obtained by varying the area or loss factor of the valve.

A clear relation can be seen between additional damping and stiffness, as is expected from the pressure phase-lag. Resonance was not observed at intermediate frequencies in the steady-state response, due to highly dissipative nature of the air-system. As a result of the damped response, the passive AO-TLCD is not able to provide a significant reaction force to the host system.

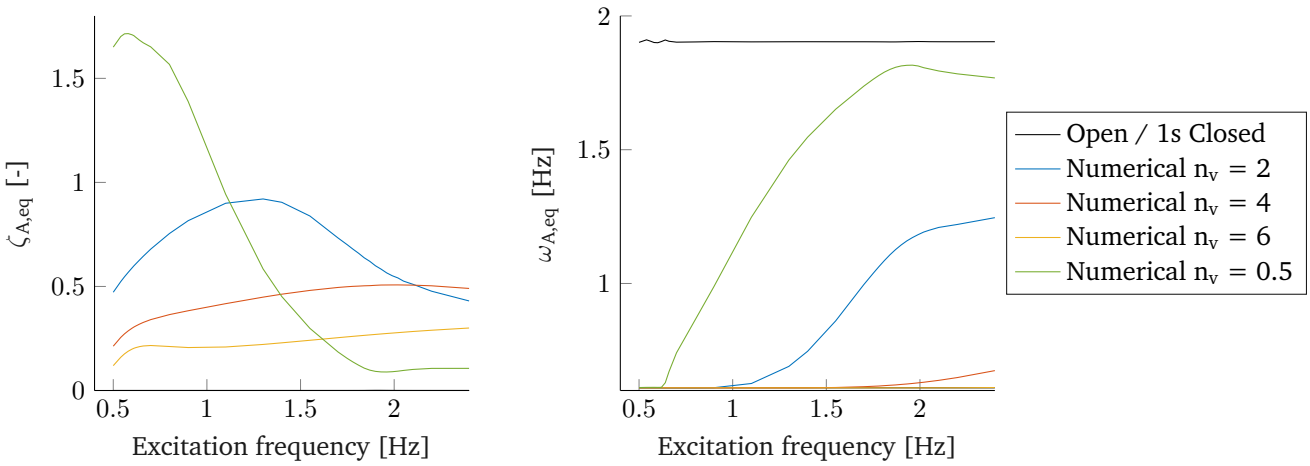

Figure 4.6: Numerical results for equivalent parameters of the AO-TLCD with variable number of open valves.

4.3.2 Dissipative mechanism airflow obstruction

The dissipative nature of the AO-TLCD can be explained by the viscous losses in the air-system. Heat is generated through energy dissipation, which radiates outwards and into the liquid. In order to verify that the viscous losses account for the damping observed in the AO-TLCD, energy is compared in Figure 4.7. Here the average work performed on the liquid by the pressures is indicated by a solid line. The mean viscous dissipation in the air-system is indicated by markers.

The produced heat may affect the polytropic pressure relation, as increased temperature of the gas can affect the pressures. Though, from the validation in Section 4.2 we can conclude that these effects are negligible.

4.3.3 Flow regime

Both the pressures and massflow are within their simplified regime. The flow speeds were computed to be far below the sub-sonic region, with $M < 0.05$ for all simulations. Furthermore, the regime was checked using graphs as in Figure 3.3.

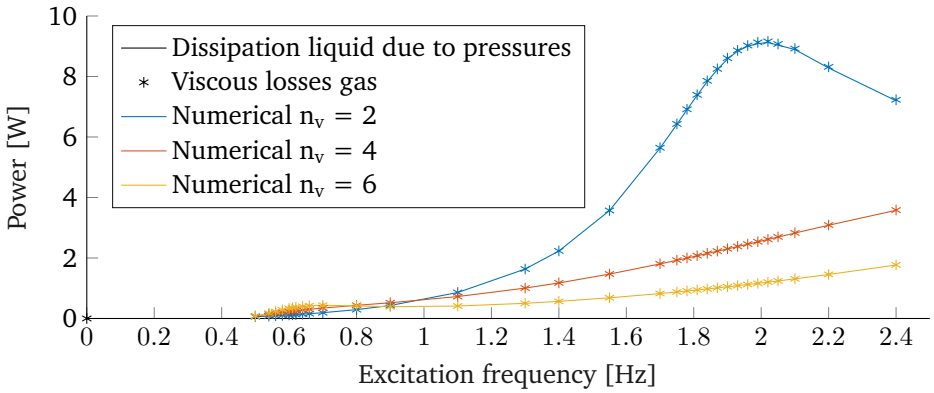

Figure 4.7: Comparison energy dissipation TLCD and gas-system for a variable number of open valves.

4.4 Modification valves

Modifications of the valves to obtain different flow behaviour does change the dissipative nature of the passive AO-TLCD:

- Design for compressible flow conditions, may improve the dissipative nature of the air-system. The increased non-linear relation of the massflow, decreases massflow at peak pressures. This yields a relative increase of the pressures at peak liquid displacement compared to the liquid zero-crossing. This improves the phase-lag of the pressures. However, dependencies to the excitation become significantly larger.
- The other way around, valves with a linear pressure drop with respect to the massflow, decrease dependencies on excitation, but negatively affect the damping/frequency ratio.

4.5 Discussion

In this section the observations and conclusions made in this chapter are summarized briefly. At the end, part I is concluded with the motivation for the second part of this thesis: semi-active control of the AO-TLCD.

Modelling of the airflow obstruction

Even though the response showed to be quite sensitive to the AO parameters, numerical results for the steady state response of the AO-TLCD showed good agreement with experimental data. Hence, we can conclude that the response of a passive AO-TLCD can be accurately predicted using the simplified model for the airflow obstruction.

Dynamical behaviour of the passive AO-TLCD

Passive AO can have a large influence on both the TLCD's stiffness and damping (Figure 4.6) – although, not independently. Passive period adjustment, to frequencies in-between the 'open' and 'closed' configuration, introduces large amount of dissipation into the system. The magnitude of the pressures and its phase-lag with the liquid displacements, are closely related (Figure 4.5). As a result, independent influence of the stiffness and damping, through AO, is limited. These observations, confirm the expectations based on valves with linear pressure drop, at the end of Chapter 3.

The response of the passive AO-TLCD is largely dependent on its properties and on the rate of compression. Hence, it is assumed to be impossible to design a passive AO-TLCD for varying excitation intensities.

Application of the passive AO-TLCD

As a result of the additional dissipation, the AO-TLCD is not effective at supplying a significant reaction force to the host system. Hence, period adjustment using passive air-flow obstruction is not a viable strategy. Though, the AO-TLCD could be used in the design process for adjustment of the headloss. Which in current practice, is designed through the geometry of the TLCD and optional orifices in the liquid.

Further development of the AO-TLCD

For the period adjustment strategy to be effective, more control over the massflow is required. The use of a semi-active control strategy is employed because:

- The dissipative nature of the AO-TLCD needs to be reduced.
- The AO-TLCD should be effective independent of the excitation frequency/intensity. Especially, if one considers time variant excitation of the host structure.

The semi-active AO-TLCD is assumed to be of low complexity compared to current adjustment methods for TLCDs and within the constraints listed in Chapter 1.

Part II

Semi-Active TLCD modification for OWT installation

Chapter 5

Semi-active control

The first part of this research showed that, without some form of control, the AO strategy is ineffective for period adjustment. Although (semi)-active devices are a relatively new concept in the bottom-founded offshore industry, these devices have been successfully deployed in the Civil industry for decades [3]. That is why these existing methods and their working principles are reviewed first. While control theory is treated later in this chapter and limited to the application of simple control laws. Fundamental concepts like observability and controllability are not included, as the main focus of this research is the technical feasibility of the period adjustment strategy, and not the fundamental control theory behind it.

Section 5.1 starts with the general idea behind semi-active control. Afterwards, existing methods for semi-active and active structural control are reviewed. Of which, methods for TLCDs are the main focus. The section concludes with a comparison of these methods with the semi-active control of TLCDs through airflow obstruction. Section 5.2 treats the modelling of semi-active AO-TLCDs. Multiple state-space representations are given of the AO-TLCD model, including a linear approximation. Moreover, the modelling input, realistic actuators and sensors are discussed. The chapter concludes with more theoretical control theory in Section 5.3, where an overview is given on potential control laws.

5.1 Semi-active structural control devices

This section elaborates further on (semi)-active devices, as they were only briefly discussed in Section 2.4. First semi-active control is discussed in general, including its features and limitations. Afterwards, relevant existing semi-active devices are reviewed. In this review, the focus is on the physical implementation and the general effectiveness of these devices.

General properties As previously defined, semi-active control strategies cannot add mechanical energy to the system through its actuators. This dissipative constraint is also referred to as the passivity constraint.

Essentially, one can change passive properties of the system on small time scales; in case this does not increase the overall mechanical energy. Still, large amounts of control can be obtained over the dynamic system. Generally, semi-active systems out-perform their passive counterparts. Moreover, they can be effective for a wide range of time-variant excitations and host system properties.

Advantages Semi-active devices are more capable of reducing peak responses in the transient regime. Multiple modes can be damped by a single device. Making it better suited for vibration reduction of excitations that are not stationary, like wind gusts, seismic activities or slamming waves [17].

The passivity constraint is both its limitation as its feature. On the downside, the freedom of the control input is limited, which may result in low effectiveness compared to an active system.

However, contrary to active systems, the host system cannot be de-stabilized, even if the controller is not implemented properly. To be more concise; semi-active devices "are proven to be unconditionally stable, regardless of the accuracy of the modal state information" [31].

Additionally, significantly less energy is required to operate the device. Often they can operate on battery power [3]. Compared to active devices, small actuators and a small number of sensors are required. In case energy supply or control components fail, a passive system remains.

Limitations Compared to passive systems drawbacks are clear. The requirement for additional components like sensors, actuators, controllers and energy sources increase complexity and reduce the reliability of the complete system.

5.1.1 Viscous Dampers

One type of semi-active structural control devices, outside the dynamic vibration absorbers field, are viscous dampers directly attached to structures/systems. These dampers are generally of the magneto rheological (MR) fluid or electro rheological (ER) fluid kind. An example is displayed in Figure 5.1 and Figure 5.2.

These devices are relevant to our application, because they have the ability to store/release energy from and back to the host. The AO-TLCD possesses similar properties, as energy can be stored in the gas and released back into the system. Some of the research in this field focusses on shaping of force-deformation loops [32] [33], which can be particularly insight-full to the semi-active nature of the AO-TLCD.

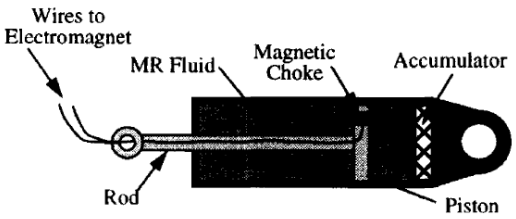

Figure 5.1: MR-fluid damper device [34].

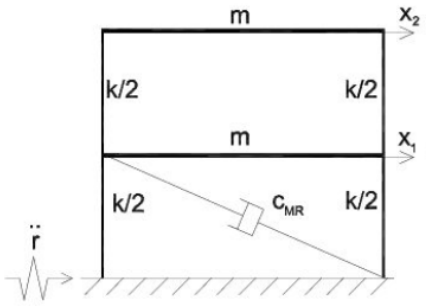

Figure 5.2: MR-fluid damper attached to a multi-story structure [35].

5.1.2 Tuned mass dampers

The actuator implementation of semi-active TMDs (STMDs) is different than for TLCDs. Still, some parallels exist between these devices. Especially, with regard to effectiveness, modelling and control laws.

Suspensions A lot of work has been performed on semi-active applications in the field of (vehicle) suspensions [36]. Depending on the model detail, these systems can be very similar to STMDs. Contrary to the application of semi-active VAs for civil structures, a great deal of control laws have been developed and studied. Especially more complex control laws have been investigated [37].

TMD: controllable component Any TMD generally requires a damper-component, like a hydraulic fluid damper. Depending on the type of TMD, a spring-like component may also be required. As a

result, most (semi)-active methods for TMDs focus on actuation through these components. Two main components exist: variable orifice- and controllable fluid dampers. The former is illustrated in Figure 5.3. For variable orifice dampers, resistance in a hydraulic fluid damper is controlled. For controllable fluid dampers, viscosity is controlled using MR/ER-fluids. These devices are semi-active by nature and give some control over the damping force (within certain bounds).

TMD: variable stiffness A different type of STMD, the semi-active continuously and independently variable stiffness (SAIVS) device, is illustrated in Figure 5.4 [38][39][40]. The SAIVS proposed by Sun [40] is capable of complete continuous stiffness control and limited on/off damping control.

Most notable, is that recently, this STMD has been studied for its application to monopile-foundation type OWTs for multi-hazards [13]. The STMD out-performed its passive counterpart. Moreover, it was consistently effective in reducing the tower response during foundation damage (changing natural frequencies). Lastly, a smaller damper stroke was observed.

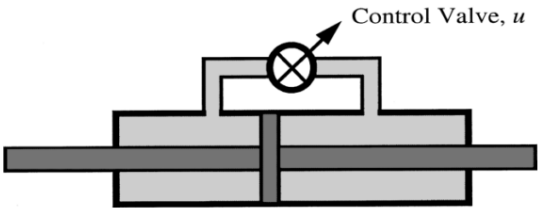

Figure 5.3: Variable orifice damper [3].

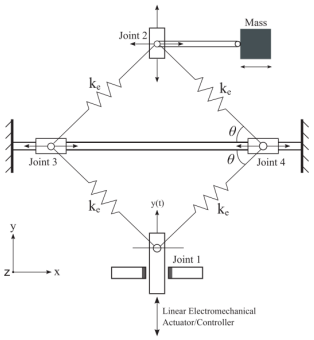

Figure 5.4: Variable stiffness STMD [40].

5.1.3 Tuned Liquid Column Damper

Obviously, (semi)-active modifications of the TLCD are most relevant to our application. Firstly, strategies aimed at controlling the internal damping are listed. These strategies generally aim to increase the effectiveness of a tuned TLCD and to decrease its non-linear characteristics. Thereafter, a semi-active and active strategy capable of period adjustment are given.

Variable damping

Variable damping strategies for TLCDs are very similar to their TMD counterparts. Instead of controlling the hydraulic fluid damper component, the TLCD fluid is controlled directly. Equivalent to the STMD approaches, this happens through either variable orifices or through controllable fluids.

Variable orifice One of the first semi-active TLCDs was introduced by Yalla [24][41]. The damping force of the TLCD is controlled through a controllable valve/orifice in the fluid as is illustrated in Figure 5.5. For white-noise excitation, an improvement of 10-15% over passive systems was observed.

A broad scope of control strategies and assumptions have been tested for this strategy. Most interestingly, bang-bang control (i.e. on/off actuators), performed as well as continuously varying actuators. The use of simple control laws with limited sensor input and included actuator dynamics, still resulted in promising results.

Controllable fluid Ni studied the use of a MR-fluid inside the TLCD. The damping was influenced through semi-active control of the fluid's viscosity [23][42], as in Figure 5.6. The use of a clipped-optimal feedback strategy showed "significant response reduction in terms of displacement, interstory drift and acceleration, in comparison with a passive TLCD."

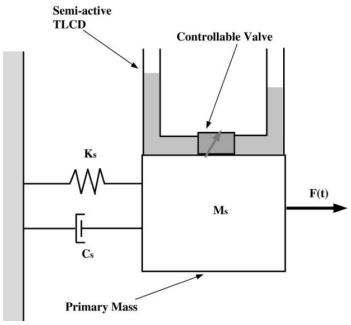

Figure 5.5: Variable orifice TLCD [41].

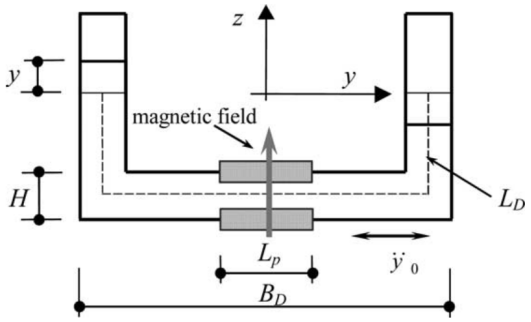

Figure 5.6: MR-TLCD [23].

Variable stiffness

Most recently, Altay investigated and validated a method for period/damping adjustment of TLCDs using movable panels in the vertical columns as can be seen in Figure 5.7 [7]. Though, in this research the controllable range was minimal. Furthermore, its effectiveness for full-scale applications is yet to be determined.

Active devices

As stated in Section 2.4.2, the AO-TLCD can be seen as a variation on the active TLCGD developed by Hochrainer [6][43], which is shown in Figure 5.8. Experiments with the active TLCGD showed that it was able to counteract multiple modes. In other words, effectiveness at largely off-tuned frequencies was obtained. While the numerical studies utilized an optimal feedback control law, experiments were performed using a limited state PD controller (proportional/derivative feedback). Additionally, the effectiveness of the active strategy was validated; while dynamics of the valve, massflow and pressures were mostly unaccounted for. Instead they assumed the pressure input to be proportional to the valve opening (using 'proportional valves').

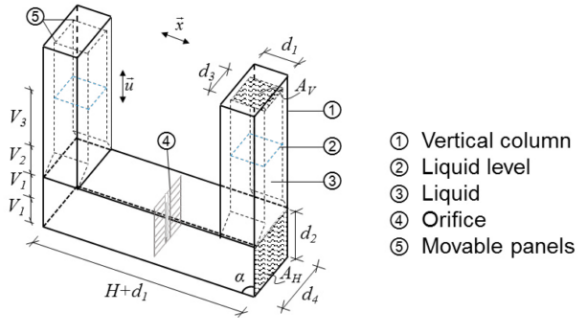

Figure 5.7: Variable column TLCD [7].

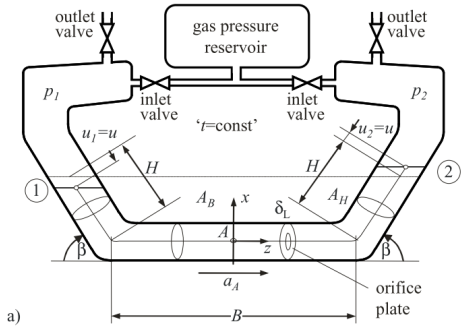

Figure 5.8: Tuned liquid column gas damper [6].

5.1.4 Semi-active airflow obstruction

The first two semi-active strategies for TLCDs focus on controlling the damping inside the TLCD. These methods only provide limited control over the viscous damping forces in the TLCD. This can be an effective approach of increasing the effectiveness of an already tuned passive system. Though, its capabilities for period adjustment are limited.

For the variable column TLCD, tuning has only been obtained for a limited range of frequencies. Moreover, its full-scale implementation for an OWT is assumed to be impractical, as the actual TLCD design will be of a more complex shape. The semi-active AO-TLCD is still considered the most viable option for non-invasive period adjustment for low frequency TLCDs.

Why it should work From the passive AO-TLCD results and from the research presented in this section we can conclude that the semi-active AO-TLCD strategy is promising because:

- Passive AO has a large influence on the internal stiffness and damping of the TLCD.
- In the field of directly applied MR-dampers, semi-active strategies were effective in storing energy from and releasing energy back to the host system. Effectively, providing control over the stiffness of the structure.
- Semi-active strategies consistently outperform their passive counterparts. Numerical investigation of period adjustment of STMDs for OWTs produced positive results [13].
- Period adjustment using the active counter-part of the AO-TLCD has been numerically analysed and experimentally validated [6][43].
- Neglecting dynamics and many non-linearities in the actuator/gas-system, effectiveness of the active TLCGD was maintained [6]. Suggesting that unmodelled dynamics of the AO-TLCD will not likely play a significant role in its effectiveness.
- The use of variable orifice TLCDs, which also includes a controllable valve, has been shown to work for simple control laws, limited sensor output and included actuator dynamics [17].

Limitations The indirect control input through an additional degree of freedom (the pressures), may prove problematic, as the restoring force magnitude can't be increased instantaneously. The non-linearities of the gas-system further complicate potential control laws. Additionally, it may be hard to obtain fully independent control over damping and stiffness.

Lastly, the actuators may be a limiting factor. Potentially large, periodically switched valves have to be employed in an offshore environment. Required closing-times and total number of valve cycles may be unrealistic. This is discussed briefly in Section 7.5, though quantitative analyses of such practical limitations are not included in this research.

5.2 Modelling and control components

With more insight in the implementation, we can now start looking at the model of the AO-TLCD. Semi-active strategies are inherently non-linear. Unfortunately, a large portion of control theory is based on linear systems. In our case, the number of non-linearities largely depends on assumptions regarding the actuator implementation. Therefore, this is the main focus of this section, namely its effects on the model complexity and on the passivity constraint. At the end of this section, the 'gap' between the model and the actual actuators and sensors is treated shortly.

5.2.1 Model semi-active AO-TLCD

Linear control theory is far less complex than its non-linear counterparts. In our case, linearisation of the system can be problematic for the massflow equation, as its derivative is infinite around zero. In order to apply linear theory, additional assumptions are required. Below, different state-space representations and actuator definitions are given. The different actuator definitions are mainly focused on the input bounds enforced by the passivity constraint. The bounding/saturation of a reference input to these bounds is referred to as clipping. The effect of clipping on the dynamical behaviour of the system is explained later in Section 5.3.

Non-linear system Combining Equation 3.31 and Equation 2.6, the state-space of a non-linear AO-TLCD attached to a SDoF host structure is obtained (Equation 5.1 to Equation 5.3). Here, $F(t)$ are the external forces acting on the SDoF host structure. For this NL system, where the inverse obstruction parameter K_{oi} of the valve is controlled (Equation 5.4), the clipping is given by the saturation in Equation 5.5. Here, * indicates the reference unclipped input (a potentially active input). Note that, according to control theory conventions, the input is denoted by u. Therefore, the liquid displacement is always denoted by subscript f.

$$\mathbf{x} = \begin{bmatrix} w & u_f & \Delta p & \dot{w} & \dot{u}_f \end{bmatrix}^T \tag{5.1}$$

$$\dot{\mathbf{x}} = -\mathbf{M}^{-1} \begin{bmatrix} 0 & 0 & 0 & -1 & 0 \\ 0 & 0 & 0 & 0 & -1 \\ 0 & 0 & 0 & 0 & -\frac{1}{\epsilon} \\ \omega_S^2 & 0 & 0 & 2\zeta_s\omega_s & 0 \\ 0 & \omega_A^2 & \frac{1}{\rho_f L_{ee}} & 0 & \delta_L|x_2| \end{bmatrix} \mathbf{x} + \begin{bmatrix} 0 \\ 0 \\ -\frac{f(x_5)}{\epsilon A_H \rho_o} \\ 0 \\ 0 \end{bmatrix} u + \mathbf{M}^{-1} \begin{bmatrix} 0 \\ 0 \\ 0 \\ 0 \\ F(t) \end{bmatrix} \tag{5.2}$$

$$\mathbf{M} = \begin{bmatrix} 1 & 0 & 0 & 0 & 0 \\ 0 & 1 & 0 & 0 & 0 \\ 0 & 0 & 1 & 0 & 0 \\ 0 & 0 & 0 & 1 & \kappa \\ 0 & 0 & 0 & \mu\bar{\kappa} & 1+\mu \end{bmatrix} \tag{5.3}$$

$$u = K_o^{-1} = K_{oi} \tag{5.4}$$

$$u = SAT[K_{oi}^\star] = \begin{cases} 0 & if\ K_{oi}^\star \leq 0 \\ K_{oi}^\star & if\ 0 < K_{oi}^\star < K_{oi,max} \\ K_{oi,max} & if\ K_{oi,\max} \leq K_{oi}^\star \end{cases} \tag{5.5}$$

Linear system Instead of the inverse obstruction, we assume the massflow to be the input. In other words, it is assumed that the massflow can be controlled directly. Together with the linearised TLCD damping this results in the linear system in Equation 5.6. The new clipping law is given by Equation 5.7. In order to follow the reference input, accurate measurements of the pressures are required.

$$u = \dot{m}$$

$$\dot{\mathbf{x}} = -\mathbf{M}^{-1} \begin{bmatrix} 0 & 0 & 0 & -1 & 0 \\ 0 & 0 & 0 & 0 & -1 \\ 0 & 0 & 0 & 0 & -\frac{1}{\epsilon} \\ \omega_S^2 & 0 & 0 & 2\zeta_s\omega_s & 0 \\ 0 & \omega_A^2 & \frac{1}{\rho_f L_{ee}} & 0 & 2\zeta_A\omega_A \end{bmatrix} \mathbf{x} + \begin{bmatrix} 0 \\ 0 \\ -\frac{1}{\epsilon A_H \rho_0} \\ 0 \\ 0 \end{bmatrix} u + \mathbf{M}^{-1} \begin{bmatrix} 0 \\ 0 \\ 0 \\ 0 \\ F(t) \end{bmatrix} \tag{5.6}$$

$$
\begin{aligned}
u = SAT[\dot{m}^\star] &= \begin{cases} 0 & if\ \dot{m}^\star \cdot sgn(\Delta p) \leq 0 \\ \dot{m}^\star & if\ 0 < \dot{m}^\star \cdot sgn(\Delta p) < |\dot{m}_{\max}| \\ \dot{m}_{\max} & if\ |\dot{m}_{\max}| \leq \dot{m}^\star \cdot sgn(\Delta p) \end{cases} \\
\dot{m}_{\max} &= f(\Delta p, K_{oi,max}) \\
K_{oi} &= f(\Delta p, \dot{m})
\end{aligned}
\tag{5.7}
$$

On/off actuators The need for exact pressure measurements can be eliminated by using bang-bang control, i.e. on/off valves, as is indicated in Equation 5.8. Since only two valve settings exist, only the sign of the pressures is required to perform the clipping. In the 'open' configuration, the pressure magnitude may be low. As a result, sensor noise may be problematic for accurate determination of the sign. In practice, the sign could be predicted from other states using an estimator.

$$
SAT[\dot{m}^\star] = \begin{cases} 0 & if\ \dot{m}^\star \cdot sgn(\Delta p) \leq 0 \\ \dot{m}_{\max} & if\ \dot{m}^\star \cdot sgn(\Delta p) > 0 \end{cases} \quad \longrightarrow u = K_{oi} = \begin{cases} 0 & if\ sgn(\dot{m}^\star \cdot \Delta p) \leq 0 \\ K_{oi,max} & if\ sgn(\dot{m}^\star \cdot \Delta p) > 0 \end{cases} \tag{5.8}
$$

The semi-active AO-TLCD is modelled with the non-linear model given by Equation 5.2 and with the clipping law given by Equation 5.8. Though, massflow may still be assumed as the input computed by a control law. The resulting active massflow input, can be clipped and mapped to the obstruction parameter input. Additionally, the complete linear state-space in Equation 5.6 may be used for the control law, e.g. to determine the control input or optimal feedback gain. Nonetheless, the resulting input is applied to the non-linear system. Unmodelled dynamics are most likely negligible, since damping non-linearities are weak.

5.2.2 Actuators

In reality we do not have direct control over the massflow, nor over the valve obstruction. Most likely, valves will be operated hydraulically or magnetically in a continuous manner. The position control of the valve, has its own dynamic properties and response.

Semi-active control, prevents the accumulation of modelling errors in the system. The use of feedback control, provides additional corrective capabilities regarding unmodelled dynamics.

The obstruction parameter has a non-linear relation with respect to the valve position. Still, a linear dependency can be fitted with reasonable accuracy. For bang-bang control non-linearities are weaker, as the open/closed obstruction are known. Only during closing/opening, some modelling errors are made.

Hochrainer obtained good controller performance neglecting many of these dependencies [6]. Therefore, the complete set of dynamic effects and non-linearities, from the actual controllable input to the valve obstruction parameter, is only taken into account through an over-damped low pass filter for the valve obstruction parameter.

5.2.3 Sensors

The main objective of the damper modification is only temporary. Therefore, low complexity is key, ergo the number of sensors should be limited.

Host accelerations and gas pressures can be measured with relative ease. Somewhat more difficult are: accurate measurements of the liquid displacement (e.g. wave gauges or pressure sensors) or accurate measurements of the massflow (e.g. massflow sensors or pilot tubes and temperature sensors).

Proving the feasibility of the semi-active AO-TLCD and investigating the dynamic effects of this implementation is more important than robust controller design. In the research available on semi-active TLCDs, a reduction of sensors or inclusion of sensor noise only led to a minor decrease in effectiveness. Inclusion of incomplete measurement requires the use of observers/estimators, which complicates the control laws and theory. Therefore, the full state is assumed to be available for control.

5.3 Control laws

With the model and input defined, we still require a way of determining the control action. This section treats these potential control laws. To provide more insight in what comprised a good control law, the effects of the semi-active constraint on the damper are discussed in Section 5.3.1. Afterwards, two semi-active control laws are derived. In Section 5.3.5 an overview is given on the control laws used in the remainder of this research.

5.3.1 Passivity constraint

The passivity constraint is typically enforced through the actuator. For example, when controlling the internal damping of a TLCD through its orifice, a damping force opposite to the liquid velocities can't be obtained. For the AO-TLCD this is also true. Independent of the valve setting, gas will never flow upstream. In other words, gas cannot be pumped by simply changing the closing of the valve. The passivity constraint is given, in terms of power $P(t)$, in Equation 5.9.

$$P(t) = -\Delta p \cdot \dot{m}/\rho_0 \leq 0 \tag{5.9}$$

Depending on the control law, this constraint is not always 'build into' the controller and/or the numerical model. Control actions, i.e. inputs, may be requested that violate the passivity constraint (and are often non-physical). Therefore, the input, or the controlled parameter has to be bounded. This bounding is referred to as clipping in the semi-active control literature.

Depending on the control law and the objective, this clipping may result in undesired dissipation. This is specifically true for actuators that can store energy from and release energy back to the system. During a cycle, the control force may not be able to follow the same force-displacement trajectory for the storage and release of energy, respectively. Effectively, 'forming' hysteresis loops. When the main objective is to provide additional stiffness, this may be an undesired side-effect.

Clipping for the AO-TLCD In the case of the AO-TLCD this undesired effect can be analysed from multiple angles. Directly from the actuator perspective or from the force acting on the to-be controlled system. In Figure 5.9 this is illustrated through a force-displacement/velocity diagram for a to be followed reference stiffness. Only forces resulting from the pressures are shown. The pressure-force has been normalized by its fully closed magnitude.

First the constraint is analysed through the TLCD perspective. in Figure 5.9a. From A to B, a desired intermediate reference stiffness can be followed by releasing gas with respect to sealed conditions. At point B, liquid velocities become negative. For the pressures to de-compress with a smaller stiffness (i.e. less quickly than for the fully sealed air-spring), mass has to flow back into the compartment. Since pressures are still positive, this is not possible. At best, the requested input can be clipped to its minimum (zero massflow). The formed hysteresis loop effectively dissipates energy from the TLCD.

From the actuator perspective, illustrated on the right, energy stored in the gas is dissipated through massflow. This is clearly visible through the force-velocity trajectory, which is only present in the dissipative quadrants. The dissipated energy must result in additional damping for the TLCD.

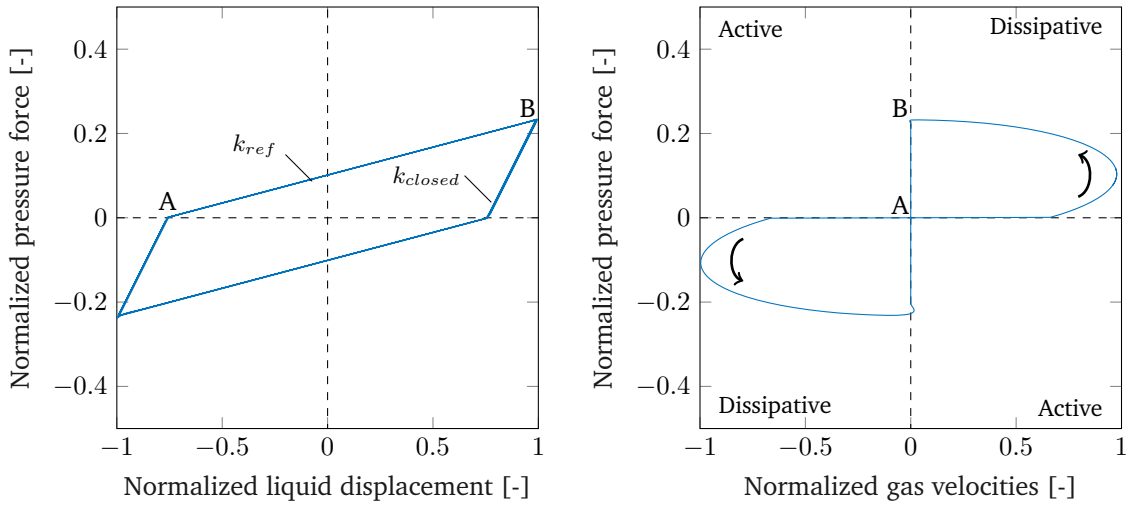

(a) Pressure-force on liquid displacements

(b) Pressure-force on gas velocities

Figure 5.9: Force-displacement/velocity diagrams: Clipping of AO-TLCD input for a followed reference stiffness.

Minimal clipping It may be better to close the valves completely for only a small period of time around the peak displacement. This has been illustrated in Figure 5.10 with force-displacement/velocity trajectories with respect to the liquid. Valves are switched around atmospheric conditions. As a consequence, no massflow occurs at the moment of switching. In other words: no dissipation is introduced through actuation. By selecting the correct closing time, the desired amount of energy can be stored and released to the liquid to achieve the desired equivalent stiffness.

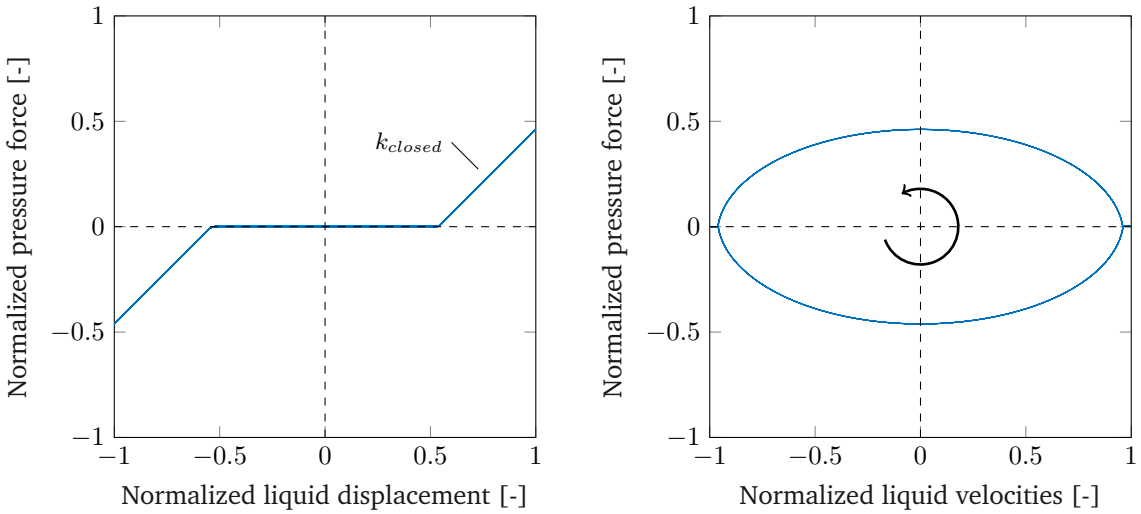

Figure 5.10: Force-displacement/velocity diagram of pressure-force on liquid: minimal clipping of AO-TLCD input.

Goal For the application to OWTs, shaping of the force-displacement loop as illustrated above, is not applicable. Stochastic loads generally require a more general approach. However, the approach gives

insight in the semi-active constraints and its physical implications for the AO-TLCD. In most cases, gas flow has undesirable effects, as it negatively affects the TLCD its reaction force through dissipation.

The rewritten EoM of the host structure, in Equation 5.10, shows that the pressures also have a direct effect on the host system. Therefore, some cases may exist where positively affecting the host vibrations outweighs negative effects on the dynamic behaviour of the TLCD with respect to the host. For additional clarity, this is illustrated in Figure 5.11. Though it is assumed, that in general, a good control law for the AO-TLCD minimizes viscous dissipation by the gas while maximizing its force on the host and TLCD.

$$\ddot{w} + 2\zeta_S\omega_S\dot{w} + \omega_S^2 w \underbrace{-\mu\bar{\kappa}\delta_L|\dot{u}_f|\dot{u}_f - \mu\bar{\kappa}\omega_A^2 u_f}_{\text{indirect}} \underbrace{-\mu\bar{\kappa}\frac{\Delta p}{\rho_f L_{eff}}}_{\text{direct}} = F(t)/M \tag{5.10}$$

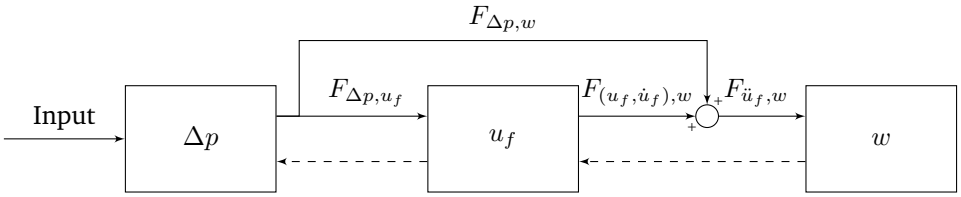

Figure 5.11: Schematic overview of effect of pressures on host and liquid.

5.3.2 Hybrid control

Hybrid systems, or hybrid control, combine continuous dynamics with discrete actions [44]. In simpler terms: a system is switched between modes based on simple (state dependent) rules. In the case of the on/off semi-active AO-TLCD this results in the simplistic model in Figure 5.12. The switching rules can incorporate the semi-active nature by themselves. In that case, no further clipping treatment of the input is required.

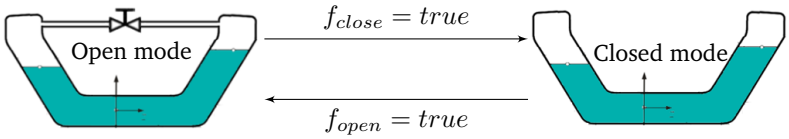

Figure 5.12: Schematic overview simple hybrid system.

Liquid based Intermittent closing, solely based on liquid displacements, is not a viable option for the semi-active AO-TLCD. The effectiveness of the damper can be quite sensitive to the switching moment and the total closing time. These switching moments and closing times are relatively unpredictable due to the stochastic excitation and the change of the system's properties.

A simplification of this method, switching only at zero-crossings of the liquid, eliminates this unpredictability. Though, the obtained equivalent frequency is constant (if the control is performed perfectly). Depending on which sides are closed and opened, the TLCD can be tuned to one of three additional 'semi-passive' frequencies.

Energy based Hybrid control laws for semi-active vibration absorbers are often based on energy flow. For example: Maximum energy absorption from the host can be the objective. Only if a control action can increase the absorption with respect to the host, it is performed. In the field of viscous dampers and suspensions a specific form is referred to as 'skyhook control' [45]. This hybrid control law for a viscous damper can be found in Equation 5.12 [46]. Here, the host displacements are denoted by subscript

s. The viscous actuating force is dependent on the relative displacements between host and damper, denoted by subscript rel.

$$F_{actuator,s} = c * \dot{x}_{rel} \tag{5.11}$$

$$c = \begin{cases} c_{min} & if\ \dot{x}_s \cdot \dot{x}_{rel} \leq 0 \\ c_{max} & if\ \dot{x}_s \cdot \dot{x}_{rel} > 0 \end{cases} \tag{5.12}$$

In the case of the AO-TLCD, the same logic can be applied. When the pressures extract energy from the host and its force can be increased through closing, the valves are closed. This has been illustrated in Figure 5.13. The resulting control law can be found in Equation 5.14. Note that when the valves are open, pressures move in phase with the liquid displacements. As a result, the pressure sign before closing is equivalent to the direction of compression after closing.

$$\begin{aligned} F_{\Delta p,w} &= -\mu \bar{\kappa} A_H \Delta p \\ \dot{p} &= \dot{u}_f / \epsilon - f(K_{oi}, \Delta p) \end{aligned} \tag{5.13}$$

$$K_{oi} = \begin{cases} K_{oi,max} & if\ -\dot{w} \cdot \Delta p \leq 0 \\ 0 & if\ -\dot{w} \cdot \Delta p > 0 \end{cases} \tag{5.14}$$

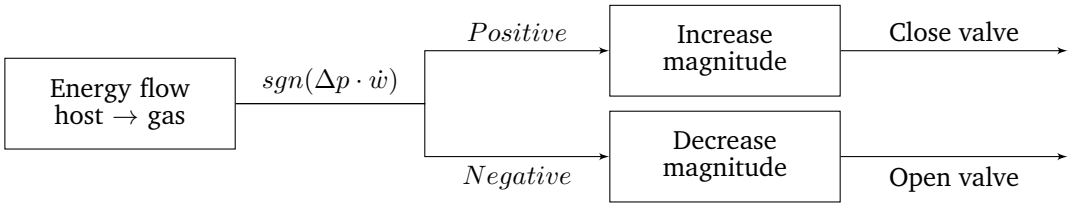

Figure 5.13: Simplified schematic of non-optimal hybrid control scheme.

Above control law does not account for potentially negative side-effects of the control action on the liquid its motion. The work performed by the pressure-force on the liquid, may result in a non-optimal phase-lag between the liquid and the host. Moreover, large amounts of energy may be dissipated, as above law may result in opening of the valve when energy is stored in the gas.

The host accelerations approximately have a 90 degree phase shift with the host velocities. Considering available measurements, the alternative form given in Equation 5.15 is preferred. As a result, valves are closed when the host velocities are large, resulting in large energy flow from the host to the gas.

Moreover, the resulting law is more favourable with respect to the liquid. The valve opening, is generally triggered by the pressure sign change, effectively minimizing the potential side effects of dissipation on the liquid motion. Hence, the control law optimizes for both the host (increase the energy absorption) and for the TLCD (only add stiffness). A simplified diagram can be found in Figure 5.14.

$$K_{oi} = \begin{cases} K_{oi,max} & if\ \ddot{w} \cdot \Delta p \leq 0 \\ 0 & if\ \ddot{w} \cdot \Delta p > 0 \end{cases} \tag{5.15}$$

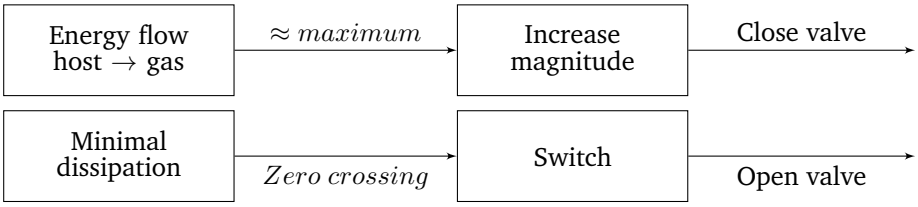

Figure 5.14: Simplified schematic of improved and final hybrid control scheme.

5.3.3 Optimal control

Many common control strategies can be classified as 'optimal' control. It deals with finding the optimal control given some performance criterion. The most commonly used method is, the 'linear quadratic regulator' (LQR). This approach is in essence an automated approach of finding the optimal full-state feedback gains for a given quadratic state- and input dependent cost function.

Especially in the field of vibration absorbers this approach is commonly used for (semi)-active control. Hochrainer applied LQR feedback for the active TLCGD [5]. Both semi-active TLCD concepts also used LQR for determining the control reference input [23][41].

LQR

What actually comprises 'optimal' control always depends on the given objective. The LQR scheme tries to find a solution that drives all states to zero at minimal cost. Consequently, the resulting state feedback depends on the choice of the cost function. A general form of this cost function, J, is given in Equation 5.16. Though, other forms of the cost criteria "might, in practice reflect the desired objectives better" [47]

In Equation 5.16, both $\mathbf{Q}$ and $\mathbf{R}$ should be positive (semi)-definite. In case $\mathbf{Q}$ and $\mathbf{R}$ are diagonal with positive individual weights, this is always valid. Moreover, all inputs must be penalized to solve the LQR problem. Without a penalty, requested inputs would potentially go to infinity.

The LQR approach assumes a linear system with full state feedback. Therefore, it results in active control of the system. Clipping of the control input results in sub-optimal performance as is discussed later.

$$J = \lim_{T\to\infty} \left\{ \int_0^T (\mathbf{x}^T \mathbf{Q} \mathbf{x} + \mathbf{u}^T \mathbf{R} \mathbf{u}) dt \right\} \tag{5.16}$$

The optimal feedback gain is found through the algebraic Riccati equation. For now, it is only relevant to know that the solution to the Ricatti equation; produces a stable and optimal state feedback gain for the given cost function. The resulting active system is given by Equation 5.17. Here, $\mathbf{K_g}$ is the feedback gain and $\mathbf{B}$ is the state-space input vector.

$$\dot{\mathbf{x}} = (\mathbf{A} - \mathbf{B}\mathbf{K_g})\mathbf{x} + \mathbf{f}(t) \tag{5.17}$$

Proper design of the weighing matrices can be a quite cumbersome and iterative process. A selection method for $\mathbf{Q}$ based on mechanical energy is mentioned by Wang [48]. Here $\mathbf{Q}$ is based on the mass and stiffness matrix including additional scaling. In that manner, the states are penalized based on their mechanical energy. This can be especially useful for MDoF host models.

The states introduced by the damper were scaled independently. Lower weights on damper states and input, increase the damper response and energy consumption and result in reduced response of the host. For an active scheme, one can use transfer functions or bode plots to find the desired weighing matrices.

The semi-active scheme does not consume energy. Moreover, low semi-active damper strokes are reported in literature. As a consequence, the individual weights for the liquid, pressures and input can be chosen much lower than for a typical active design. It should be noted that the units of states and inputs should be taken into account for the weight selection. The final form of the weighing matrices can be found in Equation 5.18.

$$\begin{aligned} \mathbf{Q} &= diag(\quad K_{1,1} \quad q_L * K_{2,2} \quad q_p \quad M_{1,1} \quad q_L * M_{2,2}) \\ \mathbf{R} &= r \end{aligned} \tag{5.18}$$

For the active system, with $q_L = 0.05$ and $q_p = r = 1e-7$ very high response reduction of the host is obtained, while maintaining liquid displacements within acceptable limits. The dynamic amplification of the host and the transfer function of the liquid are given in Figure 5.15. The off-tuned and tuned passive TLCD are given as a reference. The transfer function of the liquid has been normalized by the maximum

magnitude for tuned conditions. For the LQR scheme, and the transfer functions, a typical linear TLCD damping value was used.

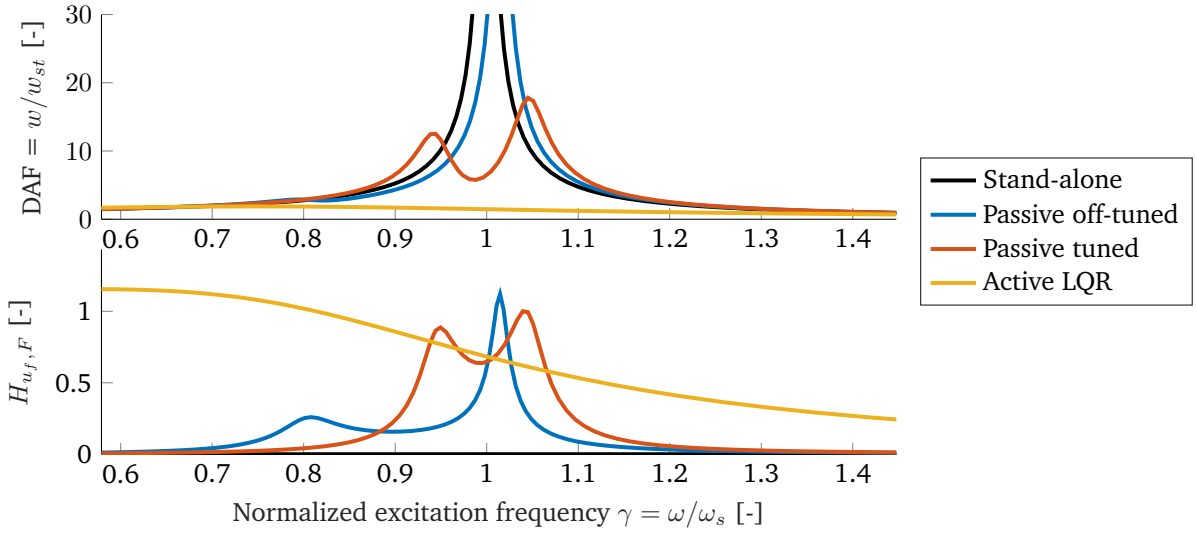

Figure 5.15: Frequency response of active LQR controlled AO-TLCD and passive TLCDs for the host and liquid displacements.

Clipped-LQR

For semi-active control, the active state feedback requires clipping. Such a clipped-LQR (C-LQR) system "only emulates the active system when the control force is dissipative" [41]. Obviously some performance is lost by changing the control input. According to Tseng: "The so-called 'clipped optimal' solution is not optimal, although its performance is generally quite close to that of the time-varying solution". "In practice, sub-optimal control laws such as the 'clipped optimal' method .... are fine engineering approximations." [49].

The clipping of a continuous C-LQR and an on/off C-LQR scheme are given by Equation 5.7 and Equation 5.8 respectively. In Figure 5.16, the active LQR input and the continuous C-LQR input are compared for a stochastic load case. For the semi-active scheme, both the clipped and unclipped input is shown. The effect of clipping on the states, is clearly visible through the increased magnitude of the reference control inputs. As a result, the clipped control input is almost equivalent to its on/off variant. Therefore, only the on/off C-LQR scheme is investigated further.

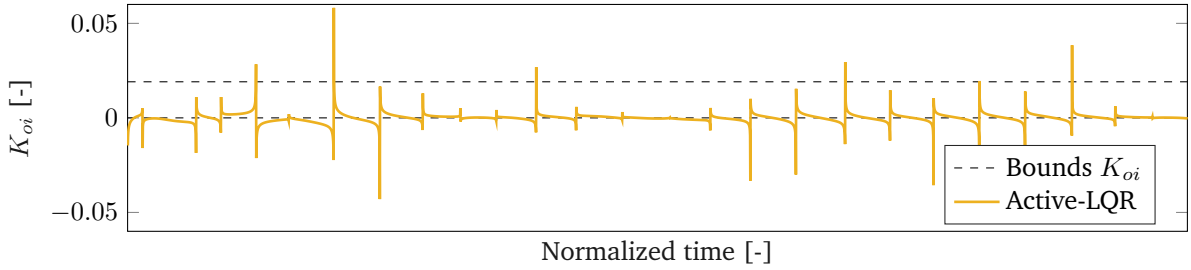

(a) Control input active LQR

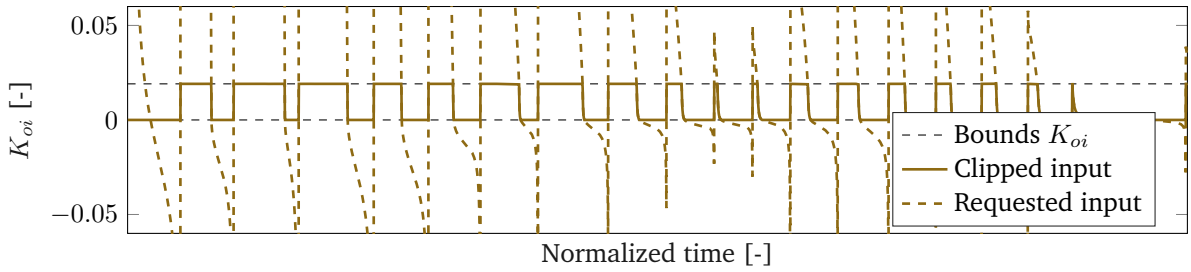

(b) Control input and reference input continious clipped-LQR

Figure 5.16: Comparison control inputs active and semi-active LQR schemes resulting from a stochastic load case.

5.3.4 Advanced methods

As noted before, both methods are not optimal in their performance. The hybrid method is not obtained using any cost function or mathematical optimisation. The LQR method does not account for the semi-active nature and bounds of the AO-TLCD.

In order to achieve optimal semi-active control (with respect to some cost function), more advanced control theory is required. In general a time-varying solution is required, as is stated by Tseng [49]. One of these methods would be model predictive control (MPC). Control actions are based on a finite time horizon instead of an infinite one as in Equation 5.16. The semi-active bounds can be included more easily in such a discrete time and finite horizon method.

Since robust/optimal controller design is not the main focus of this research, these more advanced methods are not investigated further.

5.3.5 Overview

In Table 5.1 an overview is given on the control laws used in the case study in Chapter 7. Here, 'aplied to' and 'based on' refer to which AO-TLCD model is used for the computation of the input and the response, respectively. The control inputs are determined according to Equation 5.19 - 5.21.

$$\text{Hybrid:} \qquad u = K_{oi} \qquad = \begin{cases} K_{oi,max} & if\ \ddot{w} \cdot \Delta p \leq 0 \\ 0 & if\ \ddot{w} \cdot \Delta p > 0 \end{cases} \tag{5.19}$$

$$\text{Active LQR:} \qquad u = \dot{m}^{\star} \qquad = -\mathbf{K_g B x} \tag{5.20}$$

$$\text{Clipped-LQR:} \qquad u = K_{oi} \qquad = \begin{cases} 0 & if\ sgn(\dot{m}^{\star} \cdot \Delta p) \leq 0 \\ K_{oi,max} & if\ sgn(\dot{m}^{\star} \cdot \Delta p) > 0 \end{cases} \tag{5.21}$$

Table 5.1: Overview of control laws used in case study.

Control law	Performance	Number of sensors	Based on	Applied to	Comment
Hybrid	'Sub-optimal' SA	2	Non-linear	Non-linear	
Active	'Optimal' active	5	Linear	Non-linear	Reference
Clipped-LQR on/off	'Sub-optimal' SA	5	Linear	Non-linear	

Chapter 6

Modelling of OWT installation with semi-active AO-TLCDs

The non-linear nature of semi-active control results in an excitation-dependent response. For the control strategy to be tested successfully for the OWT application, a coupled support structure and damper model needs to be deployed including stochastic environmental loading. In addition, the 'working points' of the TLCD depend on differences between its operational design and the installation phases.

Section 6.1 discusses the installation steps of an OWT and the effectiveness of a passive TLCD during these steps. Based on these two factors, the installation step for the case study is selected. In Section 6.2 details are given on the modelling of the support structure and its environmental loads. Afterwards, in Section 6.3, the model from Chapter 3 including the control law from the previous chapter is combined into the fully coupled AO-TLCD model. Furthermore, the final modal reduced form is presented. At the end of this chapter, in Section 6.4, the benchmark results are presented.

6.1 Installation case study

During installation, the support structure's mass and frequency change as components are added. In Table 6.1 typical values for these changes can be found for multiple installation steps. The properties have been normalized by the fully installed support structure. The frequency variations for a single step are a result of potential variations within an offshore wind farm.

Table 6.1: Overview normalized properties of support structure during installation steps.

Phase	Normalized frequency	Normalized modal mass
No nacelle	2.1 - 3.2	0.23
No hub	1.2 - 1.6	0.67
No blades	1.1 - 1.4	0.85
Fully installed	1.0 - 1.2	1

Site The required effectiveness of the TLCD largely depends on the specific site conditions. For very shallow sites, wave-induced vibrations are less problematic. For such sites, a damper may not be cost-effective for the operational phase; let alone for the installation phase. In order to analyse the potential benefit a deep-water offshore wind farm site was selected which is located in the North Sea.

Workability For us to differentiate between sufficient and insufficient effectiveness, the goal of the research has to be quantified in more detail. Installation workability can be dependent on many variables.

However, the focus of this research is on wave-induced vibrations only. To be more specific, only the wave-induced vibrations that occur when all other variables allow for installation are important.

To visualize the effect of wave induced vibrations on the workability; probability of non-exceedance plots were created for the case study site (i.e. workability plots). Response to a 20 year set of wave-conditions were computed with a frequency domain tool. In Figure 6.1 this workability can be found, filtered for wind speeds below 16 m/s. Here, the results are shown scaled to 4 % LogDec equivalent structural damping.

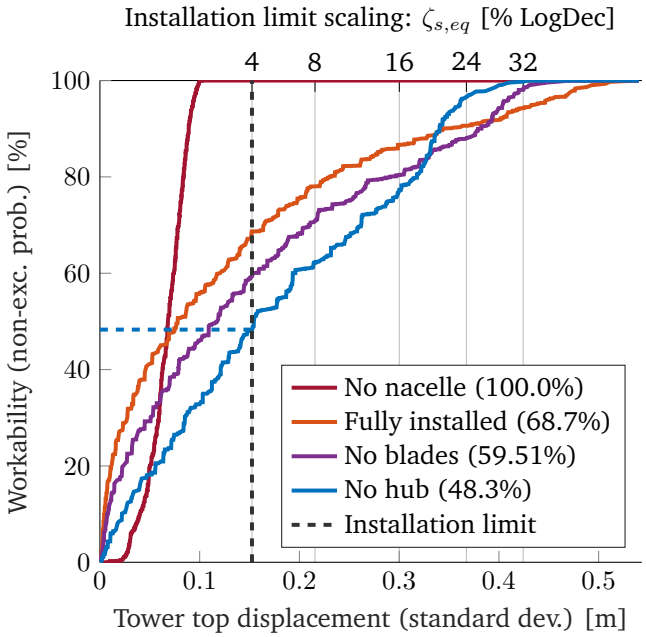

Figure 6.1: Installation workability graph for case study site for wind-speeds $v < 16m/s$.

As a rule of thumb, 90 % non-exceedance of 0.25m for the tower top displacements can be used as a limit for installation. This corresponds to a standard deviation of approximately 0.15m.

The hub-installation is most critical. Without any damper, 50% of the responses exceed the installation limit. Compared to the fully installed OWT, overlapping wave spectra are milder for this step. However, these conditions are more likely to occur.

Sensitivity to effectiveness The response of a lightly damped linear single DoF structure to white noise excitation with spectral density S_f can be approximated by Equation 6.1 [19][50]. From this, Equation 6.2 can be derived for the displacement variation as a function of structural damping variation. This relation has been verified for the case illustrated in Figure 6.1 with simulations for different values of structural damping. To provide insight in the effects of the damper, an additional axis is included in Figure 6.1, that shows the approximate scaling of the installation limit for different equivalent structural damping values. For example, for 16% LogDec, TT displacements are approximately reduced by 50%. The regular x-axis, including the installation limit, shifts with respect to the non-exceedance plots. For this example, this would results in approximately 75% workability for the hub-installation step.

$$\sigma_w = \sqrt{\frac{\pi S_f}{2\omega_s^3 \zeta_{s,eq}}} \tag{6.1}$$

$$\frac{\sigma_{w,new}}{\sigma_{w,old}} = \sqrt{\frac{\zeta_{s,eq,old}}{\zeta_{s,eq,new}}} \tag{6.2}$$

TLCD effectiveness In terms of TLCD effectiveness the hub-installation step is also most critical. In Figure 6.2 the hub installation step is indicated in the passive TLCD effectiveness graphs from Chapter 2. The TLCD is most likely under-damped during installation. Low internal damping results in a more narrow-banded effect of the passive TLCD. Therefore, Figure 6.2 may give an optimistic view.

For hub installation, the workability is hardly improved. For the other installation steps, the availability is higher than indicated in figure 6.1, as the equivalent damping is larger due to less off-tuning of the TLCD.

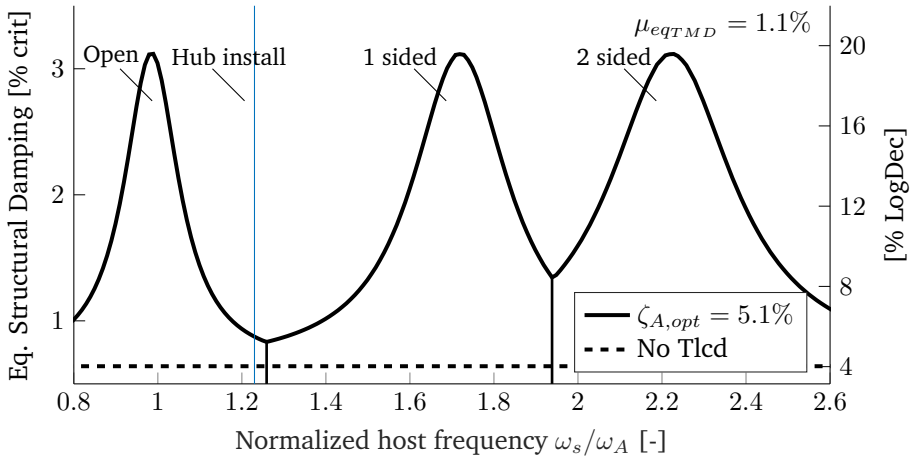

Figure 6.2: Effectiveness optimally damped TLCGD attached to a white noise excited host structure, including hub-installation frequency.

6.2 Modelling of offshore wind turbines

In this section the OWT model is discussed, including environmental loads.

Structural model

The support structure is modelled with Timoshenko beams. Across different installation steps, the model is modified exclusively at the tower top node. The point mass is changed according to the installed mass. Moments of inertia are scaled linearly with respect to the point mass at the tower top.

The structure is constraint at the pile tip for displacements and rotations in the z-direction. Other boundary conditions are applied through the soil-structure interaction, which is approximated by p-y curves.

Soil-structure interaction is the main contributor to the structural damping of an OWT. For installation steps, with reduced mass, modal damping may be larger than typical operational values. Nonetheless, additional damping may still be required. Currently no good estimates for the damping during installation exist. Therefore, a typical operational value of 4% LogDec structural damping is assumed.

Environmental loading

Only hydrodynamic wave loads are of importance for accurate testing of the damper's behaviour. Vibration absorbers mainly target dynamic amplification and have a narrow banded effect. Therefore, currents can be neglected. The aerodynamic load spectrum is significantly lower than the first natural frequency of the support structure. Moreover, aerodynamic loads are negligible during installation/idling cases.

The wave load time series were generated using in-house tools from Siemens Gamesa Renewable Energy. Wave kinematics were obtained from the Johnswap spectrum using stream function wave theory. Wave load time series were computed using Morison's equations including Mach Fuchs theory for diffraction. Afterwards, these loads were translated to the a finite element model of the structure. Lastly, these in-house tools were used to compute the modal reduction of the full structural model.

Load cases Time domain computation limits the amount of load cases that can be analysed. Four representative load cases with high occurrence were selected in a range around the natural frequency of the structure and with some spread on the significant wave height Hs. An overview can be found in Table 6.2. Here the peak natural frequencies of the wave spectrum are normalized by the natural frequency of the hub-installation support structure.

Additionally, tower-top standard deviations were obtained for the stand-alone hub installation support structure. The response was computed using multiple time-domain simulations for the full model with a certified in-house tool. The total weight of a bi-directional TLCD was added to the stand-alone support structure.

Clearly, load case III is most critical. Based on Equation 6.2, an equivalent structural damping of 18% LogDec is required to meet the installation limit. Such effectiveness would require near optimal-passive performance of the semi-active damper.

Table 6.2: Hydrodynamic load cases and stand-alone tower response including total weight TLCD.

Load case	**I**	**II**	**III**	**IV**
Hs [m]	0.875	1.375	1.875	2.625
Normalized peak frequency [-]	1.38	1.18	0.93	0.74
St. dev. TT displacements [m]	0.044	0.137	**0.292**	**0.214**
St. dev. TT accelerations [m]	0.057	0.173	0.355	0.259
Required additional damping [% LogDec]	-	-	18	9

6.3 Coupled model of OWT and AO-TLCD

An overview of the complete model can be found in figure 6.3.

Full model

The SA AO-TLCD model is attached to the full model at specific locations through the coupling forces with position vector $\mathbf{s}$. No direct coupling exists between the host and the air system for the form given in Equation 6.3. In case the TLCD location does not correspond to a structural node of the support structure, the interaction forces are distributed linearly over the two nearest nodes.

$$\begin{aligned} \mathbf{M}\ddot{\mathbf{w}} + \mathbf{C}\dot{\mathbf{w}} + \mathbf{K}\mathbf{w} &= \mathbf{F}(t) - \mathbf{s} \cdot m_f(\mathbf{s}^T\ddot{\mathbf{w}} + \bar{\kappa}\ddot{u}) \\ \ddot{u}_f + \delta_L|\dot{u}_f|\dot{u}_f + \frac{\Delta p}{\rho_f L_{eff}} + \omega_A^2 u_f &= -\kappa\mathbf{s}^T\ddot{\mathbf{w}} \\ \mathbf{s} &= [0, .., 1, ..., 0]^T \end{aligned} \tag{6.3}$$

Modal reduced form

Modal reduction is performed on the stand-alone OWT. The total mass of the TLCD perpendicular to the modal direction, is added as a point mass. The structural mass of the TLCD parallel to the modal direction is also added. The structural TLCD mass is assumed to be 40% of the total TLCD mass (the fluid mass is 60%).

The TLCD is coupled through the reaction forces using the position vector and the mode shapes. The final modal reduced coupled AO-TLCD model is given by Equation 6.4. Here, the modal coordinate of mode j is indicated by q_j, the mode shape of mode j by $\boldsymbol{\phi}_j$, actuator properties are denoted by subscript v, the input is indicated by u and the liquid displacements are indicated by u_f. Actuator dynamics can be eliminated by setting the inertia and damping of the actuator to zero. Consequently, directly controlling K_{oi} in the pressure DoF. Additional generalized parameters are introduced for mode j according to Equation 6.5 to Equation 6.7.

It is assumed that the effects of not taking the sub-structure interface into account during the reduction has negligible effects on the response.

$$\begin{bmatrix} 1+\mu_{gen} & \mu_{gen}\bar{\kappa}/(\boldsymbol{\phi}_j^T\mathbf{s}) & 0 & 0 \\ \kappa\mathbf{s}^T\boldsymbol{\phi}_j & 1 & 0 & 0 \\ 0 & 0 & 0 & 0 \\ 0 & 0 & 0 & 1 \end{bmatrix} \begin{bmatrix} \ddot{q}_j \\ \ddot{u}_f \\ \Delta\ddot{p} \\ \ddot{K}_{oi} \end{bmatrix} + \begin{bmatrix} 2\zeta_s\omega_j & 0 & 0 & 0 \\ 0 & \delta_L|\dot{u}_f| & 0 & 0 \\ 0 & \epsilon^{-1} & 0 & 0 \\ 0 & 0 & 0 & 2\zeta_v\omega_V \end{bmatrix} \begin{bmatrix} \dot{q}_j \\ \dot{u}_f \\ \Delta\dot{p} \\ \dot{K}_{oi} \end{bmatrix}$$
$$+ \begin{bmatrix} \omega_j^2 & 0 & 0 & 0 \\ & \omega_A^2 & (\rho_f L_{eff})^{-1} & 0 \\ & 0 & 0 & 0 \\ & 0 & 0 & \omega_V^2 \end{bmatrix} \begin{bmatrix} q_j \\ u_L \\ \Delta p \\ K_{oi} \end{bmatrix} = \begin{bmatrix} f_{gen} \\ 0 \\ 0 \\ 0 \end{bmatrix} + \begin{bmatrix} 0 \\ 0 \\ 0 \\ \omega_V^2 u \end{bmatrix} + \begin{bmatrix} 0 \\ 0 \\ -\epsilon^{-1}K_{oi}sgn(\Delta p)|\Delta p|^{0.5} \\ 0 \end{bmatrix} \tag{6.4}$$

$$\mu_{gen} = \frac{\boldsymbol{\phi}_j^T\mathbf{s}m_f\mathbf{s}^T\boldsymbol{\phi}_j}{\boldsymbol{\phi}_j^T\mathbf{M}\boldsymbol{\phi}_j} = (\boldsymbol{\phi}_j^T\mathbf{s})^2\mu \tag{6.5}$$

$$\omega_j = \frac{\boldsymbol{\phi}_j^T\mathbf{K}\boldsymbol{\phi}_j}{\boldsymbol{\phi}_j^T\mathbf{M}\boldsymbol{\phi}_j} \tag{6.6}$$

$$f_{gen} = \frac{\boldsymbol{\phi}_j^T\mathbf{F}(t)}{\boldsymbol{\phi}_j^T\mathbf{M}\boldsymbol{\phi}_j} \tag{6.7}$$

The generalized modal mass ratio μ_{gen} which affects the TLCD effectiveness, is lower when the TLCD is located below the tower top, since the modal contribution of the TLCD reaction force, $\boldsymbol{\phi}_j^T\mathbf{s}$, is never larger than 1. In the case study an equivalent TMD generalized modal mass ratio of 1.1% was used. In other words, the TLCD from the case study is approximately equivalent to a TMD with a modal mass ratio of 1.1% located at the tower top.

6.4 Verification and benchmark coupled model

The modes of the support structure are widely spaced. Significant excitation of the second mode by the non-linear SA damper is unlikely. Using only a single mode for the stand-alone support structure, tower top standard deviations were obtained within 1% of the full model solution.

In Figure 6.4 the tower top and liquid displacements can be found for the benchmark solutions. This includes: the stand-alone tower including TLCD weight, the off-tuned passive TLCD designed for the operational life and an optimally tuned passive TLCD. The fully open air-system used by the AO-TLCD, introduces additional damping. For both passive TLCD set-ups, the internal damping matches that of the fully open passive AO-TLCD. Consequently, the effectiveness of the off-tuned TLCD is somewhat over-estimated.

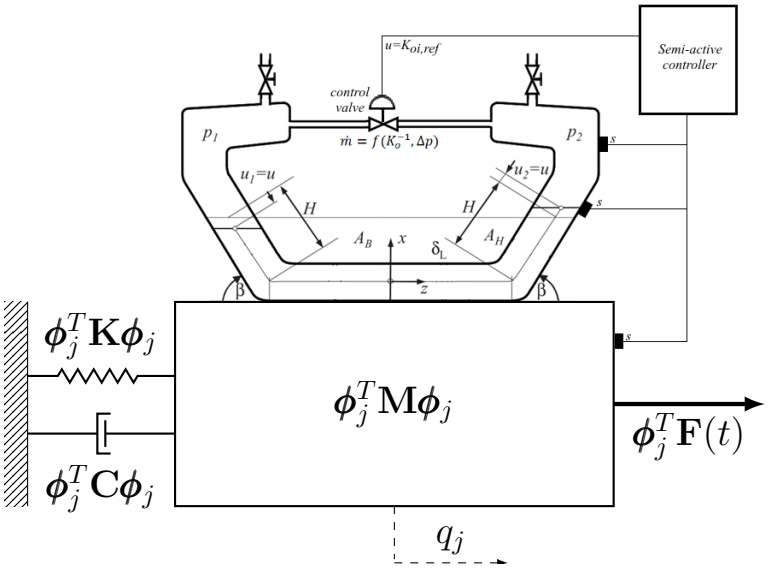

Figure 6.3: Diagram OWT-coupled SA AO-TLCD.

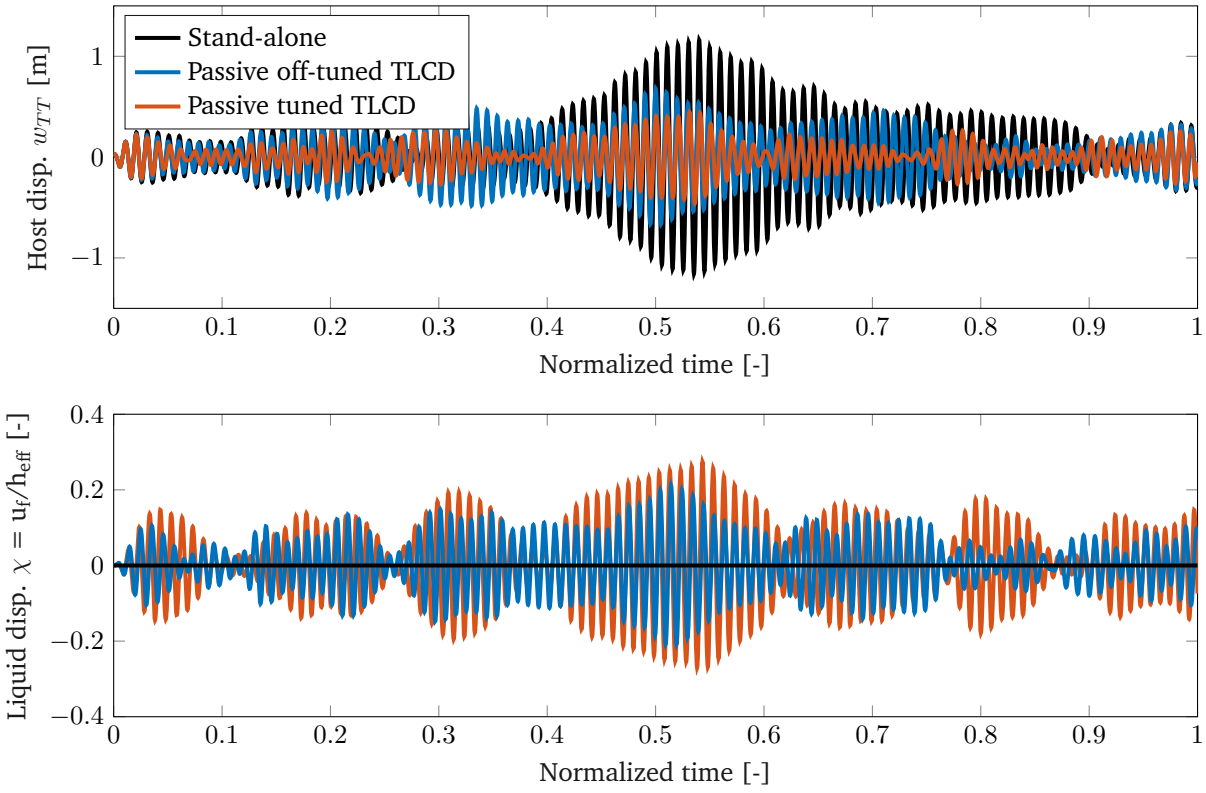

Figure 6.4: Displacements benchmark solutions for critical loadcase III seed 1.

TLCD effectiveness Equivalent properties were analysed for both the host and the TLCD. The resulting 'working points' are indicated by markers in figure 6.5. The effectiveness of a linear TLCD for white noise excitation is also given. The off-tuned and tuned conditions are indicated by blue and orange respectively.

As expected, the passive TLCD is under-damped during the installation phase. Since additional damping has been added to account for the fully open air system, the actual TLCD damping is even lower.

For load case III, a large deviation in effectiveness is observed for the tuned TLCD compared to the white-noise approximation. For other working points only slight deviations are observed. These deviations can be contributed to the narrow banded excitation in combination with the narrow banded effect of an under-damped TLCD. As a result, the differences are large for load case III, with a peak frequency near the support structure and tuned TLCD their natural frequencies.

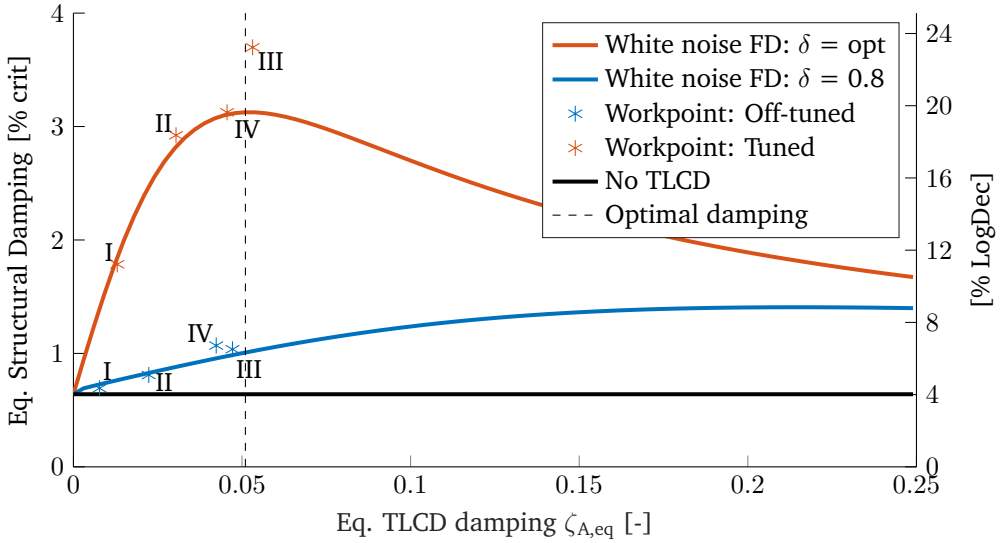

Figure 6.5: Comparison between working points of benchmark solutions with linear TLCD effectiveness for a white noise excited host structure.

Chapter 7

Results Case Study

First, the results for the hub-installation case study are presented using ideal controller assumptions. Section 7.1 focusses on some general statistical results across all load cases. Section 7.2 includes more in depth analysis of load case III, the most critical load case. Afterwards, Section 7.3 and Section 7.4 focus on model sensitivities to stiffness variations and actuator dynamics, respectively. In Section 7.5 the results are discussed further, including some additional context.

7.1 General statistical results

To provide a good overview on the semi-active strategies their performance, some statistical data is presented first. The benchmark solutions and the active LQR controller have been included for comparison. In Figure 7.1 the average standard deviations of the tower top displacements can be found. Both semi-active control strategies, out-perform the optimal passive damper.

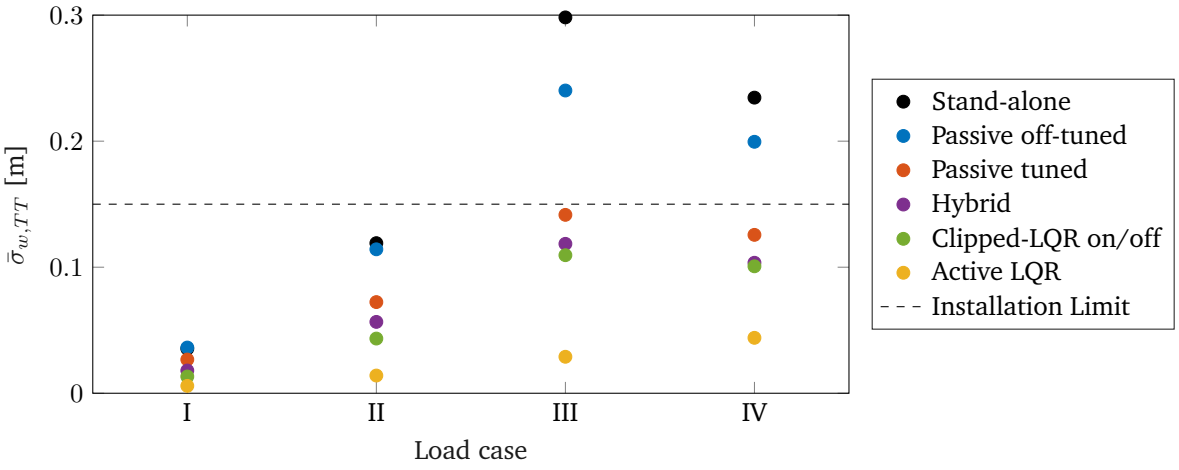

Figure 7.1: Average standard deviation TT displacements semi-active across seeds.

More detailed information can be found in Table 7.1 for load case III. Here the standard deviation reduction can be found compared to the stand-alone support structure. The liquid displacement standard deviations have been normalized by the effective height of the gas compartment. Lastly, the equivalent structural damping, i.e. effectiveness, is included.

The semi-active strategies show similar TLCD strokes for increased effectiveness. Only the active LQR scheme results in a significant TLCD response increase.

The active LQR scheme vastly out-performs its clipped-LQR counterpart. This can be mostly contributed to the weights chosen to determine the optimal feedback. Low penalties for the liquid response and the input were used because these were not likely to be constraints for the semi-active strategy. If the design of an active control scheme was the objective, larger penalties for these states would be preferred to limit energy consumption and the liquid response. This would also result in a less optimistic performance of the active scheme compared to the semi-active strategies.

Table 7.1: Performance passive and semi-active strategies for load case III.

Strategy	$\sigma_{w,TT}$ reduction [%]	Effectiveness [% crit]	σ_{χ_f} [m]
Passive off-tuned	-22	1.04	0.07
Passive tuned	-53	3.70	0.10
Hybrid	-60	4.54	0.10
Clipped-LQR on/off	-63	5.46	0.11
Active LQR	-90	-	0.19

Spread time-domain responses

As noted in the previous chapter, both the environmental loads and the dynamic systems are narrow banded. Depending on its statistical parameters and its specific realisation, the wave spectrum intensity may deviate largely across the frequency band of the host. Especially the lightly damped set-ups experience large deviations across different seeds.

The 90% confidence error of the mean tower top standard deviations can be computed according to Equation 7.1. Here, t_N is the 90% student's t-distribution for N number of simulations. The errors are normalized by the mean of the standard deviations. The convergence of this confidence error is displayed in Figure 7.2 for load case III across all set-ups. Twelve different seeds per load case are assumed to be sufficient for accurate estimation of any average performance indicators.

$$\text{90\% confidence error} = t_N \frac{std(\sigma_{w,N})}{\sqrt{N} mean(\sigma_{w,N})} \tag{7.1}$$

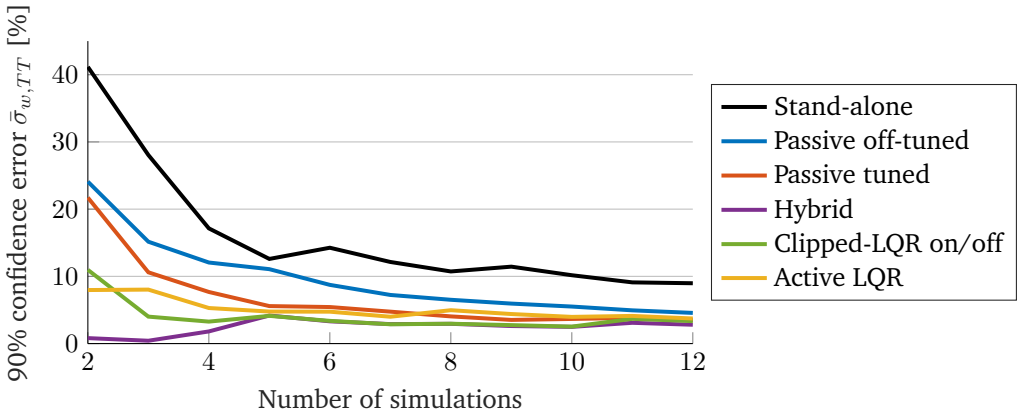

Figure 7.2: Convergence mean tower-top displacement standard deviations for load case III.

7.2 Additional observations

In this section the results are analysed in more detail. First, the response of the host is analysed in the frequency domain across all set-ups. Afterwards, the controller behaviour is illustrated in time-domain.

Dynamic amplification host

The dynamic amplification of the host displacements for load case III can be found in Figure 7.3. The dynamic amplification was obtained using multiple seeds. All dynamic amplifications are according to expectations.

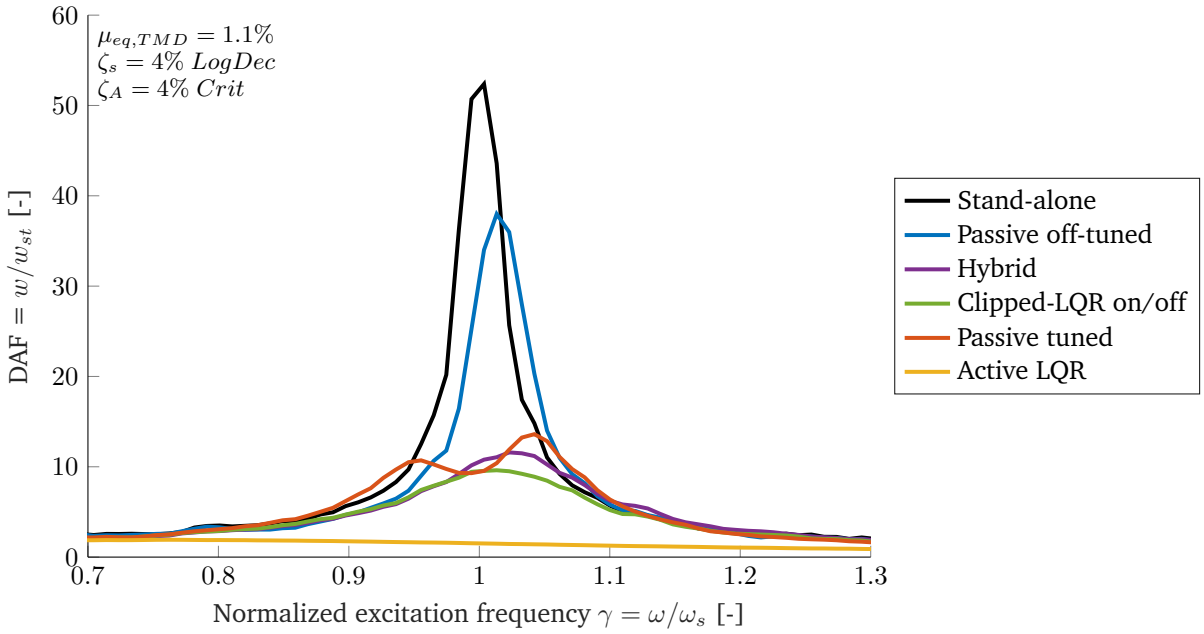

Figure 7.3: Dynamic amplification host for all set-ups for load case III.

Controller behaviour

In order to get a proper insight in the controller behaviour, the force-displacement/velocity diagrams are given for the hybrid controller in Figure 7.4. A single simulation of 'critical' load case III is shown.

To isolate the behaviour of the controller, the pressure-force trajectories are given with respect to both the liquid and the host. Across all diagrams, the pressure-force has been normalised by the maximum restoring force due to the liquid its weight. A small portion of the total time-series has been highlighted for clarity.

With respect to the liquid, the control law behaves as intended. This is clearly visible in the force-displacement diagram in the top left. The valves are closed around the peak liquid displacement, temporarily 'adding' a secondary stiffness. The other part of the cycle, some equivalent damping is 'added' through the losses in the air-system. No additional hysteresis is observed around the switching of the valves. In the force-velocity diagram in the bottom left, it can be observed that the additional damping is slightly non-linear.

With respect to the host, the control law also behaves accordingly. This can be mostly observed through the force-velocity diagram in the bottom right. The trajectories are mostly present in the 'dissipative' quadrants. As the hybrid control law did not prohibit energy release back to the host, some

trajectories go through the 'active' quadrants. Note that these quadrants do not violate the passivity constraint because the energy is only released back to the host and not introduced through the actuator.

For the control action, an optimum has to be found between direct dissipation from the host and optimal liquid response. It is assumed that the minimal viscous dissipation observed in the gas system, out-ways the energy-flow back to the host. In other words, for this specific case the valve opening is performed optimally. Though, it is unclear if the closing of the valve is optimal. As different closing cycle lengths may result in a larger effectiveness of the semi-active damper.

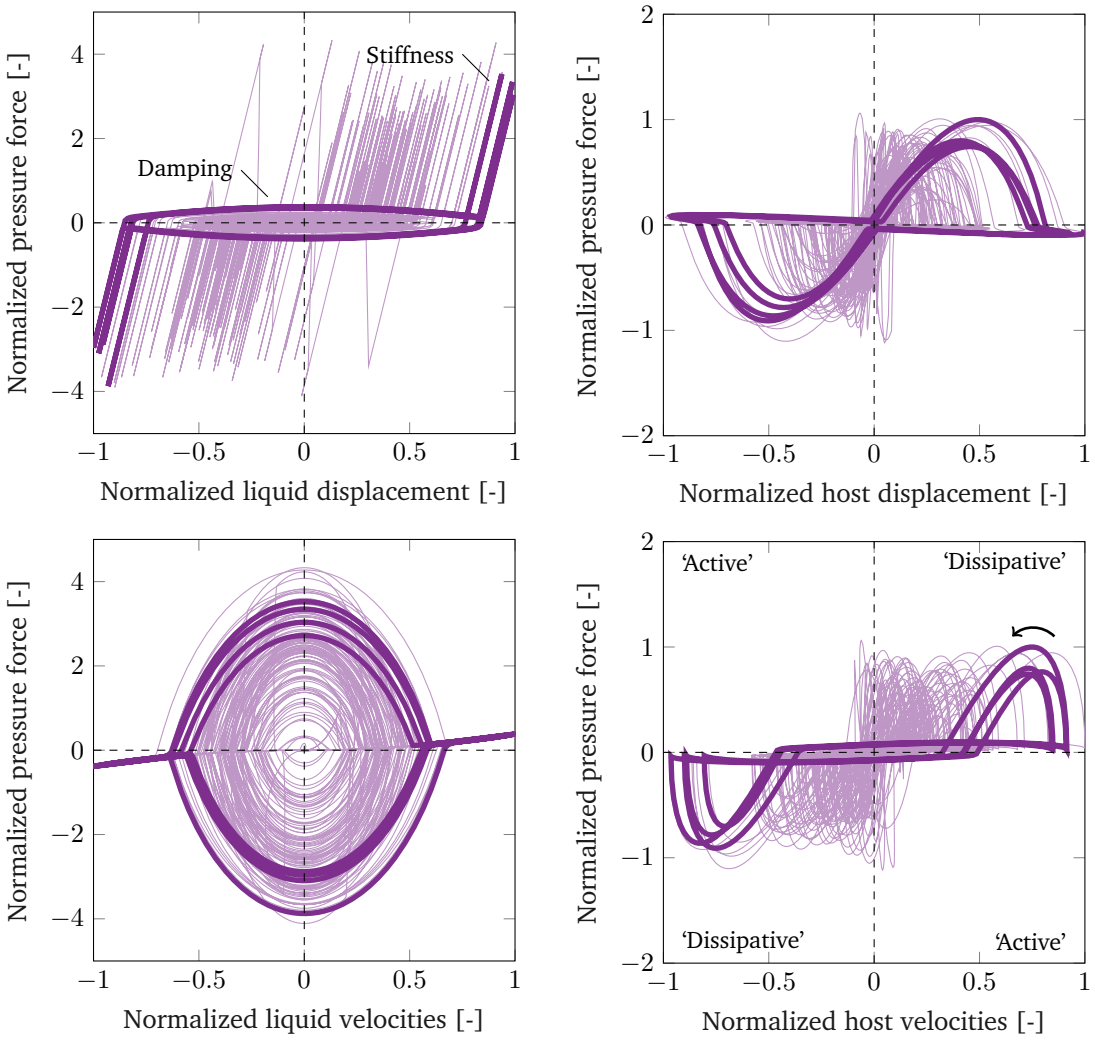

(a) Pressure-force on liquid

(b) Pressure-force on host

Figure 7.4: Force-displacement/velocity diagrams for hybrid control strategy load case III seed 1.

The on/off clipped-LQR scheme shows almost exactly the same behaviour and can be found in Figure B.1. For the clipped-LQR scheme, slightly less presence in the active quadrants w.r.t. the host is observed. Furthermore, slightly larger forces, i.e. larger closing cycles, are observed. Even though the additional host vibration reduction is small, it confirms the suspicion that the hybrid valve closing is not optimal.

7.3 Sensitivity to frequency variations

The sensitivity to passive TLCD frequency variation is investigated to check the robustness of the proposed strategies.

Method for frequency variation The frequency of the TLCD is adjusted exclusively through an additional variable in the TLCD equation of motion. As a result, all geometric factors, including the TMD equivalent modal mass ratio remain the same. The stand-alone host including the environmental loads are also unaffected. Since the air-system also remains the same, the natural frequency ratio between the two TLCD modes (open and closed) does change. The computed LQR feedback gain changes due to changes in the TLCD frequency.

Results The sensitivity to TLCD natural frequency variations is shown in detail in Figure 7.5 for load case III. Both the hybrid and clipped-LQR strategies are effective over a wide range of off-tuning.

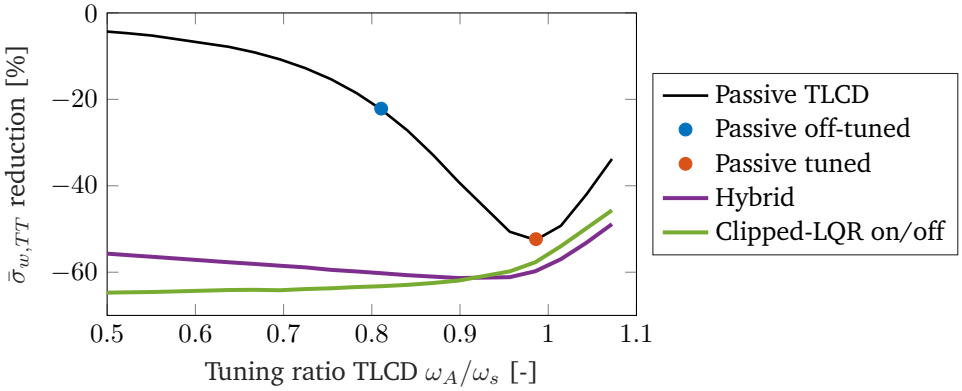

Figure 7.5: Sensitivity of semi-active control strategies to adjusted 'open' TLCD stiffness for load case III.

For more insight, the equivalent internal properties have been illustrated in Figure 7.6. At optimal tuning, both the passive and semi-active systems have near-optimal internal damping. One can conclude, that the increased effectiveness for the semi-active strategy is not solely due to improved TLCD parameters; but due to its semi-active nature. Hence, the semi-active damper out-performs its passive counterpart.

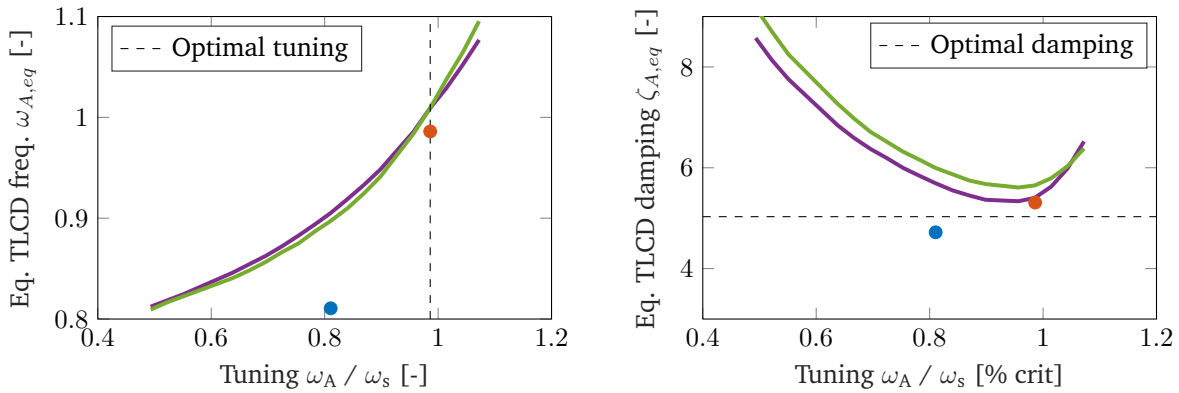

Figure 7.6: Equivalent internal properties TLCD for semi-active control strategies with variable 'open' TLCD stiffness for load case III.

7.4 Sensitivity to actuator dynamics

Until now, actuator dynamics have been neglected. Inclusion of the actuators may give rise to additional dynamic behaviour. Slow closing/opening of the valves introduces additional dissipation in the system. Large delays in the control action, may render the semi-active strategy completely ineffective.

First, the method is discussed briefly. Afterwards, the results for the closing time sensitivity are presented for load case III. At the end of this section, the behaviour of the 'slow' actuator is compared to the instantaneous control for a single simulation.

Method for actuator dynamics As mentioned in Section 6.3, a second order low pass filter is used for the actuator dynamics. The rise time t_r is varied, which represents the duration for the valve to respond up to 95% for a step input. In all cases the actuator frequency is much larger than the natural frequency of the support structure. Therefore, dynamical interaction does not occur.

For two typical valves, the step response is given in Figure 7.7. For the valves, the rise times have been normalized by the support structure its natural period. A rise time of 10% is already quite considerable, as valves are switched multiple times per cycle.

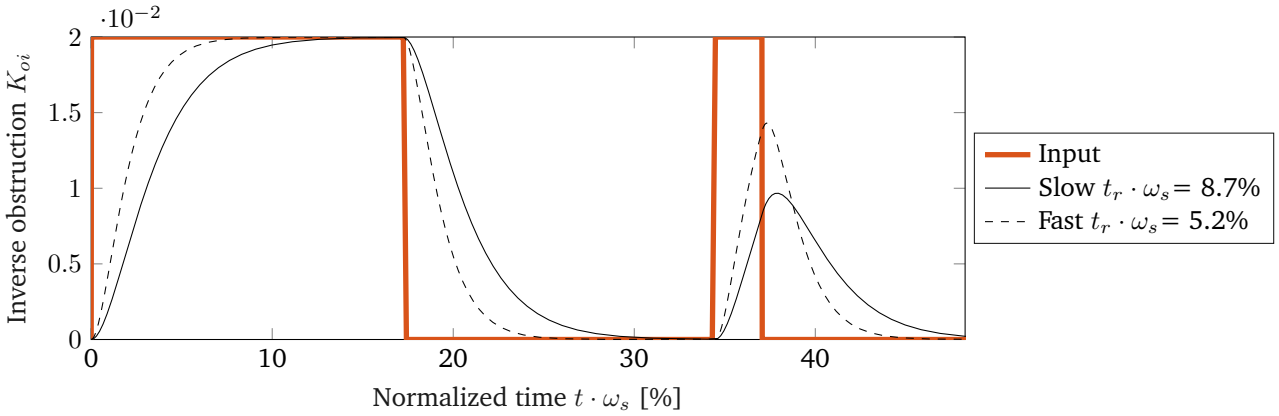

Figure 7.7: Step response of a 'slow' and 'fast' actuator to control input.

General results The sensitivity to normalized rise-time is shown in detail in Figure 7.8 for load case III. As actuator dynamics are likely to be uncertain, they were not included in the LQR feedback gain determination. In other words: unlike for the frequency sensitivity, the same feedback gain was used across all C-LQR simulations.

Both control strategies have reasonable performance up to large valve closing times. Further improvements can potentially be achieved through inclusion of the actuator dynamics in the LQR scheme or by using more advanced control schemes.

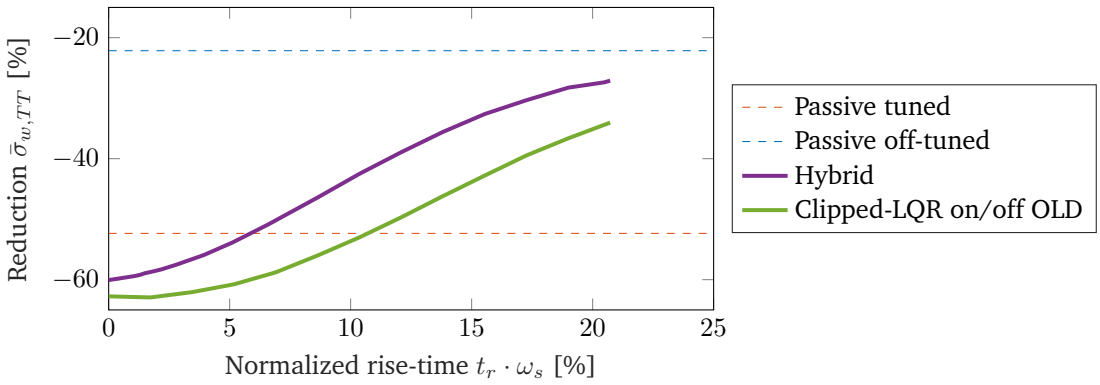

Figure 7.8: Sensitivity of semi-active control strategies to actuator rise time for load case III.

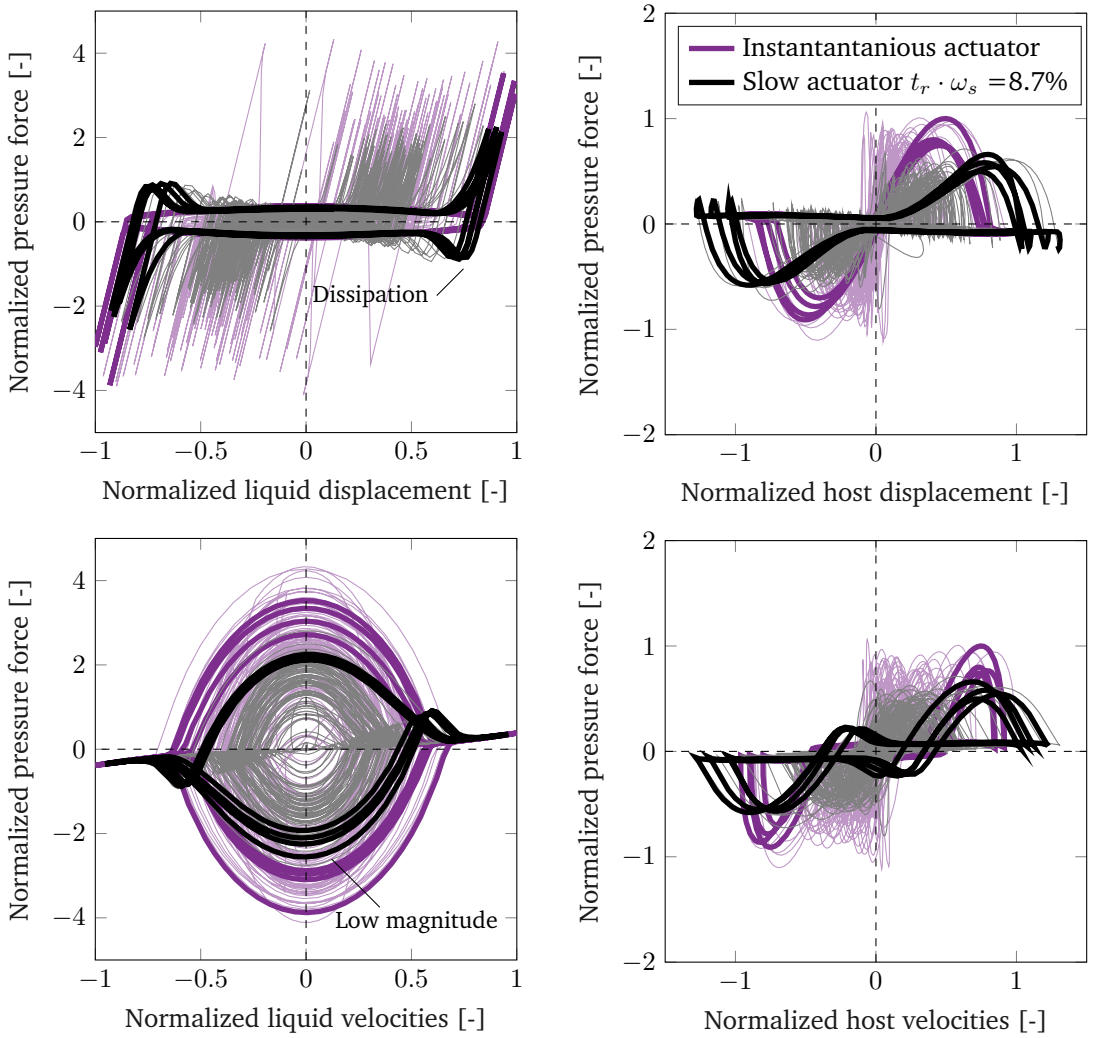

(a) Pressure-force on liquid

(b) Pressure-force on host

Figure 7.9: Force-displacement/velocity trajectory comparison hybrid control strategy with and without actuator dynamics for load case III seed 1.

Specific results To show the effect of the actuator dynamics on the control action, a comparison between the instantaneous and the 'slow' actuator is given in Figure 7.9. Both cases are normalized with respect to the instantaneous actuator set-up. Across all diagrams, forces are normalized with the maximum liquid weight restoring force. Displacements are normalized by their maximum. Again, part of the total time-series has been highlighted.

Most of the differences between the two cases can be explained with respect to the liquid. For the slow actuator, less pressure is built up. Partly due to delayed closing and partly due to pressure release during the closing. The reduction in pressure magnitude is most clearly visible in the force-velocity diagram in the bottom left. Furthermore, energy is dissipated around the closing, resulting in additional internal damping in the TLCD. In the force-displacement diagram, this is illustrated by the additional area described by the hysteresis loop around the valve closing/opening.

Except for the lower force magnitude, the effects with respect to the host are less clear. Delay on valve opening seems to increase the presence in the active quadrants slightly.

7.5 Discussion

In this section the observations made in this chapter are summarized and discussed briefly. Moreover, towards the end of this section additional context is given to the results and on the general development of the SA AO-TLCD.

Controller performance Figure 7.4 and Figure B.1 demonstrated that both control schemes minimize viscous dissipation in the gas system, i.e. massflow of the gas. This suggest that the assumptions in Chapter 5 on what comprises good semi-active control of the AO-TLCD are correct. Consequently, one can conclude that qualitatively, both control schemes are well designed.

For the clipped-LQR scheme, a slightly unpredictable sensitivity to its cost function was observed. Smaller weights for the control input or liquid response, did not necessarily result in improved response with respect to the host. The deviations in the effectiveness of the clipped-LQR control were not significant enough to result in different conclusions. However, it does confirm that quantitatively both control laws are sub-optimal in their performance.

Effectiveness period adjustment The semi-active AO-TLCD is able to reduce host vibrations by around 60% independent of the excitation intensity and the degree of passive off-tuning (Figure 7.1 and Figure 7.5). Moreover, for tuning ratios larger than 1, the semi-active damper out-performed its passive counterpart by more than 10%. The latter is in agreement with literature on semi-active VAs in general and for OWTs in specific [13].

Installation workability Because the performance is independent of the TLCD's passive natural frequency, we can conclude that a tower-top standard deviation reduction of 60% can be achieved across all installation steps. Looking at Figure 6.1, this results in a workability increase up to 90%.

Actuator dynamics and valve sizing As for the variable orifice TLCD [41], sensitivity to actuator dynamics is relatively low (Figure 7.8). Still, full-scale applications in civil structures may require large valves. Low frequency cyclic switching is not a standard application for valves of these sizes. This, or the performance loss due to actuator dynamics in general, can be mitigated partially by proper design of the valves and the controller.

Additional resistance in the fully open air system, for smaller valves, may be worthwhile in case of faster actuation. In other words, a decrease in actuator losses may outweigh an increase in losses due to passive obstruction. Furthermore, performance improvements may be achieved through inclusion of actuator dynamics in the controller design.

SA AO-TLCD for the operational phase The additional effectiveness around tuned conditions is low for the proposed control strategies. Potential losses due to sensor noise, limited sensor data, un-modelled dynamics and actuator dynamics make it even less attractive. In case internal damping is a constraint for the operational phase, the air-system including a sufficiently fast actuator, may introduce to much additional headloss. Furthermore, additional components may reduce the overall reliability of the OWT.

Still, an improvement of only 10% assumes the passive TLCD to perform optimally over its operational lifetime. As was demonstrated in Figure 2.5, this is not the case. Furthermore, research suggests that semi-active control may prove more beneficial for extreme or transient load cases. Therefore, it may still be worthwhile to investigate the application of the SA AO-TLCD for the OWT's operational life.

Off-tuned by design Improving geometric factors, resulting in a larger equivalent TMD mass ratio, would result in larger 'open' TLCD frequencies. The semi-active strategies are not effective for passive tuning ratios significantly larger than 1. Therefore, one can not find a more optimal geometric operational TLCD design by including the semi-active AO-TLCD.

Activation levels Requirements on components may be improved through the use of activation levels. In other words, the

For both its application to installation and the operational life of an OWT, For the purpose of increased workability, the semi-active AO-TLCD is only required to reduce wave-induced vibrations above a certain threshold, during the actual installation. With the host measurements, an activation level for the semi-active strategy can be set, above which the controller is active. Below this level, a passive AO-TLCD setting can be set, with optimal internal damping for the off-tuned conditions. In this manner, requirements on the components, like energy supply and number of valve switching, can be reduced.

Chapter 8

Periodically time-variant systems framework

In the previous chapter the performance of non-linear semi-active AO-TLCDs was evaluated for two sub-optimal control schemes. Robust performance of the AO-TLCD was obtained, though real insight in the dynamical system was not obtained. As a result, performance and stability were only measured qualitatively, in a post a-priori manner. As the observed response was not chaotic, more insight can be gained by further simplification and generalisation of the SA AO-TLCD. This chapter places the semi-active system in a periodic linear time-variant (LTV) systems framework.

Firstly, the definition of a general LTV system is given in Section 8.1, including an overview of the methods for analysis of such systems. Afterwards, in Section 8.2 a numerical approximation method is treated based on Floquet's theorem. In order to strengthen the understanding of LTV systems and to compare the numerical method with literature, the approximation method is applied to SDoF systems in Section 8.3. Finally, in Section 8.4 the semi-active AO-TLCD is simplified to a homogeneous periodic LTV system and analysed with a Floquet based approximation method. The solution is analysed for both stability and performance. Lastly, in Section 8.5 the results are discussed and compared with case study results from Chapter 7.

8.1 Linear time varying systems

A great deal of dynamical systems can be described as linear ordinary differential equations with (periodically) varying coefficients, i.e. periodic linear time-variant (LTV) systems. For this chapter we are most interested in the general response and stability of the AO-TLCD. For this, the homogeneous system is sufficient. A general description of a homogeneous LTV system is given in Equation 8.1. The matrix $\mathbf{A}$ can be a periodically varying matrix with period T according to Equation 8.2[1].

$$\dot{\mathbf{x}} = \mathbf{A}(t)\mathbf{x} \tag{8.1}$$

$$\mathbf{A}(t+T) = \mathbf{A}(t) \tag{8.2}$$

The system $\mathbf{A}$ is linked to a dynamical second order system as is given in Equation 8.3. Here, $\mathbf{M}$ indicates the mass matrix. The variational parts of the stiffness and damping matrices are indicated with $\mathbf{K}^*$ and $\mathbf{C}^*$ each varying with a period T.

$$\mathbf{A}(t) = \mathbf{M}^{-1}\begin{bmatrix} 0 & \mathbf{I} \\ -(\mathbf{K}+\mathbf{K}^*(t)) & -(\mathbf{C}+\mathbf{C}^*(t)) \end{bmatrix} \tag{8.3}$$

[1]With respect to LTV systems, the period T is reserved for the modulation period. Any other periods will be denoted by additional subscripts.

Depending on the objective, various ways exist to solve these systems. Though, most involve some kind of approximation - namely finite series, perturbations or numerical approximations. With regards to stability, most methods can be classified under the following [51]:

- Hill's method of infinite determinants
- Perturbation methods (including method of multiple scales)
- Floquet theorem

The former method can be cumbersome when applied to complex or MDoF systems. The second class of methods, e.g. the Lindstedt Poincoire method, is limited to cases where the "periodicity in the coefficients of the system, can be expressed in terms of some small parameter" [51]. The latter is from a numerical point of view very attractive and relatively straightforward. Moreover, besides analysis of the stability some methods allow for computation of the system its response.

8.2 Stability of LTV systems

In this section a brief review on the solution of LTV systems is given. Of which the main focus is on the stability of periodic LTV systems. As noted in the previous section, approximation methods based on Floquet's theorem are treated.

8.2.1 Solution of LTV systems

A set of linearly independent solutions of a linear system, as described in Equation 8.1, can be put in a $n \times n$ matrix, called the *fundamental matrix* $\boldsymbol{\phi}(t)$. Since the solutions are independent, the determinant of this matrix, the *Wronskian* w, must be non-zero.

$$\boldsymbol{\phi}(t) \equiv [\mathbf{x}_1(t), \mathbf{x}_2(t), ..., \mathbf{x}_n(t)] \tag{8.4}$$

The *transition matrix* $\boldsymbol{\Phi}$, or *principle matrix*, is defined to relate the (transient) response at time t to the initial values at time t_0 (Equation 8.5). In other words, a single term in $\boldsymbol{\Phi}$ relates state j at time t to the initial value of state i at time t_0 [52]. The transition matrix can be derived from the fundamental matrix according to Equation 8.6. In essence, the inverse of the fundamental matrix $\boldsymbol{\phi}^{-1}(t_0)$, eliminates potential linear transformations of independent solutions in the fundamental matrix.

$$\mathbf{x}(t) = \boldsymbol{\Phi}(t, t_0)\mathbf{x}(t_0) \tag{8.5}$$

$$\boldsymbol{\Phi}(t, t_0) = \boldsymbol{\phi}(t)\boldsymbol{\phi}^{-1}(t_0) \tag{8.6}$$

From Equation 8.6 we can derive that the transition matrix can be split up into consecutive parts as is given in Equation 8.7. Additionally, the transition matrix equals identity at $t = t_0$. Both these properties also become clear by solving x at discrete times according to Equation 8.5.

$$\boldsymbol{\Phi}(t, t_0) = \boldsymbol{\Phi}(t, t_1)\boldsymbol{\Phi}(t_1, t_0) \tag{8.7}$$

Since $\boldsymbol{\Phi}$ contains linearly independent solutions of x, one can also state that

$$\dot{\boldsymbol{\Phi}}(t, t_0) = \mathbf{A}(t)\boldsymbol{\Phi}(t, t_0) \tag{8.8}$$

Any linear combination of $\boldsymbol{\Phi}$ through a constant non-singular matrix $\mathbf{C}$ is also a transition matrix of $\mathbf{A}(t)$, since Equation 8.8 still holds. Though it is important to note that a transition matrix of $\mathbf{A}(t + \tau)$ may not be a transition matrix of $\mathbf{A}(t)$. In other words, the fundamental solution set of the system changes due to time varying properties.

8.2.2 Floquet theorem and stability criterion

In case the LTV system is periodic according to Equation 8.2, Floquet theorem can be applied. As indicated at the start of this chapter, the main purpose of Floquet's theorem is to determine the stability of a periodic LTV system. The two main consequences of the theorem are [53]:

- The stability can be determined through knowledge of the transition matrix at the end of a single period ($\mathbf{\Phi}(T,0)$).
- The solution of the homogeneous system at any time can be determined with knowledge of the transition matrix over a single period ($\mathbf{\Phi}(t,0)$ with $0 \leq t \leq T$).

In the remainder of this section, above consequences are derived and discussed in greater depth. Moreover, stability criteria are given.

Definitions

Due to periodicity of the system matrix, Equation 8.8 yields that the transition matrices across a period T are related through a constant non-singular matrix $\mathbf{C}$.

$$\mathbf{\Phi}(t+T,t_0) = \mathbf{\Phi}(t,t_0)\mathbf{C} \tag{8.9}$$

Using Equation 8.7, we can define that this matrix $\mathbf{C}$ must be related to the transition matrix at the end of a single period, called the *growth matrix*. Moreover, we define a constant matrix $\mathbf{R}$ as is given in Equation 8.10. Where, for notational simplicity $\mathbf{\Phi}_0(t)$ denotes $\mathbf{\Phi}(t,t_0)$ with $t_0 = 0$ and $\mathbf{x}(t_0) = \mathbf{x}_0$.

$$\mathbf{\Phi}_0(T) = \boldsymbol{C} \equiv \exp(\mathbf{R}T) \tag{8.10}$$

Moreover we define that there exists a non-singular matrix $\mathbf{P}(t)$ that relates the transition matrix to the constant matrix $\mathbf{R}$ as in Equation 8.11. It can be shown that this matrix $\mathbf{P}(t)$ also is periodic with period T.

$$\mathbf{\Phi}_0(t) \equiv \mathbf{P}(\mathbf{t})\exp(\mathbf{R}t) \tag{8.11}$$

It is important to note that $\mathbf{R}$ only defines the system at the end of each period T. Only at these instances the solution of $\mathbf{x}$ can be computed directly, as $\mathbf{P}(t)$ cannot be proven to equal identity at other instants. Therefore, it does not describe the response at other instants. Hence, the matrix may not correspond to the approximate or average system of $\mathbf{A}(t)$.

Stability

Using these definitions, we can rewrite the solution of the homogeneous system as

$$\mathbf{x}(t' + sT) = \mathbf{\Phi}_0(t')\mathbf{\Phi}_0(T)^s\mathbf{x}_0 \tag{8.12}$$

where s denotes the number of complete periods and $0 < t' < T$. Looking at Equation 8.12 it clear that the growth matrix, or the constant matrix $\mathbf{R}$, define stability. The n-distinct eigenvalues of the growth matrix, Λ_i, are called the *characteristic multipliers*. The n-distinct eigenvalues of $\mathbf{R}$, λ_i, are called the *characteristic exponents*. These two are related according to equation 8.13.

$$\Lambda_i = \exp(\lambda_i T) \tag{8.13}$$

The criteria for global asymptotic stability (GAS) are given by Equation 8.14.

$$|\Lambda_i| \leq 1 \; or \; Re(\lambda_i) \leq 0 \text{ for } i = 1, 2, ..., n \tag{8.14}$$

Performance

As stated before, full knowledge of the transition matrix over a single period provides the solution at any time instant. Though, analysing the performance of a certain system with knowledge of the transition matrix, without obtaining the full time-domain solution, may prove difficult.

The growth matrix, or the matrix $\mathbf{R}$, only describe $\mathbf{x}$ at $t = sT$. Therefore, its eigenvalues may not represent the average system of $\mathbf{A}(t)$. Moreover, in case of MDoF systems eigenvalues may be hard to relate to physical properties, like equivalent damping. Lastly, the modulation period T may be unrelated to the natural period(s) of the system. Looking at the states at time sT may not represent a full cycle of a certain state.

8.2.3 Approximation of the transition matrix

One of the most straightforward method for computing the growth matrix has been proposed by Hsu [54]. Additional overviews of this method and more practical applications have also been provided in literature [51] [55].

The periodic continuous, or piecewise continuous, system $\mathbf{A}(t)$ is approximated through a series of step functions. The period T is discretised into K parts with a constant matrix $\mathbf{A}_k$. In Figure 8.1 a visual representation is given in case just a single parameter is periodic.

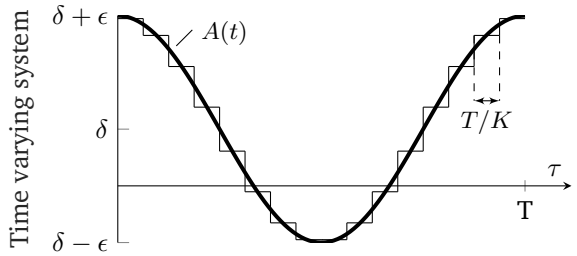

Figure 8.1: Discretised system matrix $\mathbf{A}(t)$ over period T with a single periodic parameter.

The constant system $\mathbf{A}_k$ is computed according to Equation 8.15, which is in essence just the average of $\mathbf{A}(t)$ over time interval Δ_k which is defined between t_{k-1} and t_k.

$$\mathbf{A}_k = \frac{1}{\Delta_k} \int_{t_{k-1}}^{t_k} \mathbf{A}(s) ds \tag{8.15}$$

Thus, the system from Equation 8.1 is approximated by Equation 8.16. Where, the discrete $\mathbf{A}_k$ is put in a piecewise continuous form through a summation of heaviside step functions as in Equation 8.17. The subscript A indicates an approximate solution.

$$\dot{\mathbf{x}}_A(t;k) = \mathbf{A}(t;k)\mathbf{x}_A(t;k) \tag{8.16}$$

$$\mathbf{A}(t;k) = \sum_{m=-\infty}^{\infty} \sum_{k=1}^{K} \mathbf{A}_k \left[U(t - sT - t_{k-1}) - U(t - sT - t_k) \right] \tag{8.17}$$

The theory for linear time-invariant (LTI) systems allows us to write the general solution of a first order system as in Equation 8.18. Where the exponential is the matrix exponential, which is computed through the power series expansion given in Equation 8.19.

$$\mathbf{x}(t) = e^{\mathbf{A}t}\mathbf{x}(0) \tag{8.18}$$

$$e^{\mathbf{A}t} = \sum_{n=0}^{\infty} \frac{1}{n!}(\mathbf{A}t)^2 = \mathbf{I} + \mathbf{A}t + 0.5\mathbf{A}^2t^2 + O(3) \tag{8.19}$$

Using the general solution for the discrete system in Equation 8.16, the approximate solution during a single period can be written according to Equation 8.20 and Equation 8.21. By evaluating the transition matrix up to $k = K$, the growth matrix is obtained. Floquet theorem can be used for analysis, though its accuracy depends on various factors.

As $K \to \infty$ the approximate transition matrix goes to the actual solution [54]. For a piecewise continuous system $\mathbf{A}(t)$, errors solely depend on the Taylor series in Equation 8.15. For a continuous system $\mathbf{A}(t)$, errors are of the order $O(\Delta^2)$ [54].

$$\mathbf{x}_A(t';k) = \mathbf{\Phi}_A(t';k)\mathbf{x}(0) \tag{8.20}$$

$$\mathbf{\Phi}_A(t';k) = e^{\mathbf{A}_k\Delta_k}e^{\mathbf{A}_{k-1}\Delta_{k-1}}...e^{\mathbf{A}_1\Delta_1} \tag{8.21}$$

$$\text{where } 0 \leq t' \leq T \tag{8.22}$$

8.3 Modulation of Single DoF systems

To further strengthen the understanding of periodic LTV systems, Floquet's theorem is applied to SDoF second order differential equations. The main advantage of these SDoF systems, is that the fundamental matrix can be obtained analytically and does not require the use of the matrix exponential. Moreover, obtained results are more general and can be compared with literature. The main disadvantage is that the results may be too general and not applicable to actual dynamical systems.

Firstly, in Section 8.3.1, stiffness is modulated in a discrete manner. The main purpose is comparison of the numerical method with literature. Afterwards, in Section 8.3.2, damping is modulated. The main purpose is to study modulation of damping in general. Both SDoF systems do not represent the physical behaviour of the AO-TLCD.

8.3.1 Stiffness modulation

One of the most commonly studied periodic differential equation is 'Hill's equation'. It can represent a variety of physical phenomena including an (inverted) pendulum with vertical excitation of its hanging point. The EoM is given by Equation 8.23, where the time-scale τ is normalized based on the modulation frequency. Furthermore, the squared frequency ratio δ, the normalized damping ratio γ and the modulation depth ϵ are introduced.

$$\ddot{x} + \gamma\dot{x} + (\delta + \epsilon p(\tau))x = 0 \tag{8.23}$$

$$p(\tau + 2\pi) = p(\tau) \tag{8.24}$$

$$\tau = 2\Omega t\ ,\ \gamma = 2\zeta\omega/2\Omega = \zeta\delta\ ,\ \delta = (\omega/2\Omega)^2\ ,\ \epsilon = (k^*/m2\Omega)^2 \tag{8.25}$$

Depending on the modulation shape $p(\tau)$ and the depth of modulation ϵ, different methods can be applied to analyse the stability.

Meissner's equation

A special form of Hill's equation is Meissner's equation. It assumes a piecewise modulation shape as is given by Equation 8.26 and illustrated in Figure 8.2. In this form, the growth matrix can be obtained analytically with relative ease.

$$p(\tau) = sgn(cos(\tau)) \tag{8.26}$$

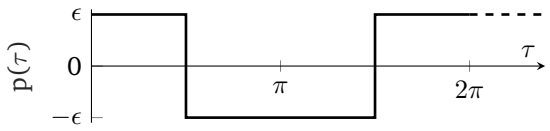

Figure 8.2: Shape of modulation signal $p(t)$ of Meissner's equation.

The system can be described by two time invariant systems, with different constants. Their first order form is given in Equation 8.27. Here $\mathbf{A}^+$ and $\mathbf{A}^-$ represent the system for positive and negative modulation, respectively.

$$\mathbf{A}^{\pm} = \begin{bmatrix} 0 & 1 \\ -(\delta \pm \epsilon) & -\gamma) \end{bmatrix} \tag{8.27}$$

The general solution is given by Equation 8.28. Here $r_{1,2}$ represent the complex roots, or eigenvalues, of Equation 8.27. These can be obtained directly from the second order form or through solving the eigenvalue problem of the first order system.

$$x(t) = c_1 \text{exp}(r_1 t) + c_2 \text{exp}(r_2 t) \tag{8.28}$$

As explained in section 8.2.2 one can use the eigenvectors as independent solutions to form the fundamental matrix and subsequently compute the transition matrix. Alternatively, Equation 8.28 can be solved for a unit displacement and unit velocity separately. In this manner, the transition matrix can be found directly.

In Equation 8.29, these two solutions are indicated by x_i with $i = 1, 2$ each having their own solutions c_{1i} and c_{2i} to the initial value problem. To complete the set, $\dot{x}_i$ is obtained through differentiation. Δt is the time interval over which $\mathbf{A}^+$ and $\mathbf{A}^-$ act. The full derivation can be found in Appendix A.6.

$$\mathbf{\Phi}_0^{\pm}(t) = \begin{bmatrix} x_1 & x_2 \\ \dot{x}_1 & \dot{x}_2 \end{bmatrix} = \begin{bmatrix} c_{11}\text{exp}(r_1\Delta t) + c_{12}\text{exp}(r_2\Delta t) & c_{21}\text{exp}(r_1\Delta t) + c_{22}\text{exp}(r_2\Delta t) \\ c_{11}r_1\text{exp}(r_1\Delta t) + c_{12}r_2\text{exp}(r_2\Delta t) & c_{21}r_1\text{exp}(r_1\Delta t) + c_{22}r_2\text{exp}(r_2\Delta t) \end{bmatrix} \tag{8.29}$$

$$\text{where: } c_{11} = \frac{r_2}{r_2 - r_1}\ ,\ c_{12} = -\frac{r_1}{r_2 - r_1}\ ,\ c_{21} = \frac{1}{r_1 - r_2}\ ,\ c_{22} = -\frac{1}{r_1 - r_2}$$

The growth matrix can be obtained through multiplication of the fundamental matrices over a half period. Logically, these two fundamental matrices each depend on their own set of eigenvalues in case $\epsilon > 0$.

$$\mathbf{\Phi}_0(T) = \mathbf{\Phi}_0^+(0.5T)\mathbf{\Phi}_0^-(0.5T) \tag{8.30}$$

The stability diagram is given in Figure 8.3 for different damping values. Here, some unstable regions are indicated by U. Existence of instability 'pockets', indicated by U^*, depends on damping. The results agree with other methods found in literature [56]. The origins of the stability 'tongues' correspond to $\omega = n * \Omega$ with $n = 0, 1, ..., i$. Additional damping mainly reduces instabilities that occur at low modulation depth.

8.3.2 Damping modulation

In an analogous manner, modulation of the dissipative term in Equation 8.23 can be investigated. By studying Equation 8.31, some conclusions can be drawn on damping modulation in general. These conclusions can be extended to semi-active damping control of MDoF systems.

$$\ddot{x} + (\gamma\dot{x} + \epsilon p(\tau)) + \delta x = 0 \tag{8.31}$$

$$p(\tau + 2\pi) = p(t) \tag{8.32}$$

$$\tau = 2\Omega t\ ,\ \gamma = \zeta\delta\ ,\ \delta = (\omega/2\Omega)^2\ ,\ \epsilon = \Delta\zeta \cdot \delta \tag{8.33}$$

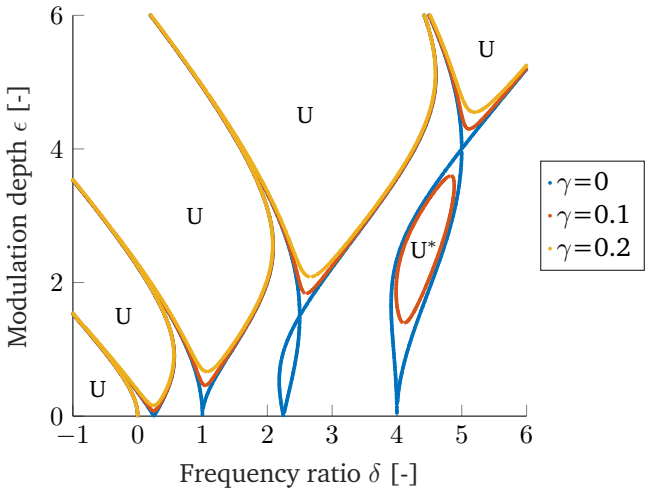

Figure 8.3: Stability chart for Meissner's equation with variable damping.

For a sinusoidal shape of $p(\tau)$, analytical and numerical approximations exist in literature. The main result is that "instability is possible in a system for which the average dissipation is positive"[57]. However, a system can only become unstable in case damping is negative over at least part of the cycle. The latter statement is quite obvious, as without negative damping, no energy can be introduced through the parametric forcing term.

The limit of the modulation depth, for which the system becomes unstable, depends on the shape of the modulation signal $p(\tau)$. For a sinusoidal shape, the system is unstable for $\epsilon > 2\gamma$ at the most critical modulation frequency $\delta = 0.25$ [57][58].

For an on average undamped system, instabilities only originate from uneven modulation frequency ratios ($\omega = n\Omega$ with $n = 1, 3, ...$) [58].

Analogous to the previous section, stability curves for square modulation are obtained and can be found in Figure B.2. Furthermore, the relation for a sinusoidal shape have been duplicated using Equation 8.29 using the approach illustrated in Figure 8.1.

8.4 Semi-active AO-TLCD

Proper analysis of the behaviour of the semi-active AO-TLCD requires more degrees of freedom. Attempting to obtain an equivalent SDoF system with damping/stiffness modulation will be an unfruitful exercise. The system will be too specific to make general statements and to simplistic to ensure representation of the AO-TLCD.

In this section the semi-active AO-TLCD is simplified to a MDoF periodic LTV system and analysed for its stability and performance using the numerical approximation method given in Section 8.2.

Homogeneous periodic LTV form of the AO-TLCD

As mentioned before, modulation of stiffness does not represent the AO-TLCD. The restoring force of the gas-spring is contained in an additional degree of freedom. With respect to the liquid, the equivalent additional 'spring element' will depend on the closing moment. This has been visualized with an equivalent system in Figure 8.4, where u_c is the fluid displacement at the moment of closing. Hence, the restoring force for this representative system will depend on the relative displacement $u_{gas} = u_f - u_c$.

Moreover, free modulation of the damping is also not applicable to the semi-active system. Negative damping values can't be obtained through semi-active actuators like valves. Consequently, the additional damping c^*, will always be larger than zero.

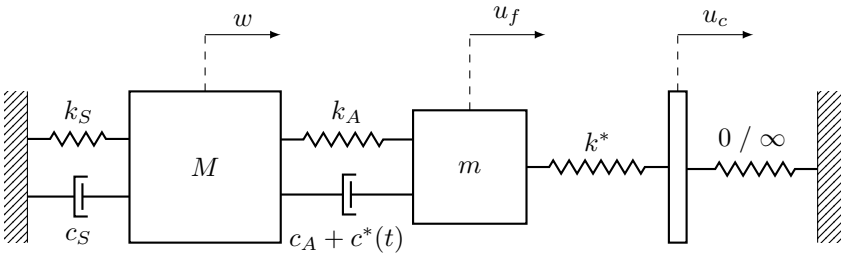

Figure 8.4: Diagram of the periodically varying LTV semi-active AO-TLCD.

The on/off control, can be simplified to a square modulation signal. Both k^* and c^* are assumed to switch between zero and its maximum value. The resulting modulation signal $p(t)$ is shown in Figure 8.5. Here, the duty cycle D is the modulation width w normalized by the period T. The signal is shown for a duty cycle of 30% over two modulation periods.

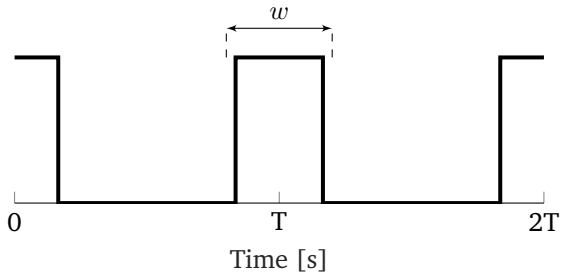

Figure 8.5: Square modulation signal over two modulation periods with $D = 0.3$.

With these definitions the linear system from Equation 5.6 can be transformed to the desired form in Equation 8.34. For simplicity the opposite modulation signal is denoted as $p_-(t) = 1 - p(t)$. Looking at the pressures, the gas spring and the massflow are switched on and off intermittently by the modulation depth ω_A^{2*}. To ensure instantaneous decoupling of the gas-spring, the reaction force is also modulated. Lastly, the damping modulation depth ζ_A^* is in essence the resistance of the 'open' gas system.

$$\dot{\mathbf{x}} = -\mathbf{M}^{-1} \begin{bmatrix} 0 & 0 & 0 & -1 & 0 \\ 0 & 0 & 0 & 0 & -1 \\ 0 & 0 & |\omega_A^{2*}|\rho_f L_{eff} \frac{K_{oi}}{A_H \rho_0} \cdot p_-(t) & 0 & -\omega_A^{2*} \rho_f L_{eff} \cdot p(t) \\ \omega_S^2 & 0 & 0 & 2\zeta_s \omega_s & 0 \\ 0 & \omega_A^2 & \omega_A^{2*} \cdot p(t) & 0 & 2\omega_A \left(\zeta_A + \zeta_A^* \cdot p_-(t)\right) \end{bmatrix} \mathbf{x} \tag{8.34}$$

Without modulation, e.g. a duty cycle equal to zero or one, the transient response of the LTV model is identical to that of the non-linear model. For the SA AO-TLCD, the response of the on/off C-LQR AO-TLCD can be described with reasonable accuracy. In Appendix B.2.2, Figure B.3, a time-domain comparison can be found for an unit initial displacement of the host.

Modulation of the AO-TLCD

In Chapter 7, the SA AO-TLCD was controlled by two sub-optimal schemes resulting in quasi-periodical modulation. Moreover, only one design was used for the gas system. In this section we will modulate the homogeneous LTV system from Equation 8.34 for a broader range of variables. These variables, and some additional assumptions, can be found in Table 8.1.

The main variables are the duty cycle D and the modulation depth. The duty cycle, represents all closing cycles between fully open and fully closed. The modulation depth ω_A^{2*}, related to the air spring stiffness, is evaluated up to negative values in order to assess the limits of the system in terms of stability.

Especially for the evaluation of the performance, the phase t_ϕ of the modulation signal may be of importance. For the whole range of phase shifts, the worst and best case scenario are extracted in terms of stability and performance, respectively. This will be explained later in more detail.

The modulation frequency is set to two times the host natural frequency ($\delta = 0.25$). Typically this is the most critical modulation frequency with respect to stability. Furthermore, this corresponds to the semi-active control defined in Chapter 5. At different modulation frequencies, the system is in all likelihood more stable with respect to parametric resonance and less optimal in terms of performance. Ill-design of the controller, i.e. deviating modulation frequencies, enhances the dissipative nature of the AO; further increasing the stability.

From the SDoF results in Section 8.3.2, we can conclude that positive modulation of damping will not increase instabilities. Therefore, the modulation depth of the damping is assumed to be constant and equal to 50% of the internal TLCD damping, corresponding to the fully open valves in the case study.

Table 8.1: Variables and constants used in the stability and performance analysis of the LTV SA AO-TLCD.

Name	Variable	Range	Units
Modulation depth stiffness	ω_A^*/ω_A	[-1 10]	[-]
Duty cycle	D	[0 1]	[-]
Modulation signal phase	t_ϕ	[0 T]	[s]
Modulation frequency	δ	0.25	[-]
Modulation depth damping	ζ_A^*/ζ_A	0.5	[-]

Evaluation of stability and performance

With the representative periodic LTV model and the modulation parameters defined, we still need to define the evaluation of the system. An overview of the computational procedure can be found in Figure 8.6.

For all combinations of variables listed in Table 8.1, the growth matrix $\mathbf{\Phi}_0(T)$ is obtained. Stability can be evaluated directly from the characteristic multipliers using Equation 8.14.

As mentioned in Section 8.2.2, evaluation of the performance is less straightforward. States have a combined response, i.e. the system has its own set of modes. One cannot assume that states respond with the same frequency as they would individually. As a consequence, the states will not be at a constant phase at $t = sT$ where the response can be computed. To overcome this, the total mechanical energy E in the system is computed at $t = sT$. For this, the response is computed for an initial unit displacement of the host structure. In Appendix B.2.2, Figure B.4, this is visualized through the comparison of a time-domain solution obtained using the complete transition matrix, and the periodic solution obtained with the growth matrix.

The host time-domain response is not known. Therefore, the approach of finding the equivalent structural damping used in the first two parts of this research, cannot be applied. Instead the dissipated energy over s cycles is matched with the dissipated energy for a SDoF host structure. For this the general solution for a unit displacement and its derivative are used, listed in the first column of Equation 8.29.

Results

The stability and performance is shown in Figure 8.7. Here, the duty cycle is plotted on the x-axis. Where, $D = 0$ and $D = 1$ represents the fully open and closed system, respectively. The y-axis indicates the depth of modulation, i.e. the normalised gas-spring stiffness. Unstable regions are indicated by black.

For the stable regions the equivalent structural damping, i.e. the effectiveness, is plotted in % critical. Points corresponding to the two passive TLCD set-ups are indicated. Lastly, the depth of modulation

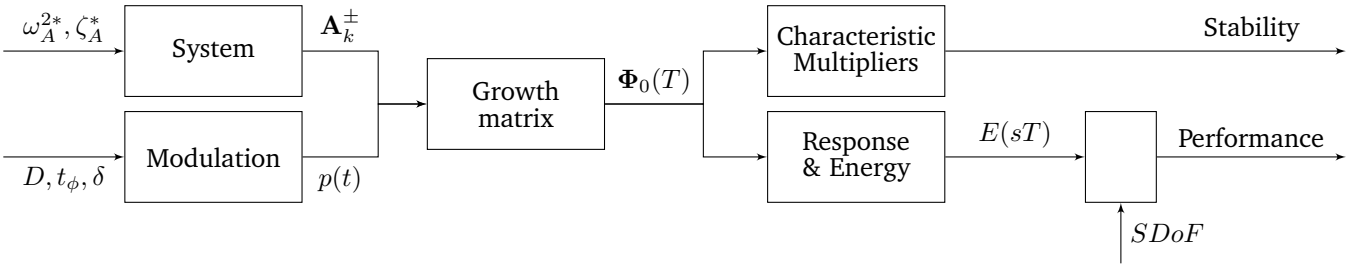

Figure 8.6: Computational procedure stability and performance of the homogeneous LTV SA AO-TLCD.

corresponding to the gas-spring stiffness in the case study is given. Duty cycles observed in the case study for the semi-active damper can be found in Figure B.7. For load case III, 50% of the case study duty cycles lie within 0.4 and 0.5.

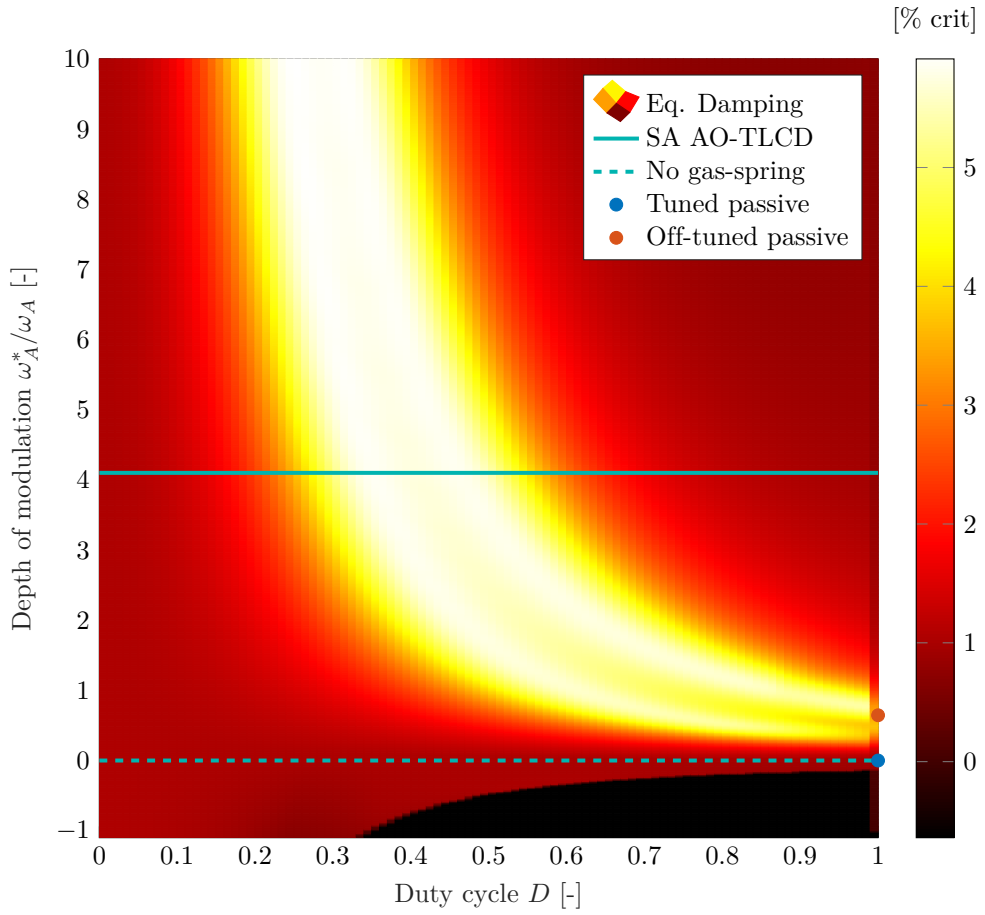

Figure 8.7: Stability and performance of the periodical LTV system.

In Table 8.2, specific points corresponding to the benchmark solutions of the TLCD can be found. The results are almost identical to Table 7.1. In Appendix B.2.2, Figure B.5, one can find a cross section of Figure 8.7 at $D = 1$, corresponding to the passive TLCD without additional air system damping. Furthermore, cross sections are included in Figure B.6 for a modulation depth equivalent to zero and to the SA AO-TLCD used in the case study.

Table 8.2: Effectiveness of the LTV system at specific points corresponding to passive AO-TLCD settings.

Meaning	Duty cycle [-]	Modulation depth [-]	Effectiveness [% crit]
No TLCD	1	High	0.64
Passive off-tuned	0	Any	1.04
Passive tuned	0	0.46	3.66

8.5 Discussion

Below the results from this chapter are discussed with the main focus on the comparison with the case study results and the link to the physical device.

Stability of the SA AO-TLCD

In Figure 8.7, it can be seen that instabilities do not occur for positive modulation, i.e. for positive gas-spring stiffness. This is expected for a semi-active system, i.e. a system that cannot increase mechanical energy through its actuators.

For the actual damper, a negative gas-spring stiffness cannot be obtained. Inclusion of the TLCD's non-linear damping improves stability. Different modulation frequencies result in less parametric resonance and may result in large amounts of dissipation in the gas system due to improper control of the AO. Lastly, the damping is always positive throughout its modulation and therefore it cannot result in an unstable system.

Hence, it can be concluded that the semi-active AO-TLCD indeed is inherently stable.

Performance of the SA AO-TLCD

In Figure 8.7, regions exist with larger effectiveness than were obtained with the semi-active control laws. However, differences are small when one considers reduction of host vibrations instead of equivalent damping. Still, more optimal and advanced control schemes may provide additional 'buffers' for losses due to actuator dynamics, limited sensor input and unmodelled dynamics.

Sensitivity of the SA AO-TLCD

From Figure 8.7 one can also conclude that the damper is not sensitive to its specific AO design. Increased performance can be obtained for any positive gas-spring stiffness. A single AO design is effective over quite a broad range in terms of closing cycles.

Required modelling detail

Similar results were obtained compared to the OWT installation case study. The periodic LTV model, or an inhomogeneous variant, may be sufficient for the evaluation of the semi-active damper's general performance. Though, due to the constant modulation, its applicability is limited.

In case of stochastic excitation or more advanced controller implementation, constant modulation will not represent actual control of the valves. Still, in these cases, a non-periodic inhomogeneous LTV model may be sufficient.

For more detailed actuator implementation or precise evaluation of the effect of the damper; the non-linear model is required.

Chapter 9

Conclusions and Recommendations

The main goal of this thesis was: *'reduction of wave-induced vibrations during OWT installation by a novel non-invasive strategy for period adjustment of off-tuned TLCDs'*. In Chapter 2, consideration of modification methods for TLCDs including OWT constraints resulted in a new period adjustment strategy; the Airflow Obstructed TLCD. In the remainder of the research, this strategy was investigated and developed. The work was structured into two parts:

1. Development and validation of a passive stand-alone AO-TLCD model.
2. The performance of a semi-active AO-TLCD and its application to OWT installation.

In Section 9.1, the conclusions are given according to the thesis its structure. Afterwards, some recommendations are made in Section 9.2 regarding the use of the AO-TLCD and future work on its development.

9.1 Conclusions

In this section, the conclusions from this research are summarized, including important observations. These are further structured into separate paragraphs. Each paragraph ends with one of the main conclusion of this research.

9.1.1 Part I: passive (stand-alone) AO-TLCD

The conclusions from part I fulfil the first two sub-objectives of this research: '*development and validation of a simple numerical model*' and '*investigation of the dynamical behaviour of the passive AO-TLCD*'. Moreover, a potential application of the passive AO-TLCD is discussed.

Modelling of the passive AO-TLCD In Chapter 3, a numerical model was developed for the stand-alone AO-TLCD. To allow for numerically efficient and insightful analyses, the goal was to develop a simplistic model describing the gas dynamics of the AO-TLCD. Based on literature on TLCGDs, pressures were computed through polytropic relations. Empirical relations were used for the pressure losses in the quasi-steady massflow. Both compressible and incompressible flow were analysed.

For the operational conditions of the AO-TLCD, simplified forms of the massflow and pressure equations have differences smaller than 10% compared to their fully non-linear and incompressible counterparts. in In Section 4.2, the model was validated to accurately predict the steady-state response of the passive AO-TLCD using small-scale experimental data. Hence, the use of a simplified model for the AO-TLCD is justified.

Dynamical behaviour of the passive AO-TLCD In Section 4.3.1 it was shown that passive AO can have a large influence on both the TLCD's stiffness and damping – although, not independently. A close relation exists between the magnitude of the pressures and its phase-lag with the liquid displacements.

As a result of this dependency, adjustment to off-tuned frequencies introduces large amounts of viscous dissipation into the system; effectively reducing the restoring force. Therefore, period adjustment using passive airflow obstruction is not possible while maintaining significant effectiveness of the TLCD with respect to the host.

Application of the passive AO-TLCD Typically, regular TLCDs require detailed design on the internal resistance of the fluid compartment in order to achieve the required internal damping. For low obstruction, a large influence of the AO-TLCD on the internal damping of the TLCD was observed; without affecting other properties of the system. Hence, passive airflow obstruction can be used as an alternative design parameter for internal damping of a regular TLCD.

9.1.2 Part II: Semi-active AO-TLCD for OWT installation

The conclusions from part II of this research, fulfil the third and fourth sub-objectives of this research: '*robust period adjustment of the AO-TLCD*' and '*evaluation of the effect of the AO-TLCD on installation workability*'. To further fulfil sub-objective three, conclusions from Chapter 8, investigation of the SA AO-TLCD through a periodic linear time-variant (LTV) systems framework, are included. Lastly, the main goal of this research is discussed.

Passive TLCDs for an installation casestudy In Chapter 6, an OWT installation case study is defined for a realistic deep-water site. Overlap of the support structure's natural frequency with highly probable wave spectra, resulted in workability reductions as high as 50%.

For this case study, the effectiveness of a passive TLCD designed for the operational life of an OWT was evaluated in Section 6.4. In accordance with estimations in Chapter 2, damping was only increased up to 6% LogDec, resulting in insufficient improvement of the installation workability. Hence, modifications of the off-tuned TLCD are required during next-generation OWT installation.

Semi-active AO-TLCD for period adjustment In order to increase the effectiveness of the damper, the AO is controlled semi-actively. In Chapter 5 it is defined that proper semi-active control of the damper involves minimizing the viscous dissipation of the AO-TLCD; i.e. the massflow. Based on literature on semi-active VAs, two sub-optimal on/off control laws were defined: simplistic hybrid control and clipped-LQR. In Section 7.2 it can be seen that both laws indeed result in minimal massflow.

In Chapter 7 the semi-active damper's performance was evaluated for the installation case study. For both control laws, the SA AO-TLCD was able to reduce wave induced tower-top displacements by up to 60% for critical installation load cases. The semi-active damper out-performed its optimally tuned passive counterpart by more than 10%. It can be concluded that semi-active AO is an effective strategy for period adjustment.

Periodic linear time-variant systems framework The inherent stability of the semi-active damper was further demonstrated in Chapter 8. Moreover, in Figure 8.7 similar results were obtained for the LTV model, in terms of the equivalent structural damping, compared to the case study. The performance of the two control laws are close to optimal, especially with respect to host vibration reduction.

For general evaluation of the SA AO-TLCD its performance, an inhomogeneous time-domain form of the LTV model may be sufficient. Though, for complex actuator or controller implementation the non-linear model is required.

Improvement installation workability with SA AO-TLCDs In Figure 7.5 it was demonstrated that, the semi-active AO-TLCD is effective in reducing host vibrations, independent of its passive natural frequency. Furthermore, low actuator speeds were not detrimental to the AO-TLCD its effectiveness. Results from Chapter 8 further demonstrate the robustness of the proposed strategy.

Thus we can conclude that the semi-active AO-TLCD can be sufficiently effective in reducing wave-induced vibrations over the whole OWT installation and operational frequency range.

9.2 Recommendations

For deep water sites and next-generation turbines with installation frequencies around highly probable sea states, the implementation of semi-active AO is recommended. However, further development of the concept is required before the SA AO-TLCD can be successfully deployed. Below some recommendations are made regarding this future work.

Even though improvements are not sufficient, until the full development of the semi-active AO-TLCD has been completed, temporary placement of passive airflow obstruction is recommended. As it is a cost-effective approach for increasing the effectiveness of the damper during installation phases.

- Experimental validation of the proposed semi-active AO-TLCD is required. Most importantly, unmodelled dynamics that are potentially introduced through semi-active control of the valves, should be investigated. For this, proper scaling of the AO in the experimental design will be key.
- Robust controller design, using more realistic sensor data, should be investigated for the semi-active AO-TLCD. This includes both the use of state-estimation, as the inclusion of sensor-noise on the measurements.
- More advanced control strategies should be deployed to determine optimal semi-active control of the AO-TLCD. Most importantly, the control strategy should include the semi-active bounds of the AO-TLCD. This 'optimal' semi-active control of the AO-TLCD is required to either improve performance or to further justify the use of the 'sub-optimal' control schemes proposed in this research.
- The use of semi-active AO-TLCDs during operational life, to decrease excitation dependencies and to reduce specific critical load case scenarios may prove beneficial. Though, investigation of the general feasibility may be required first, including the practical considerations; namely, the additional demands on components and the effects on the TLCD its reliability.

Appendices

Appendix A

Methods

A.1 Energy considerations extended

In this research, the mechanical system is analysed using an energy perspective multiple times, to obtain more insight into its behaviour. This perspective is explained further in this section. First, the energy balance of the dynamical system is given. Afterwards, equations for equivalent parameters are given. Lastly, some of those equations are solved for specific cases assuming a linear harmonic response. For simplicity, the liquid displacement is denoted without its subscript f.

A.1.1 Energy balance

Assuming a stationary stochastic input and ergodicity the expectation of energy flow becomes the time average of the product of the force and velocities over a number of periods. Alternatively this can be viewed as the time derivative of the work done by a general force. Where the work done is the integration of a force over its displacement path.

$$m \cdot E\left[f\left(t\right)\dot{x}\left(t\right)\right] = m \cdot \int_0^{nT} f\left(t\right)\dot{x}\left(t\right)dt = m \cdot \frac{\delta}{\delta t}\left(\int f(t,x)dx\right) \tag{A.1}$$

For the host and TLCD the energy balance is given as:

$$E\left[\left(1+\mu\right)\ddot{w}\dot{w}\right] + E\left[2\zeta_S\omega_s\dot{w}\dot{w}\right] + E\left[\omega_s^2 w\dot{w}\right] = -E\left[\mu\kappa\ddot{u}\dot{w}\right] \tag{A.2}$$

$$E\left[\ddot{u}\dot{u}\right] + E\left[\delta_L|\dot{u}|\dot{u}^2\right] + E\left[\frac{\Delta p}{\rho_f L_{eff}}\dot{u}\right] + E\left[\omega_A^2 u\dot{u}\right] = -E\left[\kappa\ddot{w}\dot{u}\right] \tag{A.3}$$

For a system in steady state the expectation of the change of kinetic and potential energy must equal zero. This becomes especially clear for the harmonically excited linear system in Equation A.11 for a phase-lag equal to 0 and 180 degrees.

$$\begin{gathered} E\left[\ddot{u}\dot{u}\right] = E\left[u\dot{u}\right] = E\left[\ddot{w}\dot{w}\right] = E\left[w\dot{w}\right] \approx 0 \\ E\left[2\zeta_S\omega_s\dot{w}\dot{w}\right] = -E\left[\mu\kappa\ddot{u}\dot{w}\right] \\ E\left[\delta_L|\dot{u}|\dot{u}^2\right] + E\left[\frac{\Delta p}{\rho_f L_{eff}}\dot{u}\right] = -E\left[\kappa\ddot{w}\dot{u}\right] \end{gathered} \tag{A.4}$$

A.1.2 Equivalent (non)-linearisation

Equivalent parameters can be found which match the same dissipative- and/or potential energy as the non-linear terms in the dynamical system [59].

$$E\left[\mu\kappa\ddot{u}\dot{w}\right] \rightarrow \Delta\zeta_S$$

$$E\left[\frac{\Delta p}{\rho_f L_{eff}}\dot{u}\right] \rightarrow \Delta\zeta_A,\ \Delta\omega_A$$

For the host, the additional equivalent linear structural damping can be described as:

$$\Delta\zeta_s = \frac{\mu \cdot E\left[\ddot{u}\dot{w}\right]}{2\omega_s \cdot E\left[\dot{w}^2\right]} \tag{A.5}$$

For the TLCD, the additional equivalent damping can be described as:

$$\Delta\zeta_A = \frac{E\left[\Delta p\dot{u}\right]}{\rho_f L_{eff} 2\omega_A E\left[\dot{u}^2\right]} \quad or \quad \Delta\delta_L = \frac{E\left[\Delta p\dot{u}\right]}{\rho L_{eff} E\left[|\dot{u}|\dot{u}^2\right]} \tag{A.6}$$

For the TLCD the regular linear damping can be described as:

$$\zeta_A = \frac{E\left[\delta_L|\dot{u}|\dot{u}^2\right]}{2\omega_A E\left[\dot{u}^2\right]} \tag{A.7}$$

For the TLCD the additional equivalent stiffness can be derived by the potential energy, V, stored and released during a cycle of a force (that has no net energy flow) [59]. For a force, which is partly dissipative the equivalent frequency can be found by Equation A.9. Here t_i indicate the quarter cycle times, i.e. the zero crossings and peak displacements of the liquid.

$$4V = \int_0^{u_{max}} f\left(u\right) du - \int_{u_{max}}^0 f\left(u\right) du + ... = \sum_1^4 |\int_{t_i}^{t_{i+1}} f\left(u\right) \dot{u} dt| \tag{A.8}$$

$$4V = \int_0^T |\Delta\omega_A^2 u\dot{u}| dt = \sum_1^4 |\int_{t_i}^{t_{i+1}} \frac{\Delta p}{\rho_f L_{eff}}\dot{u} dt| - \int_0^T \frac{\Delta p}{\rho_f L_{eff}}\dot{u} dt \tag{A.9}$$

A.1.3 Harmonic linear response

Equations listed in the previous paragraph can be solved partially in case the response is known. For a linear response to a stationary harmonic excitation the energy flow simplifies to Equation A.11. Where ϕ indicates the phase-lag between the force $f(t)$ and the displacements u.

$$u(t) = U_0 cos(\omega t) \tag{A.10}$$

$$E\left[f\left(t\right)\dot{u}\left(t\right)\right] = \int_0^T F_0 cos\left(\omega t + \phi\right) \cdot U_0 \omega sin\left(\omega t\right) dt = 0.5 F_0 U_0 \omega \left[-sin\left(\phi\right) + \int_0^T sin\left(2\omega t + \phi\right) dt\right] \tag{A.11}$$

TLCD damping

Using Equation A.11, Equation A.7 can be solved resulting in the harmonic linearisation as in Equation A.12 [5] [18].

$$\zeta_A = \frac{4}{3\pi}\frac{\omega}{\omega_A} U_0 \delta_L \tag{A.12}$$

Low-obstruction

The pressure difference across the reservoirs is assumed to be negligible. As a consequence, we may assume the gas flows freely and in phase with the liquid velocities. Contradictory, it is still assumed losses occur due to this flow. This results in a relation for the pressure losses due to the gas flow as a function of the liquid velocities.

$$\Delta p \approx 0.5 \rho_0 K_j \left(\frac{\dot{u}}{n_v, j \beta_j^2} \right)^2 \tag{A.13}$$

(A.14)

Using Equation A.11 the non-linear form of Equation A.6 can be solved now the flow-speeds are known.

$$\Delta \delta_L = \frac{\rho_0}{2} \frac{K_j}{n_v, j^2 * \beta_j^4} \frac{1}{L_{eff} \rho_f} = \frac{K_O^2}{L_{eff} \rho_f} \tag{A.15}$$

A.2 Derivation spring-element concept

For a massless piston, with a linear spring stiffness k_p equation we can assume that the piston displacement u_p is linearly dependent on the liquid displacements u_f. As a result, the pressures can be approximated by Equation A.16.

$$\Delta p = \frac{N_c n p_0}{V_0}(A_H u_f - A_p u_p) \tag{A.16}$$

Since both displacements are dependent on each other the work performed by such a pressure on the liquid and on the piston is:

$$E_p = 0.5\Delta p A_H u_f - 0.5\Delta p A_p u_p \tag{A.17}$$

As a consequence the full expression for kinetic and potential energy are given by:

$$E_k = 0.5\left(2\rho_f A_H H \left|\begin{matrix}0\\ \dot{u}_f\end{matrix}\right|^2 + \rho_f A_B B \left|\begin{matrix}\dot{u}_f\alpha\\ 0\end{matrix}\right|^2\right) \tag{A.18}$$

$$E_p = \rho_f g A_H(H^2 + u_f^2) + 0.5 N_c k_p u_p^2 + \frac{N_c n p_0}{V_0}\cdot 0.5(A_H^2 u_f^2 + A_p^2 u_p^2 - 2A_H A_p u_f u_p) \tag{A.19}$$

Using LaGrange, the coupled system is given by:

$$\ddot{u}_f + \delta_L|\dot{u}_f|\dot{u}_f + \frac{2g}{L_{eff}}u_f + \frac{1}{\epsilon\rho_f L_{eff}}(u_f - \frac{A_p}{A_H}u_p) = 0 \tag{A.20}$$

$$-\frac{A_p}{\epsilon}u_f + \frac{A_p^2}{\epsilon A_H}u_p + N_c k_p u_p = 0 \tag{A.21}$$

Rewriting gives:

$$\ddot{u}_f + \delta_L|\dot{u}_f|\dot{u}_f + \omega_A^2 u_f = 0 \tag{A.22}$$

$$\omega_A^2 = \frac{2g}{L_{eff}} + \frac{1-f_p}{\epsilon\rho_f L_{eff}} \tag{A.23}$$

$$u_p = f_p\frac{1}{\beta_p^2}u_f \tag{A.24}$$

Where

$$f_p = \frac{1}{1+\frac{V_0 k_p}{n p_0 A_p^2}} = \frac{1}{1+\frac{N_c k_p \epsilon}{A_H \beta_p^2}} \tag{A.25}$$

$$\epsilon^{-1} = \frac{N_c n p_0}{h_e f f} \tag{A.26}$$

$$\beta_p^2 = A_p/A_H \tag{A.27}$$

A.3 Extended review of gas dynamics

In this appendix, some additional equations regarding gas dynamics are given. In Section A.3.1 the laws of conservation are given in their general derivative form. The difference between the equations listed here and the steady 1D forms given in Section 3.2.1 can provide insight in the assumptions of Section 3.1.1. Moreover, to fully understand the physics behind concepts like compressibility, these derivative forms are required.

In Section A.3.3 the isentropic compressible flow equations are given. These flow equations are necessary to successfully apply the compressible flow equations in Section 3.2.2 to the AO-TLCD model.

A.3.1 Fundamental equations extended

In addition to Section A.3.1, the conservation laws are given below in their general derivative form. Here, spatial vectors are displayed in bold. For a more thorough review of the conservation laws and thermodynamics the interested reader is referred to Chapter 2 and Chapter 7 of Anderson respectively [25].

Algebra

The substantial derivative, which is a derivative for a moving control volume with velocity $\mathbf{v}$, is given by:

$$\frac{D}{Dt} = \frac{\partial}{\partial t} + \mathbf{v}\bigtriangledown \tag{A.28}$$

The divergence, which can be seen as a 3D spatial derivative, is given by

$$\bigtriangledown = \mathbf{i}\frac{\partial}{\partial x} + \mathbf{j}\frac{\partial}{\partial y} + \mathbf{k}\frac{\partial}{\partial z} \tag{A.29}$$

where $\mathbf{i}, \mathbf{j}, \mathbf{k}$ are unit vectors in the x-, y- and z-direction, respectively.

Laws of conservation

The conservation of mass is given by the continuity equation:

$$\frac{1}{\rho}\frac{\partial \rho}{\partial t} + \bigtriangledown (\rho \mathbf{v}) = 0 \tag{A.30}$$

The conservation of momentum is given by

$$\rho\frac{D\mathbf{v}}{Dt} = -\bigtriangledown p + \rho\mathbf{g} + \mu \bigtriangledown^2 \mathbf{v} + \frac{1}{3}\,\mu\mathbf{v}\,(\bigtriangledown\mathbf{v}) \tag{A.31}$$

where $\mathbf{g}$ includes the gravitational direction and μ is the viscosity of the fluid or gas. The conservation of energy is given by

$$\rho\frac{D\left(e + 0.5\mathbf{v}^2\right)}{Dt} = \rho\dot{q} - \bigtriangledown p\mathbf{v} + \rho\,(\mathbf{fv}) \tag{A.32}$$

where e and $0.5\mathbf{v}^2$ indicate the internal energy and kinetic energy per unit mass, respectively. The heat flux vector is indicated by $\dot{q}$ and $\mathbf{f}$ are the external forces acting along velocities $\mathbf{v}$.

A.3.2 Thermodynamics extended

The enthalpy for a caloric perfect gas are given by

$$h = c_p T \tag{A.33}$$

where c_p is the specific heat at constant pressure. The isentropic relation, is given by Equation A.34. Here, γ is the isentropic constant which equals 1.4 for air around atmospheric conditions.

$$\frac{p}{\rho^\gamma} \tag{A.34}$$

A.3.3 Isentropic compressible flow

For a steady isentropic flow with negligible body forces, the continuity equation can be combined with the energy equation to form an expression for the total enthalpy along a streamline. If all streamlines originate from a common uniform free stream then total enthalpy, and thus the total temperature, is constant for each streamline.

$$h + 0.5V^2 = h_0$$

With this definition and assuming a caloric perfect gas, the flow equation can be derived for the temperatures as a function of the flow speed.

$$\frac{T_0}{T} = 1 + \frac{\gamma - 1}{2} M^2 \tag{A.35}$$

Using the isentropic relation given by Equation A.34, one can arrive at similar formulas for the pressure and density [25] as a function of the flow speed.

$$\frac{p_{0i}}{p_i} = \left(1 + \frac{\gamma - 1}{2} M^2\right)^{\gamma/(\gamma-1)} = \left(\frac{T_{0i}}{T_i}\right)^{\gamma/(\gamma-1)} \tag{A.36}$$

$$\frac{\rho_{0i}}{\rho_i} = \left(1 + \frac{\gamma - 1}{2} M^2\right)^{1/(\gamma-1)} = \left(\frac{T_{0i}}{T_i}\right)^{1/(\gamma-1)} \tag{A.37}$$

A.4 Massflow

A.4.1 Loss factor comparison

Often manufacturers use the flow factor K_v or flow coefficient C_v instead of the loss factor K. The flow factor is given by

$$K_v = 3.6 \cdot 10^4 Q \sqrt{\frac{\rho}{\Delta p}} \tag{A.38}$$

where Q is the flowrate (m^3/s); Δp is the pressure loss (Pa) and ρ is the density (kg/m^3). The flow factor is related to the flow coefficient as a consequence of non-SI units:

$$K_v = 0.86 C_{v,US} \tag{A.39}$$

$$K_v = 1.03 C_{v,UK} \tag{A.40}$$

As defined before, the loss factor K is defined according to equation A.41, where v is the flow speed (m/s) and A is the nominal area (m^2).

$$\Delta p = 0.5 \rho K v^2 = \frac{0.5 \rho K}{A^2} Q^2 \tag{A.41}$$

Rewriting result in the relation between the loss factor and flow factor:

$$K = \frac{2A^2}{360^2} K_v^{-2} \tag{A.42}$$

A.4.2 Empirical expressions loss factors

A realistic approximation of the losses in the gas system, requires a good estimate of the system its loss factor. In order to do so multiple local losses were accounted for. This was done using simple theoretical and empirical equations/values for the loss factor found in Chapter 6 of White [27].

For area changes across the flow, formulas for 'sudden expansion' (SE) and 'sudden contraction' (SC) were used. As a result, the flow is assumed to always flow from one finite duct to another. Moreover, the transition is sudden and sharp edged. The approximations are given by Equation A.43 and Equation A.44. Where β is the area ratio between the smaller and larger duct. The loss factor is related to the flow speed in the smaller diameter duct.

In the case of the AO-TLCD, the area ratio between the vertical compartments and the interconnecting pipe is most likely very small. As a result, the exit losses approach 1, equivalent to the loss of all kinetic energy in the flow.

$$K_{SE} = (1 - \beta)^2 \tag{A.43}$$

$$K_{SC} \approx 0.42 (1 - \beta) \tag{A.44}$$

Bends were also taken into account to have some contribution to the total loss factor. Since its loss factor contribution depend on the gas system its geometric design, the actual values are not included here.

A.4.3 Incompressible massflow for linear pressures

Simplification massflow equation

In this section the derivation for the simplified massflow equation is given. In addition to chapter 4, also parallel valves are included. The regular massflow equation over a number of parallel similar flow elements:

$$\dot{m} = A_H n_{v,j} \beta_j^2 sgn(\Delta p) \sqrt{\frac{2\rho_1 |\Delta p|}{K_j}}$$

For incompressible flow this can be rewritten assuming local and stagnation properties are the same and given the polytropic relation. To further simplify the massflow equation we can assume to neglect the upstream density changes. Both equations are displayed blow.

$$\dot{m} = A_H n_{v,j} \beta_j^2 sgn(\Delta p) \sqrt{\frac{2\rho_0 \left(\frac{p_{01}}{p_0}\right)^{1/n} |\Delta p|}{K_j}}$$

$$\dot{m} = A_H n_{v,j} \beta_j^2 sgn(\Delta p) \sqrt{\frac{2\rho_0 |\Delta p|}{K_j}}$$

Assuming linear pressures we can derive the upstream pressure from the pressure difference.

$$p_{01} = |\Delta p| / n_c + p_0$$

The most correct massflow equation assuming linear pressures is given below.

$$\dot{m} = A_H \rho_0 sgn(\Delta p) \sqrt{\frac{2 n_{v,j}^2 \beta_j^4}{\rho_0 K_j} |\Delta p| \left(\frac{|\Delta p|}{n_c p_0} + 1\right)^{1/n}}$$

$$\dot{m} = \frac{A_H \rho_0}{K_O} sgn(\Delta p) |\Delta p|^{0.5} \left(\frac{|\Delta p|}{n_c p_0} + 1\right)^{0.5/n}$$

While the simplest equation, which neglects upstream density changes, is given below.

$$\dot{m} = \frac{A_H \rho_0}{K_O} sgn(\Delta p) |\Delta p|^{0.5}$$

Here the obstruction parameter is defined as:

$$K_O = \sqrt{\sum_j \left(\frac{K_j}{n_{v,j}^2 \beta_j^4}\right) \frac{\rho_0}{2}} \; (Flow\ obstruction\ parameter)$$

The massflow equation neglecting upstream density changes has a better fit to the compressible massflow than the more complete massflow equation. The comparison can be found in Figure A.1. Since relative errors are small, the simple form is used for the remainder of this research.

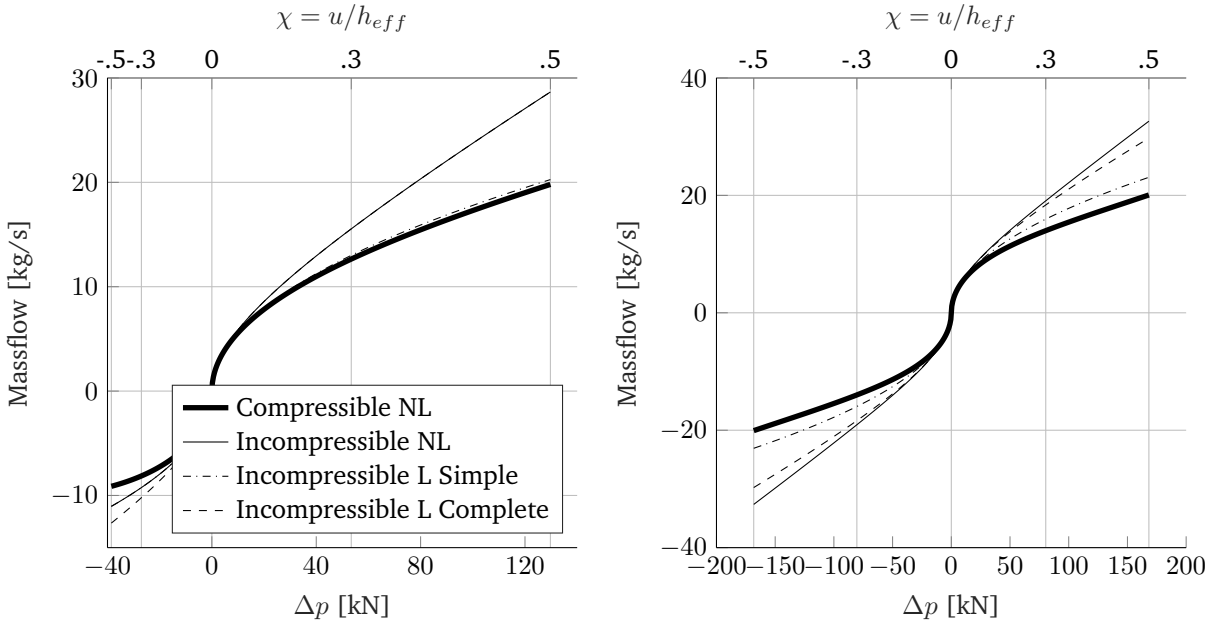

(a) 1-sided sealed

(b) 2-sided sealed

Figure A.1: Comparison massflow equations for very low obstruction with n=1.2.

A.5 Experimental calibration

In order to compare the numerical model with the experimental data, the correct TLCD and airflow parameters need to be used. The calibration of these parameters is given below.

TLCD coefficients

Especially the headloss factor is considered design specific and should be obtained experimentally for each TLCD design. But even the determination of the natural frequency and geometric factors has its uncertainties. The actual path of the streamline indicated in Figure 2.4 may vary around the bends, influencing both B and H.

Experimental results were available for an "open" TLCD with interconnecting pipe. The dynamic amplification of the liquid displacements can be seen in Figure A.2. Furthermore, using calibrated parameters, the DAF was computed with transfer function in Equation A.45 where the linear damping was obtained iteratively using harmonic linearisation.

$$H_{U,W} = \frac{\kappa}{\left(\frac{\omega_A}{\omega}\right)^2 - 1 + 2\zeta_A \left(\frac{\omega_A}{\omega}\right) i} \tag{A.45}$$

The effective length could be obtained using the natural frequency of the "open" TLCD. A geometric parameter $\kappa = 0.46$ was determined from the high frequency response. The obtained geometric parameters correspond to a streamline located around 33% in the corner. In other words, the bulk of the moving fluid cuts the corners slightly due to fluid "deadzones". From the resonant response, $\delta_L = 2$ can be obtained.

For this headloss the inter-connecting pipe, which is not present in the 1-sided small-scale set-up, has a considerable contribution. Uncertainties in the inter-connecting pipe dimensions and lack of pressure data make an exact estimation of the effect impossible. For the experimental set-up a headloss coefficient of $\delta_L = 0.5$ is assumed instead, based on theoretical loss factors [27].

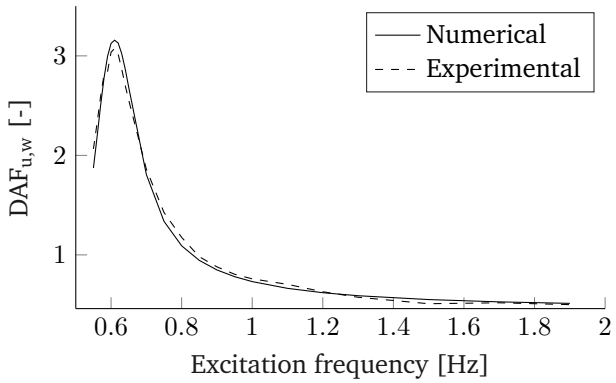

Figure A.2: Dynamic amplification liquid. Comparison calibrated model with open experimental set-up.

Other natural frequencies

In the experiments a 1-sided closed frequency around $1.9Hz$ was observed. Which corresponds to a polytropic constant around 1.2. Though, the exact frequency deviated somewhat per experiment. Furthermore, sloshing in the vertical compartments was observed at similar frequencies due to an unfavourable geometric design.

Loss factor

Assuming low-obstruction (forced flow), the total loss factor can be obtained with Equation A.13. For the steady state maximum pressure difference and displacements, Figure A.3 was obtained.

For low frequencies, sensor noise is too dominant. For high frequencies and high obstruction, the assumption of forced flow does not hold. Moreover, at these frequencies, sloshing/splashing motions distort the liquid displacement measurement.

A total loss factor of approximately $K = 8.4$ is assumed. Which is approximately equivalent to a valve loss factor of $K = 7$ if one excludes sudden expansion/compression. This value is within the typical loss factor range for small nominal diameter bend globe valves, or "angle valves" [27].

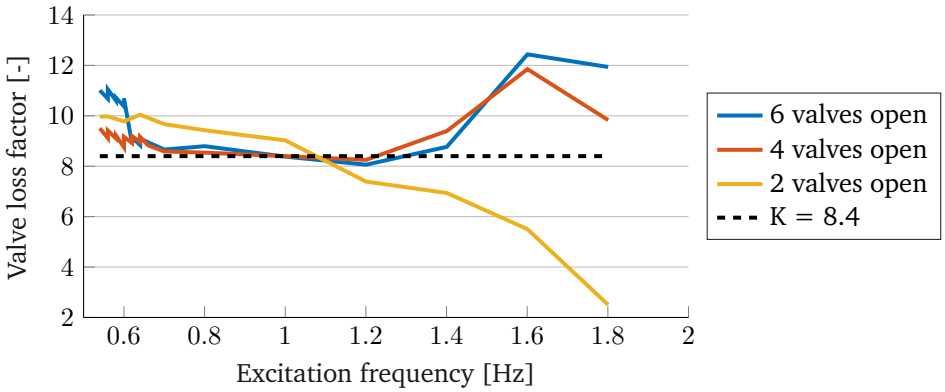

Figure A.3: Loss factor approximation for all experiments

Limitations sensor

Figure A.4 visualises the noise and distortion of the ultrasonic liquid displacement sensors. The left, represents a case where high amount of sloshing/splashing was observed and expected. The non-zero mean of the two displacement sensors suggests a constant over estimation of the peak displacements. Measurement of splashing droplets can result in such an over-estimation. Moreover, it can be seen that the peaks have been distorted. Which results in a shift in phase lag of the liquid displacements.

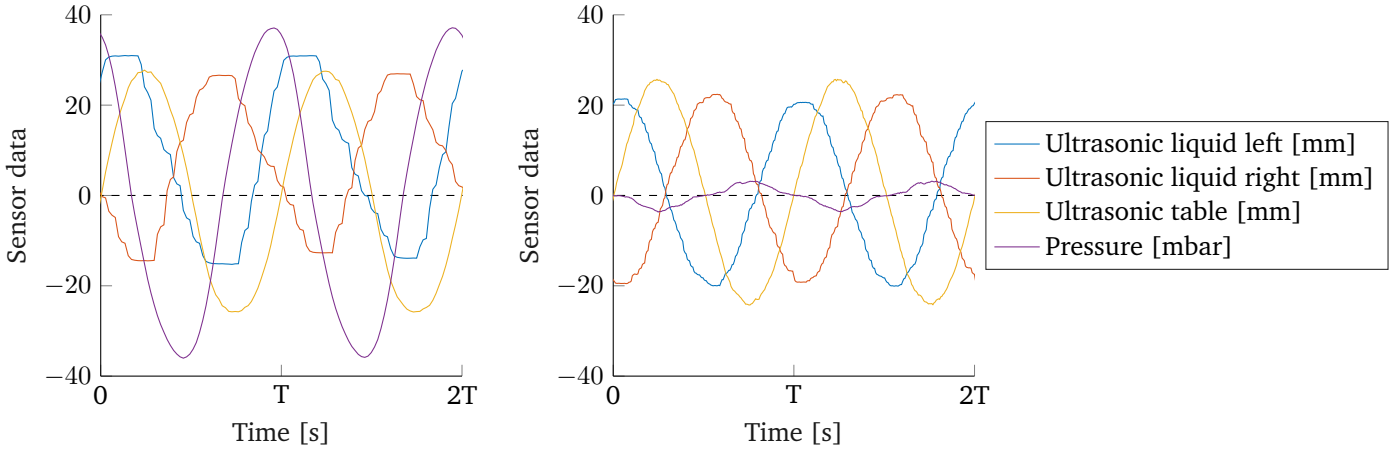

Figure A.4: Sensor noise and distortion experimental data for $n_v = 2$, $f = 1.8Hz$ and $n_v = 4$, $f = 0.60Hz$ on the left and right, respectively.

A.6 Fundamental matrix of Meissner's equation

The general solution of a second order system is restated in Equation A.46, including its derivative.

$$\begin{aligned} x(t) &= c_1 \text{exp}(r_1 t) + c_2 \text{exp}(r_2 t) \\ \dot{x}(t) &= c_1 r_1 \text{exp}(r_1 t) + c_2 r_2 \text{exp}(r_2 t) \end{aligned} \tag{A.46}$$

The first solution of the fundamental matrix $\mathbf{\Phi}_0^+(t)$ can be obtained by an initial unit displacement $x(t=0)=1$ as in Equation A.47.

$$\begin{aligned} c_1 \text{exp}(0) + c_2 \text{exp}(0) &= 1 \\ c_1 r_1 \text{exp}(0) + c_2 r_2 \text{exp}(0) &= 0 \end{aligned} \tag{A.47}$$

Solving Equation A.47 gives the constants for $x_2 1$ and $\dot{x}_1$:

$$c_{11} = \frac{r_2}{r_2 - r_1} \ , \ c_{12} = -\frac{r_1}{r_2 - r_1}$$

Analogously, the general solution can be solved for an initial velocity $\dot{x}(t=0)=1$. This results in the constants for x_2 and $\dot{x}_2$:

$$c_{21} = \frac{1}{r_1 - r_2} \ , \ c_{22} = -\frac{1}{r_1 - r_2}$$

A.7 Performance evaluation using the growth matrix

The mechanical energy E of the liquid and host is given by Equation A.48.

$$E = 0.5[\dot{w}, \dot{u}_f]^T \mathbf{M}[\dot{w}, \dot{u}_f] + 0.5[w, u_f]^T \mathbf{K}[w, u_f] + E_{gas} \tag{A.48}$$

Here, the mass and stiffness matrix are limited to the host and liquid state and given by Equation A.49 and Equation A.50, respectively. Both matrices are scaled back to their SI units by their masses M and m_{eff}. Note that m_{eff} is not the fluid mass but a result of the LaGrange derivation of the equations of motion of a regular TLCD. This scaling also results in a symmetric mass matrix.

$$\mathbf{M} = \begin{bmatrix} M & \\ & m_{eff} \end{bmatrix} \begin{bmatrix} 1 + \mu_{gen} & \mu_{gen}\bar{\kappa}/(\boldsymbol{\phi}_j^T \mathbf{s}) \\ \kappa \mathbf{s}^T \boldsymbol{\phi}_j & 1 \end{bmatrix} \tag{A.49}$$

$$\mathbf{K} = \begin{bmatrix} M & \\ & m_{eff} \end{bmatrix} \begin{bmatrix} \omega_S^2 & 0 \\ 0 & \omega_S^2 \end{bmatrix} \tag{A.50}$$

$$\text{where: } m_{eff} = n_{TLCD} L_{eff} A_H \rho_f \tag{A.51}$$

The mechanical energy of the gas is derived from the linear gas-spring and is given in Equation A.52.

$$E_{gas} = 0.5 \epsilon A_H \Delta p^2 \tag{A.52}$$

The mechanical energy of the SDoF system is computed using Equation A.53 using the general solution given in Equation A.46 at $t = sT$.

$$E = 0.5M(1 + \mu_{gen})\dot{x}(sT)^2 + 0.5M(\omega_S^2)x(sT)^2 \tag{A.53}$$

Appendix B

Figures and tables

B.1 In-depth analysis LQR strategy

In Figure B.1, forces are normalized across all diagrams with the maximum liquid weight restoring force. Displacements are normalized by their maximum. A few cycles of the total time series are indicated more clearly. Even less trajectories go through the active quadrants w.r.t. the host.

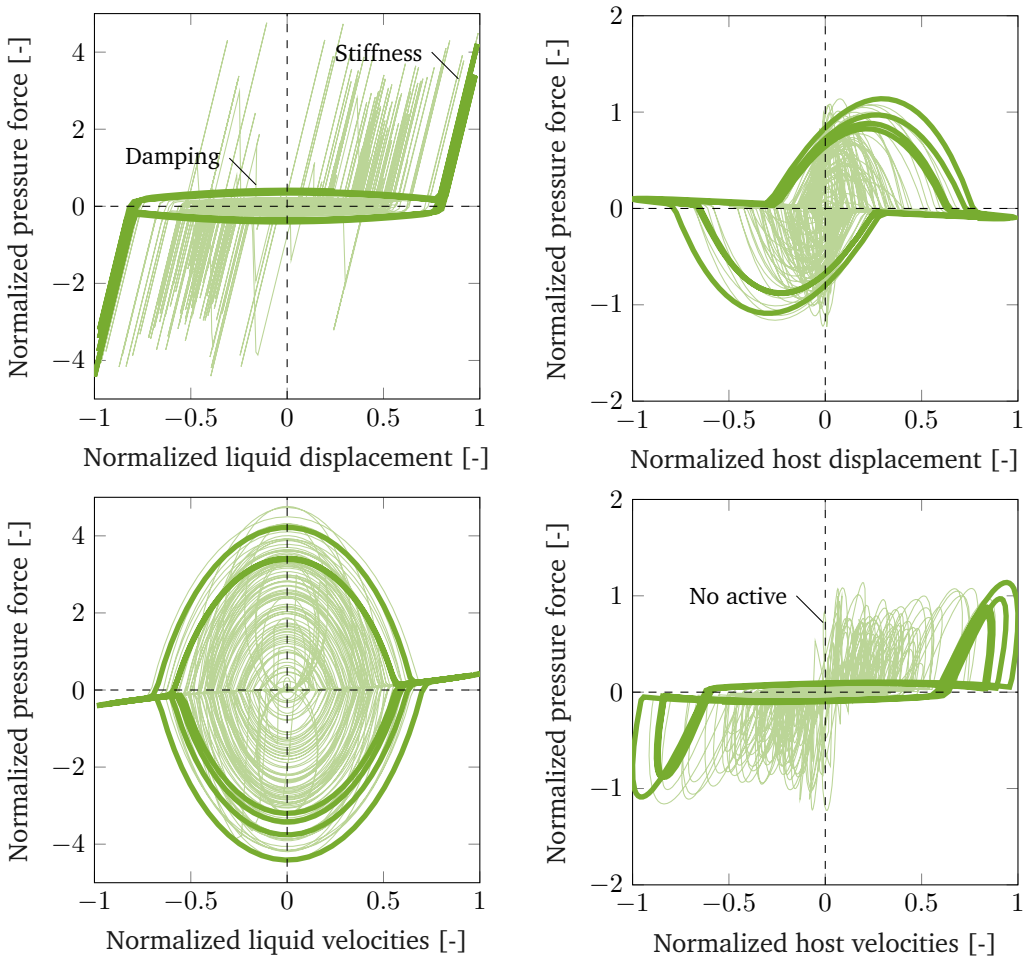

(a) Pressure-force on liquid

(b) Pressure-force on host

Figure B.1: Force-displacement/velocity trajectories for clipped-LQR strategy for load case III seed 1.

B.2 Results periodic LTV framework

B.2.1 Hill's equation

In Figure B.2 the stability graphs are shown for Equation 8.31 for a sinusoidal modulation shape on the left and a square modulation shape on the right. For both figures, a modulation frequency ratio of 2 was used ($\delta = 0.25$). In both graphs, the unstable and stable regions have been indicated by U and S, respectively. In Figure B.2a, the instability criteria of $\epsilon > 2\gamma$ is clearly visible [57]. For a square modulation signal, instabilities occur 'earlier'.

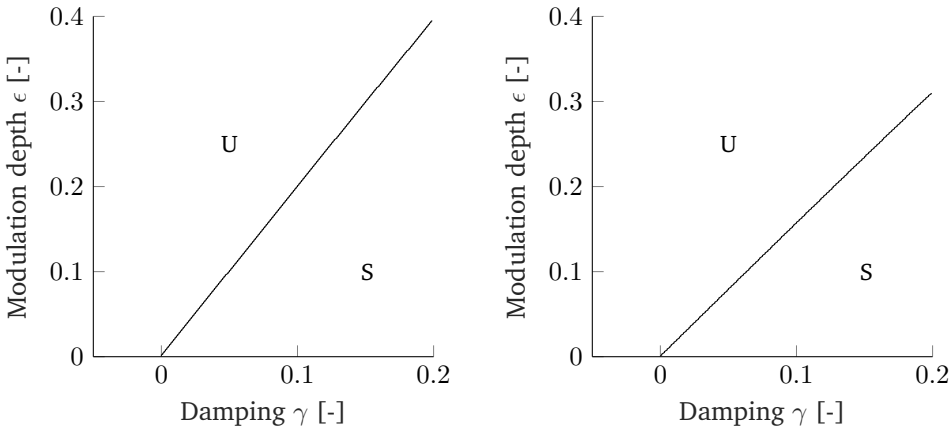

(a) Sinusoidal modulation shape.

(b) Square modulation shape.

Figure B.2: Damping modulation of a second order differential equation for δ=0.25.

B.2.2 Additional results equivalent LTV model

In this appendix section additional results from the equivalent LTV model can be found. Moreover, some comparison with the non-linear semi-active AO-TLCD model are provided.

Time domain comparison LTV and NL model

The time-domain solutions can be obtained with full knowledge of the transition matrix. In Figure B.3, this solution is compared to a time-domain solution from the semi-active AO-TLCD model. The LTV and the NL model are indicated by thick and dashed lines, respectively. Both models are excited by an unit initial displacement of the host structure.

The semi-active damper is controlled through the C-LQR on/off scheme. Moreover, the same linear damping is assumed in order to prevent strong non-linearities as a result of the large responses. For the LTV model a duty cycle of 0.4 is assumed.

As time progresses differences between the two models grow. The separation of the gas-spring and the additional damping in the LTV model can explain part of the differences in the pressure magnitude.

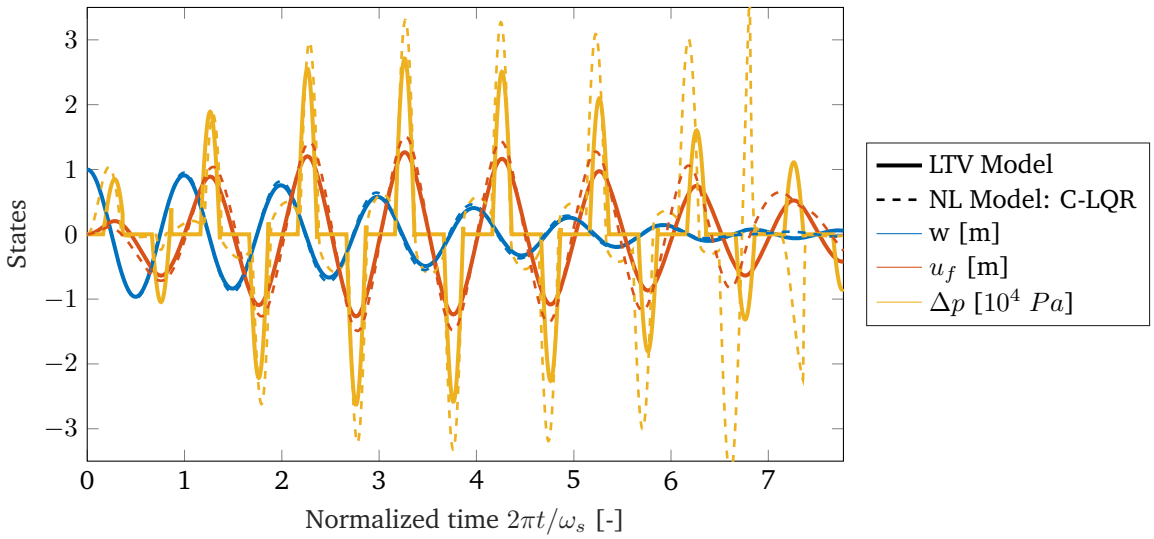

Figure B.3: Comparison of the responses between the LTV and the NL model for $D = 0.4$ and C-LQR on/off control, respectively.

Mechanical energy of the LTV model

For the same set-up as in Figure B.3 the mechanical energy is plotted in Figure B.4. Here, the solid lines indicate the time-domain solution which is obtained using the complete transition matrix. The markers, indicate the solution at $t = sT$, which is obtained with the growth matrix. The total mechanical energy is computed as in Appendix A.48. Furthermore, the energies are split up between the host, the liquid and the gas. For example, the energy of the host contains both the kinetic and the potential energy of the host structure.

In Figure B.4 it is clearly visible that the solution at $t = sT$ of the host cannot be used for the evaluation of the performance. Individual states, e.g. the host displacement, may give an even worse representation. Therefore, the total mechanical energy is used over a number of periods. For this, the first few modulation periods are neglected because of improper initial conditions (resulting in an ineffective damper around $t = 0$).

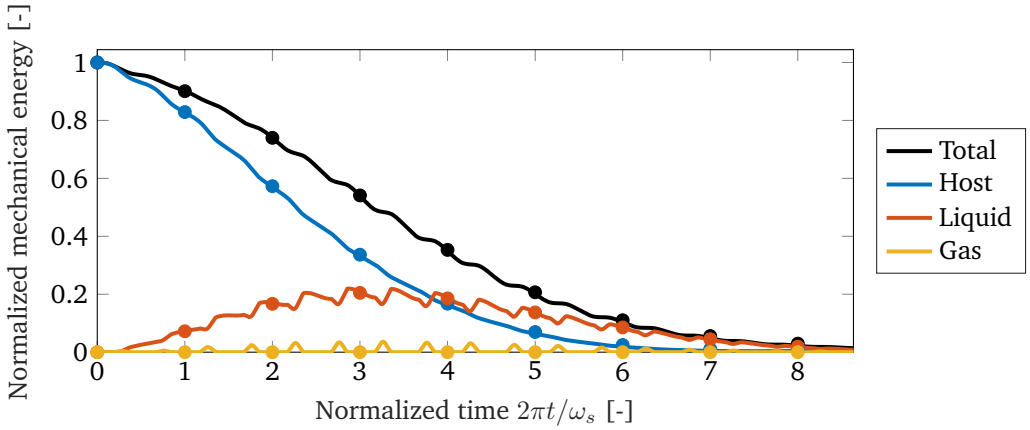

Figure B.4: Comparison of the mechanical energy computed using at $t = sT$ using the growth matrix and solved in time-domain using the transition matrix.

Cross-sections of the performance graph

In Figure B.5 and Figure B.6 three cross-sections are shown of Figure 8.7. The passive benchmark solutions from the case study are also indicated.

In essence, Figure B.5 shows a passive system which is fully closed. Instabilities occur for a normalized modulation depth of minus one. In other words, the system is unstable if the total sealed TLCD its stiffness is smaller than zero.

Figure B.6a shows the performance for variable duty cycle at a modulation depth equivalent to the gas-spring stiffness used in the case study. An effectiveness of approximately 6% critical can be obtained. This is a very slight improvement over the sub-optimal semi-active control schemes used in this research.

Figure B.6b shows the performance of the periodic LTV system for an already optimally tuned passive TLCD. Again, one can conclude that the semi-active damper out-performs its passive counterpart.

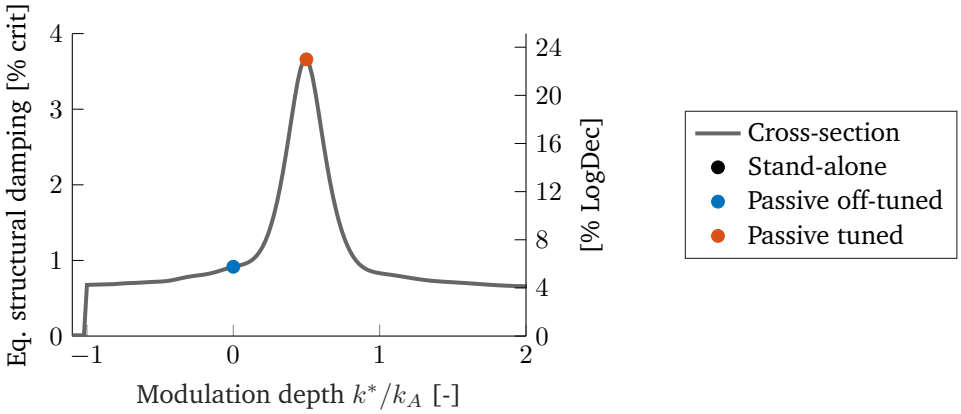

Figure B.5: Cross section of the performance figure at $D = 1$ corresponding to the passive TLCD.

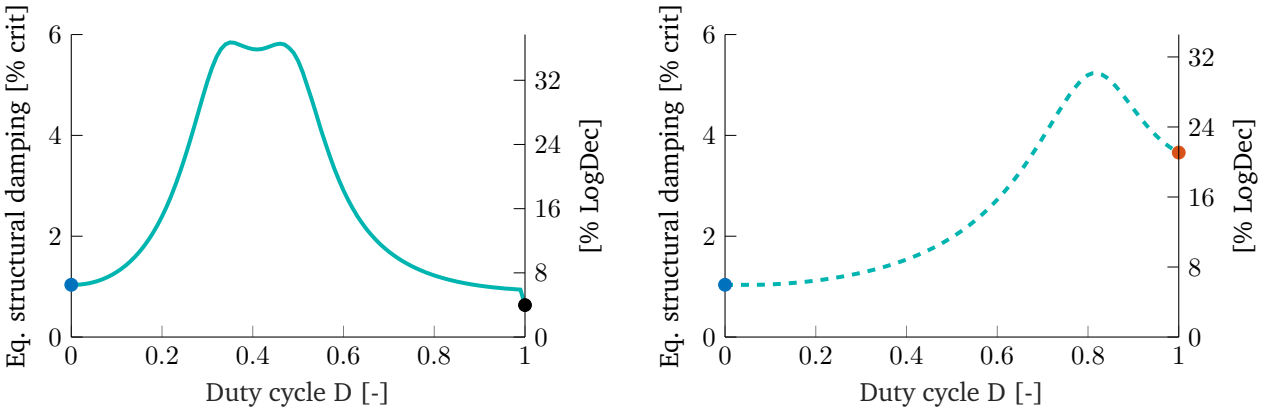

(a) Corresponding to the case study SA AO-TLCD design.

(b) Corresponding to a SA AO-TLCD for an already tuned damper.

Figure B.6: Cross section of the performance figure with variable duty cycle.

Closing times case study

In order to compare the quasi-periodic results from the case study with the periodic LTV system, data of the closing times is required. In Figure B.7 the box plots of the duty cycles is given for all load cases. The spread indicates the spread of the observed closing times. For the third, and most critical, load case 50% of the data lies within 0.4 and 0.5. Corresponding to the correct range in terms of performance in Figure 8.7 or Figure B.6a.

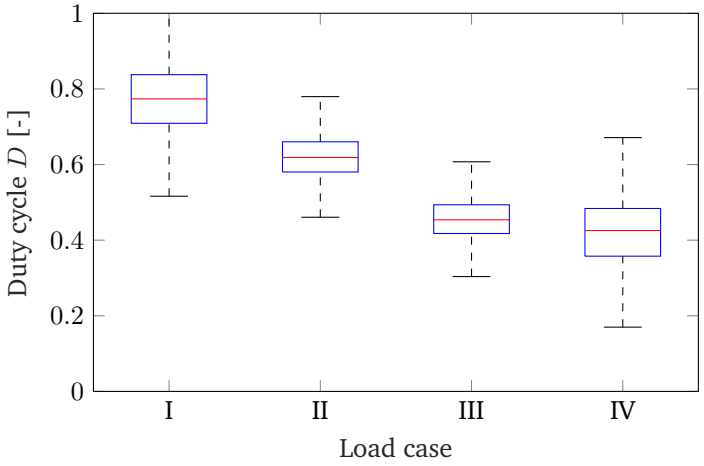

Figure B.7: Boxplot of 'duty cycles' observed in the non-linear TD simulations of the case study

Bibliography

[1] Ernst and Young. Offshore wind in europe / walking the tightrope to success. Technical report, March 2015. https://www.ewea.org/fileadmin/files/library/publications/reports/EY-Offshore-Wind-in-Europe.pdf, accessed October 2017.

[2] Department of Energy USA. Levelised Cost of Energy (LCoE). Technical report, Office of Indian Energy, 2015.

[3] B.F. Spencer and S. Nagarajaiah. State of the art of structural control. *Journal of Structural Engineering*, 129(7):845–865, 2003.

[4] G.W. Housner, L.A. Bergman, T.K. Caughey, A.G. Chassiakos, et al. Structural control: Past, present, and future. *Journal of Engineering Mechanics*, (9):897–971, 1997.

[5] M.J. Hochrainer. *Control of vibrations of civil engineering structures with special emphasis on tall buildings*. Dissertation, Vienna University of Technology, 2001.

[6] M.J. Hochrainer. Experimental investigation of active tuned liquid column gas dampers. In *Vienna Congress on Recent Advances in Earthquake Engineering and Structural Dynamics*, 2013.

[7] O. Altay, F. Nolteernsting, S. Stemmler, D. Abel, et al. Investigations on the performance of a novel semi-active tuned liquid column damper. *Procedia Engineering*, 199:1580–1585, 2017.

[8] M. Rahman, Z.C. Ong, W.T. Chong, S. Julai, et al. Performance enhancement of wind turbine systems with vibration control: A review. *Renewable and Sustainable Energy Reviews*, 51:43–54, 2015.

[9] K. Bargi, R. Dezvareh, and S.A. Mousavi. Contribution of tuned liquid column gas dampers to the performance of offshore wind turbines under wind , wave , and seismic excitations. *Earthquake Engineering and Engineering Vibration*, 15(3):551–561, 2016.

[10] M.A. Lackner. Passive structural control of offshore wind turbines. *Wind Energy*, 14(3):373–388, June 2011.

[11] G.M. Stewart and M.A. Lackner. The impact of passive tuned mass dampers and wind-wave misalignment on offshore wind turbine loads. *Engineering Structures*, 73:54–61, 2014.

[12] B. Fitzgerald and B. Basu. Structural control of wind turbines with soil structure interaction included. *Engineering Structures*, 111:131–151, 2016.

[13] C. Sun. Semi-active control of monopile offshore wind turbines under multi-hazards. *Mechanical Systems and Signal Processing*, 99:285–305, 2018.

[14] P.F. Miah. Design of an experimental model for a semi-acdtive vibration damping system on a jack-up platform. Masters thesis, Delft University of Technology, 2015.

[15] J.P. Den Hartog. *Mechanical Vibrations*. 4th edition, 1956.

[16] M. Constantinou, T. Soong, and G. Dargush. *Passive Energy Dissipation Systems for Structural Design and Retrofit*. 1998.

[17] S.K. Yalla. *Liquid dampers for mitigation of structural response: theoretical development and experimental validation*. Dissertation, University of Notre Dame, 2001.

[18] H. Gao, K. Kowk, and B. Samali. Optimization of tuned liquid column dampers. *Engineering Structures*, 19(6):476–486, 1997.

[19] C.C. Chang. Mass dampers and their optimal designs for building vibration control. *Engineering Structures*, 21(5):454–463, 1999.

[20] A. Teramura and O. Yoshida. Development of vibration control system using u-shaped water tank. In *Eleventh World Conference on Earthquake Engineering*, 1996.

[21] A. Strauss, J. Schellander, M. Reiterer, R. Wagner, et al. Reduktion von pendelschwingungen im ingenieurbau mittels flussigkeitstilgersystemen. *Bautechnik*, 90(7):421–432, 2013.

[22] B. Khalid. *Control of seismically forced vibrations of asymmetric buildings by means of a novel base isolation system*. Dissertation, Vienna University of Technology, 2010.

[23] Y.Q. Ni, Z.G. Ying, J.Y. Wang, , J.M. Ko, and B.F. Spencer. Stochastic optimal control of wind-excited tall buildings using semi-active mr-tlcds. 19(3):269–277, 2004.

[24] K. Yalla and A. Kareem. Semiactive tuned liquid column dampers: Experimental study. *Journal of Structural Engineering*, 129(7):960–971, 2003.

[25] J.D. Anderson. *Fundementals of Aerodynamics*. 5th edition, 2011.

[26] P.K. Kundu and Cohen R.D. *Fluid Mechanics*. 6th edition, 2016.

[27] F.M. White. *Fluid Mechanics*. 7th edition, 2011.

[28] L.F. Moody. Friction factors for pipe flow. *Transactions of the ASME*, 66:671–684, 1944.

[29] A. Aubault, M. Alves, A. Sarmento, D. Roddier, et al. Modeling of an oscillating water column on the floating foundation windfloat. In *Proceedings of the ASME 2011 30th international conference on ocean, offshore and arctic engineering*, 2011.

[30] A. Sarmento. Wave flume experiments on two-dimensional oscillating water column wave energy devices. *Experiments in Fluids*, 12:286–292, 1992.

[31] M. Abe and T. Igusa. Semi-active dynamic vibration absorbers for controlling transient response. *Journal of Sound and Vibration*, 198(5):547–569, 1996.

[32] F Weber and C Boston. Clipped viscous damping with negative stiffness for semi-active cable damping. *Smart Materials and Structures*, 20(4), 2011.

[33] J. Hogsberg. The role of negative stiffness in semi-active control of magneto-rheological dampers. *Structural Control and Health Monitoring*, 18:289–304, 2009.

[34] S.J. Dyke, B.F. Spencer, M.K. Sain, and J.D. Carlson. Seismic response reduction using magnetorheological dampers. In *Proceedings of the 13th IFAC World Congress*, volume L, pages 145–150, 1996.

[35] I F Lazar, D J Wagg, and S a Neild. Reducing the clipping effect of semi-active clipped optimal control of a two storey building. In *Proceedings of ISMA2012-USD2012*, pages 321–330, 2012.

[36] D. Hrovat. Survey of advanced suspension developments and related optimal control applications. *Automatica*, 33(10):1781–1817, 1997.

[37] C. Poussot-Vassal, O. Sename, L. Dugard, P. Gaspar, et al. A new semi-active suspension control strategy through lpv technique. *Control Engineering Practice*, 16:1519–1534, 2008.

[38] S. Nagarajaiah. Structural vibration damper with continuously variable stiffness, 2000. Patent, US 6098969 A.

[39] S. Nagarajaiah and E. Sonmez. Structures with semiactive variable stiffness single / multiple tuned mass dampers. *Journal of Structural Engineering*, 133(1):67–77, 2007.

[40] C. Sun and S. Nagarajaiah. Study on stmd with bariable damping and stiffness. *Structural Control and Health Monitoring*, 21:890–906, 2014.

[41] K. Yalla, A. Kareem, and C. Kantor. Semi-active tuned liquid column dampers for vibration control of structures. *Engineering Structures*, 23(11):1469–1479, 2001.

[42] J.Y. Wang, Y.Q. Ni, J.M. Ko, and B.F. Spencer. Semi-active tlcds using magneto-rheological fluids for vibration mitigation of tall buildings. In *Advances in Building Technology*, pages 537–544, 2002.

[43] M.J. Hochrainer and F. Ziegler. Control of tall building vibrations by sealed tuned liquid column dampers. *Structural Control and Health Monitoring*, 13(6):980–1002, 2006.

[44] TU Delft. Modeling and Control of Hybrid Systems SC42075, 2017. `http://www.dcsc.tudelft.nl/~bdeschutter/hs/index.html`, accessed October 2017.

[45] D Karnopp, M J Crosby, and R A Harwood. Vibration control using semi-active force generators. *Journal of Engineering for Industry*, 96(2):619–626, 1974.

[46] S. Nagarajaiah and S. Narasimhan. Smart base-isolated benchmark building. Part II: Phase I sample controllers for linear isolation systems. *Structural Control and Health Monitoring*, 13(2-3):589–604, 2006.

[47] TU Delft. Control Theory SC42015, 2017. `https://blackboard.tudelft.nl/webapps/blackboard/content/listContent.jsp?course_id=_57922_1&content_id=_2866170_1`, accessed September 2017.

[48] Z. Wang, Z. Chen, and B.F. Jr. Spencer. Self-powered and sensing control system based on MR damper: presentation and application. *Spie*, 2009.

[49] H.E. Tseng and J.K. Hedrick. Semi-active control laws - optimal and sub-optimal. *Vehicle System Dynamics*, 23(1):545–569, 1994.

[50] S.H. Crandall and W.D. Mark. *Random vibrations in mechanical systems*. 2nd edition, 1963.

[51] P. Friedmann, C. Hammond, and T. Woo. Efficient numerical treatment of periodic systems with application to stability problems. *International Journal for Numerical Methods in Engineering*, 11(6):1117–1136, 1977.

[52] H. D'Angelo. *Linear Time-varying systems*. 1st edition, 1983.

[53] P. Friedmann. Numerical methods for determining the stability and response of periodic systems with applications to helicopter rotor dynamics and aeroelasticity. *Computers & Mathematics with Applications*, 12A(1):131–148, 1986.

[54] C. S. Hsu. On approximating a general linear periodic system. *Journal of Mathematical Analysis and Applications*, 45(1):234–251, 1974.

[55] T. Insperger and R. Horvath. Pendulum with harmonic variation of the suspension point. *Periodica Polytechnica Mechanical Engineering*, 44(1):39–46, 2000.

[56] H. Broer. Tongues in parametric resonance. In *EUROMECH Nonlinear Dynamics Conference*, 2008.

[57] D.B. Batchelor. Parametric resonance of systems with time-varying dissipation. *Applied Physics Letters*, 29(5), 1976.

[58] Hartono and A.H.P. van der Burgh. A linear differential equation with a time-periodic damping coefficient: Stability diagram and an application. *Journal of Engineering Mathematics*, 49(2):99–112, 2004.

[59] M. Maslanka and Weber F. Precise stiffness control with MR dampers. In *Topics in Dynamics of Civil Structures*, volume 4, 2013.

Definitions

Off-tuning A VA operating outside of its design frequency range where it is ineffective.

Period adjustment The ability of a modified VA, to increase effectiveness at off-tuned frequencies.

Passive VA Parameters can only be changed on a time-scale much larger than the damper its natural period.

Semi-active VA Parameters of the damper can be controlled in real-time. No mechanical energy can be added through the actuator.

Active VA Full control over the damper. Mechanical energy can be added/subtracted through an actuator.

Damping Internal regular linear or non-linear damping of the TLCD.

Structural damping Inherent damping of the host structure.

Effectiveness Equivalent additional damping added to the host structure by a damper.

Clipping The process of limiting a desired, potentially active, control input to its semi-active and/or physical bounds.

Bang-bang Discrete on/off control inputs. This does not necessary imply that the actuator also responds in a discrete/instantaneous manner.

Passivity constraint The constraint for semi-active control. The control action may only dissipate energy.

Stability All states go to zero as time goes to infinity.

TU Delft Delft University of Technology

SIEMENS Gamesa RENEWABLE ENERGY